MEDIUM-TERM COASTAL MORPHOLOGY CHANGE IN THE SOUTHWESTERN BLACK SEA

by

Nick LiBassi

B.S., Geography, Texas A&M University, 2002

Submitted to the Kandilli Observatory and
Earthquake Research Institute in partial fulfillment of
the requirements for the degree of
Master of Science

Graduate Program in Geodesy

Boğaziçi University

2017

MEDIUM-TERM COASTAL MORPHOLOGY CHANGE IN THE SOUTHWESTERN BLACK SEA

APPROVED BY:

Prof. Dr. Haluk Özener ..... 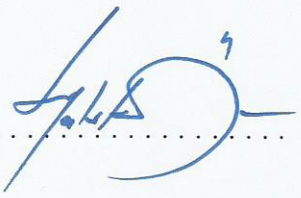
(Thesis Supervisor)

Assoc. Prof. Dr. Aslı Doğru ..... 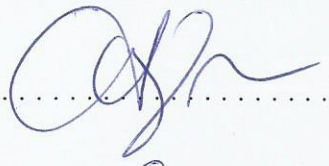
(Thesis Co-supervisor)

Assoc. Prof. Dr. Emre Otay ..... 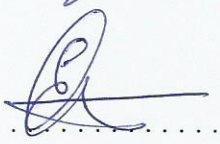

Prof. Dr. Cem Gazioğlu ..... 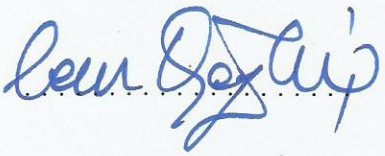
(Istanbul University)

Assoc. Prof. Dr. Yunus Kalkan ..... 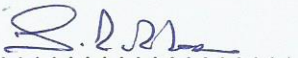
(Istanbul Technical University)

DATE OF APPROVAL: 21.04.2017

ACKNOWLEDGEMENTS

Despite their heavy workload, Dr. Haluk Özener and Dr. Aslı Doğru in the Geodesy Department always made time to answer my unending list of technical questions. I also appreciate their perspective during the times I dreamed of changing my topic to something that didn't require my swimming in the sea. I'm grateful to have benefited from their dedication to their work both in classes and throughout the duration of this project.

The staff and students at the Coastal Engineering Laboratory on Boğaziçi's Sarıtepe Campus served as survey crew members and provided support in terms of expertise, experience, data, equipment, and office space for the study. In particular, I greatly appreciate the guidance of Dr. Emre Otay. His wisdom on the nearshore environment and sediment transport and his ability to communicate them are obvious gifts of his. Mohammad Aslani freely and gladly gave of his time to conduct the surveys by serving as boat captain and resolving equipment and technical issues. Onur Akagündüz also served as boat captian and took care that the surveys were conducted without harm to crew members or the equipment. All of his assistance after the surveys was also invaluable. Beyza Özen, Çoruh Durmuş, and Pelin Uzun all helped make the March 2017 survey a success. Margarita Pozhidaeva provided general survey assistance as well as December 2015 bathymetry and shoreline data and associated metadata. Soner Kural from the Coastal Lab provided wind data.

Also from the Geodesy Department, Aslı Sabuncu helped in the search for data associated with the original surveys.

I'm also grateful to Ömer Akmanlar for his assistance in checking calculations and to Çağatay Kariptaş for his flexibility with my work schedule.

My wife Laura and children Nate, Peter, and Annie all exhibited great patience and a willingness to bear with me throughout the project.

ABSTRACT

MEDIUM-TERM COASTAL MORPHOLOGY CHANGE IN THE SOUTHWESTERN BLACK SEA

Coastal areas are in a state of continual flux, due in part to seasonal factors and in part, to influences operating over longer periods of time. Discerning between these two types of causes remains a challenge. This study compares shoreline and nearshore bathymetry surveys conducted with an interval of fifteen years in order to determine the extent of medium-term coastal change. Results of surveys completed in 2001 and 2002 in Kilyos, Turkey are compared with data collected in December 2015, September 2016, and March 2017 in the same location using GNSS equipment and an echo sounder. Average shoreline recession has been estimated at 3-4 cm/yr. The predominant bar has been found to have moved seaward at a maximum rate of 1 m/yr since 2002. Mid-term nearshore erosion has been observed at approximately 100-125 m^3/m.

ÖZET

GÜNEYBATI KARADENİZ'DE ORTA VADEDE KIYISAL MORFOLOJİ DEĞİŞİMİ

Kıyı alanları kısmen mevsimsel faktörlere, kısmen de uzun dönemli etkilere bağlı olarak sürekli bir değişim halindedirler. Bu iki etki arasındaki farkı ayırt edebilmek hala zorlu bir çalışma konusudur. Bu çalışma orta-vadeli kıyı değişiminin boyutlarını tanımlayabilmek için, 15 yıl ara ile gerçekleştirilmiş kıyı şeridi ve yakın kıyı batimetri ölçme çalışmalarını karşılaştırmaktadır. 2001 ve 2002 yıllarında Kilyos'da GNSS ve Sonar ekipmanları ile gerçekleştirilmiş ölçme çalışmalarının sonuçları, Aralık 2015, Eylül 2016 ve Mart 2017 tarihlerinde aynı bölgede aynı ekipmanla gerçekleştirilmiş ölçme çalışmalarının sonuçları ile karşılaştırılmaktadır. Ortalama kıyı erozyonu 3-4 cm/yıl olarak bulunmuştur. 2002 yılından bu yana geçen zamanda, kum yığını deniz yönünde en fazla 1 m/yıl hareket etmiştir. Orta vadede yakın kıyı erozyonu yaklaşık 100-125 m^3/m olarak bulunmuştur.

TABLE OF CONTENTS

LIST OF FIGURES

LIST OF TABLES

LIST OF SYMBOLS

L_o	Deep-water wave length

LIST OF ACRONYMS/ABBREVIATIONS

CORS	Continuously Operating Reference Station
CRAB	Coastal Research Amphibious Buggy
DEM	Digital Elevation Model
DGPS	Differential Global Positioning System
DORIS	Doppler Orbitography and Radiopositioning Integrated by Satellite
GLONASS	Global'naya Navigatsionnaya Sputnikovaya Sistema, Global Navigation Satellite System of Russia
GNSS	Global Navigation Satellite System
GPS	Global Positioning System, used to refer to GNSS in this study unless otherwise stated
HWL	High Water Line
IERS	International Earth Rotation and Reference Systems Service
IHO	International Hydrographic Organization
IMU	Inertial Measurement Unit
IRNSS	Indian Regional Navigational Satellite System
ITRF	International Terrestrial Reference Frame
ITRS	International Terrestrial Reference System
LECZ	Low-Elevation Coastal Zone
MBES	Multi-Beam Echo Sounder
MHW	Mean High Water
MSL	Mean Sea Level
NAVIC	Navigation with Indian Constellation
NMEA	National Marine Electronics Association
PDBS	Phase Differencing Bathymetric Sonar
RTK	Real-Time Kinematic
SAR	Synthetic Aperture Radar
SBAS	Satellite-Based Augmentation Systems
SBES	Single-Beam Echo Sounder

SSS	Side-Scan Sonar
THU	Total Horizontal Uncertainty
TM	Transverse Mercator
TPU	Total Propagated Uncertainty
TVU	Total Vertical Uncertainty
UAV	Unmanned Aerial Vehicle
USV	Unmanned Surface Vehicle/Vessel
VLBI	Very Long Baseline Interferometry
WGS84	World Geodetic System 1984

1. INTRODUCTION

In 2007, it was reported that roughly 634 million people worldwide live within the Low-Elevation Coastal Zone (LECZ) defined as the zone within 10 m in elevation of mean sea level [2]. A 2015 study projected these numbers to rise to 879 million and 1.4 billion by the years 2030 and 2060, respectively [3].

Over thirty years ago, the International Geographical Union's (IGU) Commission on the Coastal Environment reported recession in 70 percent of the world's coastlines [4]. Even if spread out over a few decades, a dramatic change in the world's coastlines would directly affect nearly ten percent of the world's population and would indirectly affect the entire world.

Additionally, the dynamic nature of coastal areas and the difficulty of obtaining accurate data have resulted in high demand for nearshore and coastal data. In 1999, the Coastal Services Center (CSC) in the United States surveyed 270 offices of agencies responsible for protecting and managing coastal resources in some way. Out of a possible 29 priority datasets, nearshore bathymetry ranked second after high-resolution aerial photography [5]. Nearshore bathymetry is still considered to be the variable that most restricts the accuracy of much coastal research [6].

The impact on the global population, the reality of coastal change beyond the short-term, and the difficulty of collecting the necessary data have provided the motivation for this study on changes in coastal morphology in the Black Sea.

1.1. Aims and Objectives

While coasts are naturally extremely dynamic, undergoing continual change due to daily and seasonal changes in wind and weather, medium- and long-term influences must be considered when studying coastal erosion or accretion over the course of years or decades. This study seeks to determine the extent to which medium-term coastal

erosion or accretion has occurred at the area of interest in the southwestern Black Sea.

The objectives of the study can be summarized as follows:

(i) Conduct shoreline and bathymetry surveys using GNSS and an echo sounder at Burç Beach in Kilyos, Turkey.
(ii) Compare the results of the recent studies to similar surveys conducted in the same location in 2001 and 2002.
(iii) Consider the extent to which the difference between the two sets of surveys can be attributed to processes at work beyond the short term.

1.2. Terminology and Background

1.2.1. Shore and Shoreline

The zone between the water's edge at low tide and the landward limit of the extent of wave action comprises the shore. The foreshore lies between the limits of low tide and high tide, and the backshore extends from the limits of normal high tide to locations submerged only in extreme conditions. The backshore is often bounded landward by a cliff base. Though the word *beach* may sometimes be used interchangeably with *shore*, the word *shore* is used in this study.

Similarly, although the terms *coastline* and *shoreline* are sometimes used interchangeably, research generally distinguishes between the two (see Figure 1.1). High spring tides occur twice per lunar month at new and full moons when the Earth, sun, and moon are generally aligned with each other. The coastline is defined as the edge of the land at these normal high spring tides. This study examines the shoreline, defined as the water's edge which is in a state of continual motion between low-tide shoreline and high-tide shoreline [4]. The coastal profile in the figure below depicts the coastline and shoreline among other terms.

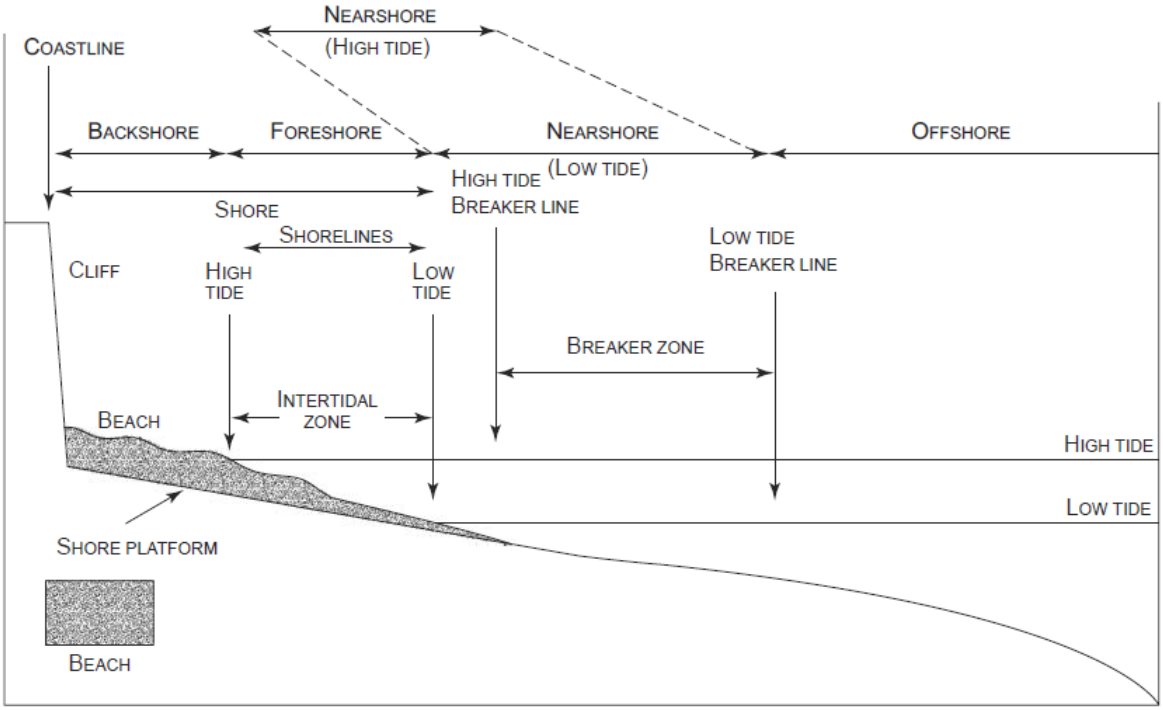

Figure 1.1. Coastal Terminology (Bird, 2008, used with permission).

1.2.2. Coastal Morphology

Coastal Morphology refers to the study of coastal landforms as well as all processes responsible for their existence and change over time. Both the effects of human and non-human intervention are considered.

1.2.3. Coastal Erosion and Accretion

Coastal erosion occurs when material along the coastal profile is worn away due to a deficit in the supply and/or the export of material from a given location. Generally, the influences of strong winds, high waves, high tides, and storm surge conditions produce coastal erosion resulting in shoreline retreat. Erosion rate is expressed in volume/length/time, while shoreline retreat is expressed in length/time, e.g. m/yr [7].

Coastal erosion is often distinguished from short-term *cutback* where the former

results in long-term shoreline retreat and/or loss of material over decades, and the latter refers to temporary loss of material or storm-induced shoreline retreat. In the case of short-term cutback, the shoreline, though dynamic, is considered to be stable as the temporarily removed sediment is later returned to the area [8].

Coastal accretion, as the opposite of coastal erosion, refers to the long-term accumulation of sediment in a nearshore environment. Any kind of laying down of sediments in a waterway is also referred to as *deposition*.

1.2.4. Medium-Term

In the context of evolution of coastal morphology, multiple definitions of *short-term*, *long-term*, and *medium-term* exist. This study will use the following definitions [9]:

- *Short-term* refers to periods as short as the duration of a single storm or a single day but including periods as long as a year.
- *Long-term* refers to periods of at least a few decades.
- *Medium-term* refers to any length of periods between a year and multiple decades.

1.2.5. Nearshore Bathymetry

The word *bathymetry* can refer to both the measurement of depth of water in oceans, seas, and lakes as well as to seafloor elevation and topography data.

The nearshore zone stretches from the region where waves begin to break, known as the surf zone, to the upper limit of the swash zone where the shore is submerged at high tide. The swash zone extends between the upper and lower levels reached by a wave on the shore, also known as *run-up* and *run-down*, respectively. While the nearshore can be concisely defined as the surf zone and the swash zone, its location varies both spatially and temporally. Accordingly, it can also be defined as the region affected by waves breaking as a result of changes in depths. While multiple definitions

have been assigned to the *offshore zone*, this study uses the term in contrast to the nearshore zone such that the offshore zone is the region unaffected by depth-induced wave-breaking. While maximum depths in the nearshore zone can exceed 40 m in certain places, typical depths range from 10 to 20 m [4].

Of the many factors shaping the coast, waves play one of the most significant roles. Due to the relationship between nearshore elevations and the speed and strength of waves approaching the shore, changes in bathymetry must be examined when attempting to determine the extent of coastal erosion or accretion in a given location. As waves reach areas of shallower depths, their velocity decreases and wave height increases.

1.2.6. Surveying

Surveying involves measuring distances, angles, and heights at a particular location for the purpose of construction or an assessment of physical phenomena.

Plane surveying involves measurements where the surface of the Earth is considered to be a two-dimensional plane. This type of surveying does not take into account the curvature of the Earth but is appropriate for study areas whose longest side is less than 10-15 km [10].

Sites with dimensions beyond this in either direction require geodetic surveying which accounts for the curvature of the Earth.

1.2.7. Reference Surfaces and Datums

Surveying and mapping utilize models of the Earth. Though the shape of the Earth is close to a sphere, the distance from its center to the equator is longer than that from its center to the poles.

The surface of the Earth is most accurately modelled by the *geoid* which results

from considering the locations of the oceans under only the influence of the Earth's gravitation and rotation and then extending these points through the continents. The geoid approximates mean sea level. Since this surface of equal gravity potential results in an irregular shape which complicates application, approximations of the the Earth's size and shape are necessary.

Rotating an ellipse about its minor axis produces an ellipsoid which serves as a mathematical model approximating the size and shape of the Earth. The term *spheroid* is also often used interchangeably with *ellipsoid*. Since no single ellipsoid fits the geoid at every location, the ellipsoid that best fits the geoid at the location of interest must be chosen for each study.

A datum consists of known locations that serve as a reference from which measurements can be taken or from which spatial relationships can be displayed. A datum defines local or global points on an ellipsoid.

Since datums take into consideration elevation on a local, regional, or global scale, lateral coordinates on the surface of the Earth vary according to the chosen datum.

Examples of regional and national geodetic datums include the European Datum 1950 (ED50) and the North American Datum 1983 (NAD83). Examples of global geodetic datums include the World Geodetic System 1984 (WGS84), the Geographic Reference System 1980 (GRS80), and the International Terrestrial Reference System (ITRS).

ITRS is a global spatial reference system that co-rotates with the Earth and is maintained by the International Earth Rotation Service (IERS) using measurements from over 500 observation stations worldwide. The positions of these observation stations are reported to be accurate to the centimeter-level and are updated using four space geodesy techniques: Global Navigation Satellite System (GNSS), Very Long Baseline Interferometry (VLBI), Doppler Orbitography and Radiopositioning Integrated by Satellite (DORIS), and Satellite Laser Ranging (SLR) [11].

The International Terrestrial Reference Frame (ITRF) refers to the realizations of the ITRS, which are the geodetic datums produced by the ITRS since 1988. As temporal changes due to tectonic or tidal deformations are observed using the space geodesy systems mentioned above, revised reference frames are published. The ITRF is widely considered to be the most accurate global reference frame.

1.2.8. Coordinate Systems and Projections

A coordinate system provides a reference for establishing positions of points in any space, and in this context, locations on or near the surface of the Earth.

A planar coordinate system defines points according to their distance from an origin consisting of two perpendicular axes.

A geographic coordinate system considers the curvature of the Earth, providing coordinates as latitude and longitude, in terms of angles between a point on the Earth's surface and the equator or Prime Meridian. Latitude, or *geodetic latitude*, is the angle between the equatorial plane and a line perpendicular to the tangent line at a given location on the reference ellipsoid. Though the word *latitude* usually refers to geodetic latitude, geocentric latitude of a given location is the angle measured between the equatorial plane and a line drawn from the center of the Earth to a given location on the surface of the reference ellipsoid [10].

Geodetic coordinates include latitude, longitude, and ellipsoidal height. In order to view or use geographic or geodetic coordinates in a two-dimensional plane, coordinates representing the three-dimensional Earth must be projected onto a planar coordinate system by means of a mathematical transformation. This often involves systematically bringing a portion of the Earth's surface into contact with a portion of a cylinder or cone. Common projections include Equirectangular, Transverse Mercator (TM), and Lambert Conformal Conic projections.

Transverse Mercator projections can be conceptualized by a horizontally-oriented

cylinder surrounding the Earth such that the Earth's surface is tangent to the inside of the cylinder. The narrow strip from pole to pole on either side of the tangent line can then be considered a two-dimensional surface. For other locations or zones in the world, a rotation of the Earth can be imagined changing the tangent line, or the central meridian of the projection. Units are measured in meters.

1.2.9. Vertical Datums

Vertical datums provide points or a surface taken as zero in order to serve as a reference in measuring heights. Tidal and geodetic datums are based on a physical surface and are used for bathymetric and topographic surveys, respectively. By contrast, an ellipsoidal datum is based on a reference ellipsoid. Since GNSS equipment produces heights based on an ellipsoidal datum, GNSS-derived heights must be transformed for use with data referred to either a tidal or geodetic datum.

1.2.10. Tidal Datums

In order to correct bathymetric and shoreline data for tidal conditions, surveyors must obtain knowledge of the water level at the time of the survey according to the ellipsoid used for vertical reference relative to a base elevation or chart datum. Since a tidal datum or chart datum provides a reference for depths used for navigational purposes, its baseline typically lies at a level below the lowest tides. Examples are Mean Lower Low Water (MLLW) and Lowest Astronomical Tide (LAT). MLLW is the arithmetic mean of the lower low water heights of each tidal day observed over a specific 19-year Metonic cycle (the National Tidal Datum Epoch). In the U.S., MLLW has been designated for use as the adopted reference National Ocean Service chart and sounding datum in most coastal tidal waters per the National Tidal Datum Convention of 1980 [12].

Mean Sea Level (MSL) is often incorporated into a national or regional datum for use in surveying and engineering purposes. MSL excludes variations due to waves and tides by averaging sea level over tidal cycles as short as 12 hours and as long as

19 years [4].

1.2.11. GNSS

Global Navigation Satellite Systems (GNSS) provide point positioning through the reception of signals from satellites orbiting the earth. Systems based in specific countries or regions include the Global Positioning System (GPS) in the U.S., GLONASS in Russia, Galileo in Europe, Beidou in China, the Quasi-Zenith Satellite System in Japan, and the Indian Regional Navigational Satellite System (IRNSS) or Navigation with Indian Constellation (NAVIC).

Each of the systems consists of a satellite constellation consisting of four to thirty-two satellites in orbit, a ground control network, and user equipment.

Trilateration uses the distances of three known points from an unknown point in order to determine the two- or three-dimensional location of the unknown point. Through electronically measuring distances between at least four satellites and a GNSS receiver, the receiver's location can be determined with an accuracy between 10 m and 1-2 cm depending on the survey method and level of corrections used. Since the orbiting satellites themselves serve as control points, or points whose precise location is known, the system relies on an ability to precisely determine the satellites' location in time.

Sources of uncertainty or error in GNSS positioning include receiver noise, satellite clocks, orbits, the ionosphere and other parts of the atmosphere, and the inability for a signal to travel the direct path between a satellite and a receiver (multipath errors).

Using a single GNSS receiver without corrections, horizontal uncertainty can be as high as 10 m. More often, two or more receivers are used so that error correction data can be sent to a rover receiver from a base receiver which has been set up over a point whose coordinates are precisely known. Since the base and rover receivers are within a certain distance of each other (10-20 km at most), the satellite signals to each receiver contain the same errors. As long as the base station is set up over a location

whose coordinates are precisely known, the extent of the errors in the signal arriving at the base station can be determined. This data is then used to correct the locations of the rover receiver through either post-processing or in real time over a radio signal. Differential GPS (DGPS) involves only one type of GNSS signal, the code-phase which provides a pseudorange accurate within a meter. A real-time kinematic (RTK) system begins with the same pseudorange from the code phase but then considers the higher frequency carrier phase which provides greater resolution. Error data based on both of these phases are then transmitted from the base station to the receiver in real-time providing horizontal accuracies between 10 mm and 1-2 cm and vertical accuracies between 15 mm and 2-4 cm.

Similar correction methods include Satellite-Based Augmentation Systems (SBAS) which arrive at the same accuracy through a network of base stations, a central station transmitting corrections to a satellite, and the satellite then broadcasting corrections to a user's receiver. Continuously Operating Reference Station (CORS) networks broadcast correction data from a nearby CORS station to a receiver [13].

The majority of the bathymetryic and shoreline survey methods described below rely on GNSS for horizontal and vertical positioning.

1.2.12. Accuracy Standards

The International Hydrographic Organization (IHO) is an intergovernmental consultative and technical organization that was established in 1921 to support safety of navigation and the protection of the marine environment [14].

The IHO Standards for Hydrographic Surveys (5th edition, February 2008) outline the minimum standards for collection of bathymetry data to be used for marine navigation. Though the data collected in this study is not used for marine navigation, the same standard is used to evaluate the quality of bathymetry data collected for research purposes.

The standards require that a geocentric reference frame based on the International Terrestrial Reference System (ITRS) be used as a horizontal reference frame. A statistical method should be employed such that positional uncertainty at the 95% confidence level can be reported. Maximum values are defined for Total Horizontal Uncertainty (THU), Total Vertical Uncertainty, and Total Propagated Uncertainty (TPU).

Of the four survey classifications outlined in their latest standards, the most rigorous, the *Special Order* classification, is appropriate for areas where "under-keel clearance is critical." This standard requires a THU of 2 m, and TVU at the 95% confidence level is defined by the following:

$$\pm\sqrt{a^2 + (bxd)^2} \tag{1.1}$$

where: a is the portion of the uncertainty that does not vary with depth, b is the portion of the uncertainty that varies with depth, and d is depth

For Special Order surveys, a is given as 0.25 m, and b as 0.0075 [15].

1.3. Methods of Conducting Coastal Surveys

A wide range of both in situ and remote sensing techniques have been used in collecting shoreline and nearshore bathymetry data.

1.3.1. In Situ Methods

1.3.1.1. Sonar. *Sonar* (originally from Sound Navigation and Ranging) describes the technique where objects on or under the surface of the water are detected using the the time interval between transmitted and returned sound waves. Bathymetry data

can be collected using echo sounders to transmit acoustic pulses which are reflected off of the seafloor providing a return time interval which is then converted into a depth. A transducer combined with a transceiver is generally mounted on the hull or the side of a boat just below the surface of the water. Single-beam echo sounders (SBES) emit a sonar wave only along a vessel's trackline. Though the width or diameter of the beam may vary from system to system, a narrow beam provides greater spatial precision. Multi-beam echo sounders (MBES) emit fan-shaped sound waves providing efficient survey of a wider area than is possible with SBES. In the nearshore, the swath collected perpendicular to the ship track would have a width to water depth ratio of anywhere between 3:1 and 12:1. Though MBES systems are more expensive, and data processing can be more complicated, they provide greater accuracy, resolution, and efficiency than can be achieved with SBES. For nearshore depths however, SBES can provide sufficient results.

Variations on this method include imaging sonar, side-scan sonar (SSS), and interferometric sonar. Imaging sonar obtains a broad sonic image as opposed to the more narrow profiles achieved through SBES or MBES. Side-scan sonar involves transducers facing perpendicular to the survey vessel, emitting pulses on both sides in order to collect data over a wider area. Both MBES and Phase Differencing Bathymetric Sonar (PDBS) or interferometric sonar employ multiple receivers and calculate the angle at which the returning acoustic pulse arrives. The depth and angle data are then used to produce a more complete model of the seafloor. MBES achieves this through *beam forming*, where the angle of each of a series of transmitted and received beams is known through the design of the device. PDBS also utilizes multiple reception elements but calculates the angle of returning pulses using the time, or phase, difference between each signal's reception at different elements.

The transducers on certain echo sounders are also able to differentiate between signals returning from the seafloor and those reflecting off of other objects on or between the seafloor, such as debris or fish. Many MBES and SSS systems can also improve bathymetric data utilizing backscatter data, information on the intensity, or amount of energy received, after reflection.

If temperature, pressure, and salinity are also measured, the local speed of sound in water can be used to calculate depths rather than the approximate figure of 1500 m s^{-1}. These parameters can be measured using a conductivity-temperature-depth (CTD) instrument.

Horizontal and vertical positions of the transducer (or a point at a known distance from it) are obtained using a GNSS receiver.

Correcting the data for the boat's heave, pitch, and roll provides further accuracy. While this can be done through one of several methods, one of the most straightforward approaches is to use a motion reference unit or attitude sensors and a gyroscope.

SBES or any method that does not produce overlapping swaths of sampled data must be interpolated to obtain a continuous surface or contours for an entire area of study. The quality of the final product in these cases is further dependent on the selected method of interpolation and its implementation.

Sonar is also utilized in surveys conducted through an Unmanned Surface Vessel/Vehicle (USV).

1.3.1.2. Amphibious Vehicle. During the early 1980s, the U.S. Army Corps of Engineers built a buggy 10.6 m in height equipped with a Zeiss Elta-2S Total Station at the top [16]. The Coastal Research Amphibious Buggy (CRAB) provided accurate, cost effective surveys of onshore topography and bathymetry up to depths of 9 m. Though limited by its height and lack of portability, its results are still often used as ground-truth data for the testing of other methods of obtaining nearshore bathymetry.

1.3.1.3. Survey Sled. Another method that originated in the early 1980s involved the use of a survey sled which collected data as it was pulled along the seafloor [17]. A winch pulls the sled first offshore and then onshore. Though this method was reported to provide reasonable results even in breaking waves as high as 5 m, its contact

with the seafloor limits its application to certain environments. Further, surveys are time-intensive, and results are limited by spatial resolution and maximum depths of approximately 10 m.

1.3.1.4. Radar. Radar data obtained from moving vessels has been used to map nearshore bathymetry and currents [18]. Although this method results in a lower horizontal resolution (50-100 m) than radar obtained from onshore stations, it provides the possibility for mapping larger areas at one time. Two datasets were obtained from a vessel travelling at a maximum speed of 14 knots. In comparing the results to an independent survey and to data from an echo sounder on the same ship, favorable results were found for depths up to 50 m.

1.3.1.5. Horizontal Distance Measurement from Shore. Though GNSS is now the preferred method for positioning, survey tape and range finders (infrared, microwave, and optic) have also been used especially in wading surveys. [19]

1.3.2. Remote Sensing Methods

Remote sensing systems acquire information about the Earth's surface without physical contact with the Earth. They can be divided into active and passive methods. Passive sensors measure naturally occurring energy while active sensors provide a source of energy which is measured in order to obtain an elevation or depth value at a given location.

1.3.2.1. Aerial Photography. Analysis of aerial photography to estimate nearshore sea depths from wave propagation characteristics began in the 1940s during World War II. Using a series of aerial photographs taken at intervals, wave speed was calculated using the wave's position relative to a baseline or fixed point. Water depth was then estimated from wave speed.

Aerial photography can be used to capture sun and sky light as it reflects both

from the seafloor and through the sea surface. The displacement between these two locations provides the sea depth at a given point. While this method can be appropriate for determining nearshore bathymetry to depths of approximately 20 m, its precision and accuracy are strongly affected by water turbidity, substances found between the surface and the seafloor (e.g. sea vegetation), solar irradiance, wave action, and the spectrum characteristics of seafloor material. It yields the most accurate results in the presence of clean sea water, strong solar irradiance, light wind-induced waves, and a sloping seafloor. The photography must also be obtained at or below 3000 m above the surface. Approximate vertical errors have been reported at 0.3 m in maximum depths of 20-30 m [20].

1.3.2.2. Lidar. Lidar (Light Detection and Ranging) is an active remote sensing technique that makes uses of pulsed lasers to determine ranges to a given object or surface. By recording the precise times of the transmission of a pulse of light and its reflection from the object or surface being imaged, the distance between the two is calculated using the speed of light.

Airborne lidar has been effectively used to determine point elevations with high accuracy and resolution from which topographic surfaces can be derived. On-board GNSS and IMU (Inertial Measurement Unit) equipment are used to obtain the x-, y-, and z- coordinates of the point on the surface and correct them for the plane's yaw, pitch, and roll. Topographic lidar uses the near-infrared portion of the electromagnetic spectrum to detect the surface, while bathymetric lidar employs the near-infrared portion to detect the surface of the sea and the green portion of the spectrum to penetrate the sea and measure bottom depths. The plane must be flown at or below 500 m.

Collection of lidar data and the final product itself make it one of the more attractive methods of obtaining elevation data. For topographic surveys, maximum vertical accuracies are reported between 2.5 and 5 cm. In 2015, The American Society for Photogrammetry and Remote Sensing (ASPRS) published their latest Positional Accuracy Standards for Digital Geospatial Data which applies to lidar among other

types of data. According to these standards, the highest class required a horizontal accuracy of 1.5 cm and a vertical accuracy of 2.0 cm with a 95% confidence interval. The recommended minimum Nominal Pulse Density (NPD) for the same class is greater than or equal to 20 pls/m^2. A typical maximum pulse or point density would be 100/m^2 for a resolution of 10 cm. Additionally, since the data is collected using a helicopter or fixed-wing airplane, large areas can be covered in a short period of time [21].

Bathymetric vertical accuracies are required to be within 0.5 m with a 95% confidence interval, and certain systems report accuracies up to 15 cm. In favorable weather conditions, data can be collected at night as well as during the day. With optimal water clarity bathymetric lidar data can be collected in maximum depths of 50-70 m.

Several aspects of lidar limit its widespread application. Though the cost of lidar data has decreased in recent years, its high price remains the primary deterrent to wider use. A lidar system consists of a laser source and detector, a scanner and controller, GNSS and IMU equipment, a high-accuracy, high-resolution clock for timing laser emissions, reflections, GNSS/IMU and scan-angle measurements as well as high-performance computers and high-capacity data recorders. Due to the cost of this equipment in addition to the aircraft and associated personnel, the price of the data often far exceeds the budget of many researchers. The quality of bathymetric lidar surveys are also highly dependent on water turbidity. Though less of a challenge now, historically, the size of data sets has also complicated its use. Adequate technological infrastructure must also exist for managing the large data.

1.3.2.3. Satellite Derived Bathymetry. Over the last few decades, nearshore bathymetry has been estimated from satellite imagery using two basic methods.

Many imagery-based techniques employ the properties of visible light as it penetrates a body of water. Since the intensity of light decreases as water depth increases due to absorption and reflection, if the level of water turbidity and substrate characteristics are known, water depth can be found using the radiation intensity received by

the satellite. This method is known as either *Photobathymetry* or the *Bottom-Reflected Radiance* method. A model to explain the relationship between bottom surface reflectance and the radiance level measured by satellite was first developed in the late 1970s [22]. While its use is limited to areas of constant water clarity/turbidity and homogeneous sea bottom substrate, as the first empirical model of its kind, it has served as a base for continued development of similar algorithms. The model involves removing from images the effects of sun glint and the water column between the surface of the sea and the sea bottom.

Since it usually requires some in situ data collection to determine the characteristics of the local water column and substrate, it is not a purely remote sensing technique. The turbidity of the water determines the degree to which light attenuates with respect to depth, and the substrate determines the bottom reflectance.

This method can offer coverage over relatively large areas at a reasonable cost with a horizontal resolution of 10-30 m. Its accuracy, however, is highly dependent on water turbidity. Though accuracy varies based on imagery used, water and weather conditions at time of data collection, as well as the chosen algorithm, in optimal conditions, vertical accuracies better than 1 m have been reported, and horizontal accuracy is typically around 5 m.

The other primary method, *Wave Kinematics*, employs the wave dispersion relationship in order to convert the motion of shoaling waves into a depth. As waves enter shallower water, their velocity decreases and wave height increases. The wave dispersion relationship is often used to find the wavelengths of waves of a known period in a known depth of water. If both wavelength and period are known, however, water depth can be obtained. A Fourier transform eventually leads to wavenumber values. Wavenumbers are easily converted to wavelengths. Wavelength and period are then used to estimate depths [23]. Since the turbidity of the water is not a factor in the calculation, in situ calibration is not required, and the method can be applied in any nearshore environment. This method was first developed to measure waves using a ship's radar [24] but has since been used with other methods.

1.3.2.4. Photo Analysis. Photos taken onshore can also be analyzed using principles similar to those described under Aerial Photography.

An approach known as *cBathy* derives bathymetry estimation from ocean wave celerity, or phase speed, as captured in photos taken using Argus cameras onshore [23]. Like Wave Kinematics Bathymetry, this method also employs wave dispersion theory. In two different locations, RMS errors of approximately 0.5 m were reported between the shoreline and water depths up to 14 m.

1.3.2.5. Synthetic Aperture Radar (SAR). As with a traditional radar system, distances between the system and the target of interest are obtained by measuring the time between the transmission of a radio pulse and its return to the antenna after reflection from the target. The two-dimensional image produced by SAR results from the range or line-of-sight distance to target or surface as well as from the azimuthal dimension perpendicular to the range. The antenna aperture or effective area is a measure of an antenna's ability to receive the power of radio waves. Traditionally a higher aperture is attained using a physically larger antenna. SAR systems are unique in the high azimuth resolution they are able to achieve through a high aperture. In order to achieve these resolutions, the system would require an antenna several hundred meters long. Rather than using an impractically large antenna, aperture is synthetically increased by using the orbit of the satellite and processing received series of signals as if they had arrived over a larger distance. The distance covered by the satellite during the processing of a given series of signals is the synthetic aperture.

Efforts to estimate bathymetry using SAR have been ongoing since 1978 when the first SAR was sent into orbit aboard NASA's SEASAT satellite. With revisits of any given portion of the Earth's surface every few days, SAR can provide easily obtainable data at a much higher temporal resolution than most other techniques. Unlike satellite imagery, it is not dependent on water clarity.

Bathymetry derived from SAR results from the analysis of a high resolution two-

dimensional representation of the sea surface. Since SAR microwave signals cannot penetrate water beyond a few centimeters, bathymetry data must be obtained indirectly through seafloor-induced surface effects. While the magnitude of offshore surface effects is not sufficient for analysis, SAR imagery can be used for nearshore bathymetry retrieval. One method makes use of variations in flow speeds of currents resulting from the morphology of the seafloor. These variations can be sensed as sea surface roughness increases thereby increasing radar backscatter in the area. This method requires the existence of a surface current (which is usually a tidal current). Another approach monitors changes in wave propagation direction and wavelength as swell waves move from deep to shallow water. Offshore storms produce swell waves that travel long distances propagating with a uniform wavelength, height, and direction until reaching shallower later. Since a surface current can interfere with swell wave characteristics, current velocities must be slight to non-existent [25].

SAR-derived nearshore bathymetry has been produced both independently of and in conjunction with other data collection methods. Maximum vertical accuracy of SAR-derived bathymetry has been reported at 0.4-0.5 m in favorable conditions [26].

1.3.2.6. Satellite Altimetry. Vertical differences in sea surface exist due to underlying changes in bathymetry. While these slight differences at the surface cannot be seen, they can be detected by a radar altimeter on a satellite. Although this method is briefly mentioned due to its general relevance, its application is only appropriate in deep sea regions rather than the nearshore zone.

1.3.2.7. Video Analysis. Updated estimates of bathymetry can be obtained through analysis of video recorded over a period of time. A project at the Coastal Imaging Lab of Oregon State University uses an array of five Argus cameras to capture video. Methods of analysis vary but all provide high temporal resolution despite the limited spatial range. One effort reported a 0.3-0.5 m RMS error [27].

1.3.2.8. Radar. Radar from either ships or onshore stations has been used to collect data on wave height, currents, and other variables since the mid-1980s. More recently, methods have been developed to obtain nearshore bathymetry from radar as well. Good results have been found in depths up to 20 m provided that certain conditions are met. Accuracy is highly dependent upon the quality of data acquisition and the height of the radio antenna above sea level, for example [28].

1.3.2.9. UAV-Collected Data. Unmanned Aerial Vehicles (UAVs) have also been utilized to collect bathymetry data in recent years. Data collection methods include lidar and aerial photography.

1.4. Methods of Shoreline Surveying

Of the methods listed above, the following can be used to obtain both bathymetry and shoreline data: aerial photography, satellite imagery, land-based photos, an amphibious buggy (CRAB), and video analysis.

The obvious advantage in shoreline surveying is the possibility of the use of terrestrial methods in many areas. As compared to bathymetry surveys, traditional land surveying techniques as well as space-based surveying (GNSS) generally provide data of much higher accuracy with much less effort. The time-intensive nature of terrestrial methods, however, limits the scale of results.

Another factor when conducting shoreline surveys is the determination of the shoreline indicator to serve as a proxy for the ever-changing shoreline. Surveys conducted for engineering research purposes, as opposed to navigation, often use tidal datums such as Mean High Water (MHW) or the High Water Line (HWL). The ease of identifying the HWL makes it one of the most commonly used indicators [29]. Other approaches involve multiple measurements seaward and landward of each shoreline point. One way of doing this would be to measure the limits of both run-up and run-down for each point in the alongshore direction.

1.5. Previous Related Work

In the winter and summer months of 2001 and 2002, shoreline and nearshore bathymetry surveys were conducted at the study location in Kilyos, Turkey by a team from the Coastal Engineering Laboratory and Geodesy Department of Boğaziçi University [30].

A total of 23 benchmarks were determined, three of which were installed as permanent concrete benchmarks designated as 5001, 5002, and 5003. Benchmark coordinates are found in [1].

Figure 1.2. Benchmarks from 2001-2002 surveys. Concrete benchmarks are labeled.

Shoreline surveys were performed using both terrestrial and space geodetic methods in June 2001, February 2002, and June 2002.

In conjunction with the shoreline surveys, topographic surveys were conducted along nine transects with two to three temporary benchmarks along each transect. Surveys were continued into the sea along the same transects using a 5-m survey rod as long as the rod could be seen from shore or until the waves prevented the seaward advance of the crew member carrying the rod.

Bathymetry data was collected in June 2001 and July 2002 using an echo sounder and DGPS. The June 2001 survey found an average slope of 0.014 and an alongshore bar at a depth of 4 meters. Thirteen months later, the alongshore bar had moved out to a depth of 7 meters.

Between June 2001 and February 2002, the shoreline was found to have receded by an average distance of 11 m, with recession reaching a maximum value of 36.3 m. While some of the recession may be attributed to natural, seasonal fluctuations, the shoreline study in June 2002 revealed an average coastal accretion of only 1.5 m [31].

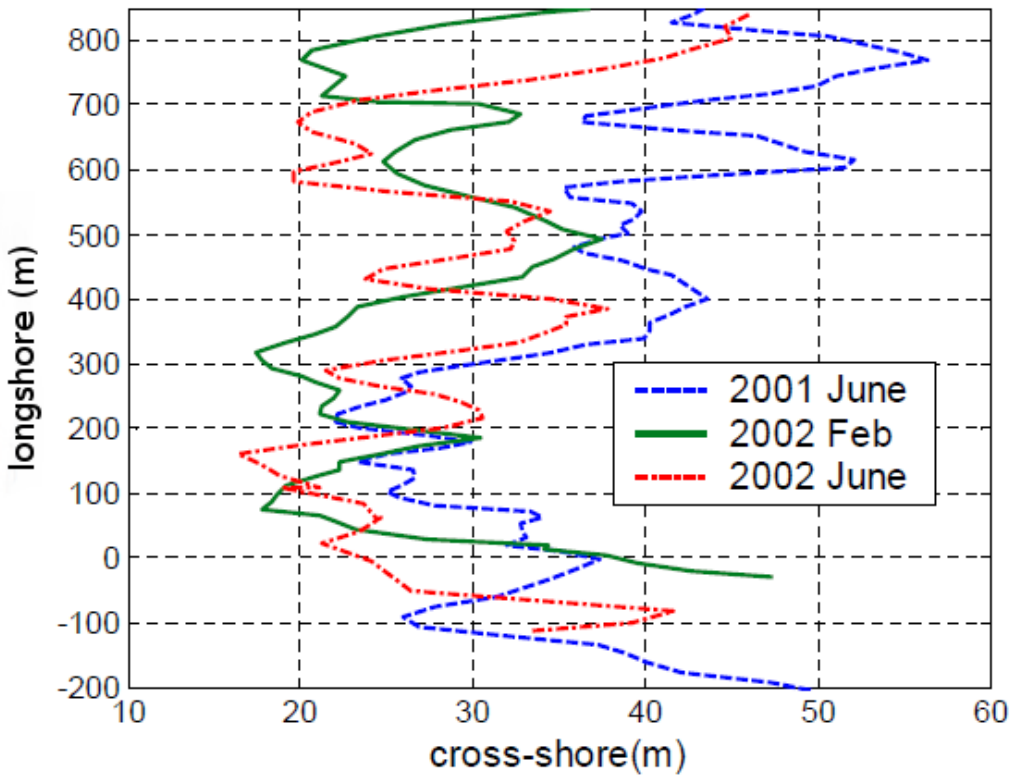

Figure 1.3. Shoreline position at Kilyos, June 2001, February 2002, and June 2002 [1].

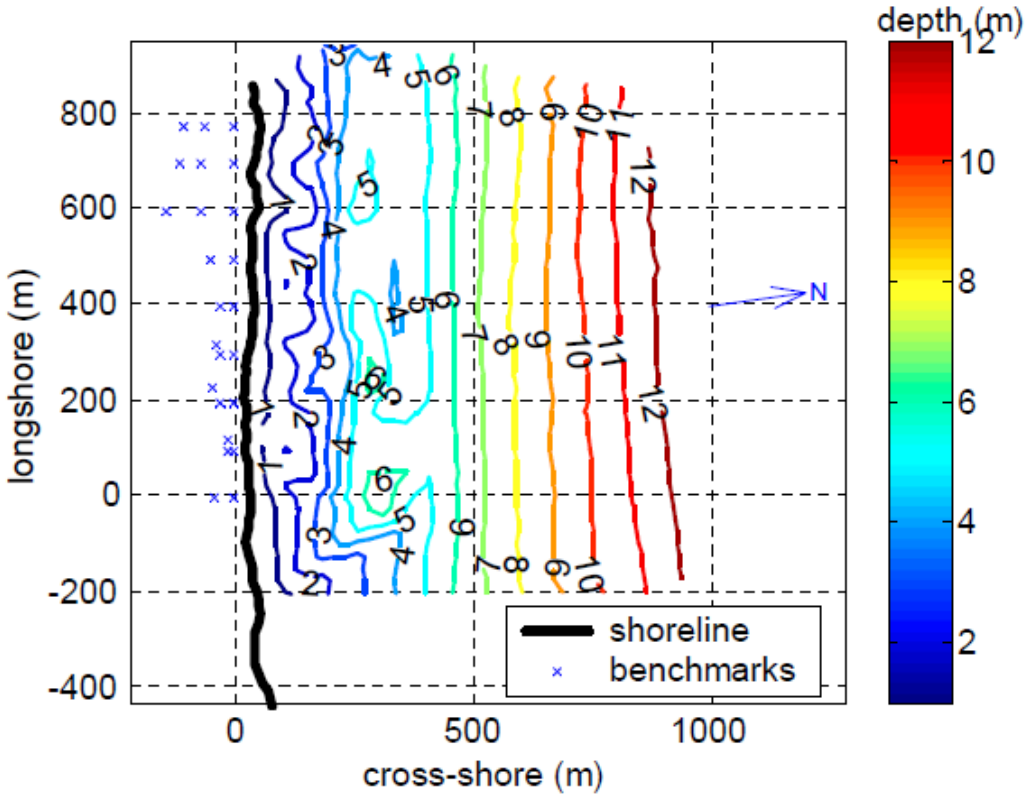

Figure 1.4. Bathymetry of Kilyos, June 2001 [1].

Interpolated results along profiles from the most landward benchmarks to the most seaward portion of the study were obtained from the Coastal Engineering Laboratory. Profile point distribution and plots of each of the profiles from 2001 and 2002 are found in Figures 1.5 and 1.6-1.14, respectively.

Figure 1.5. Profile point distribution [1].

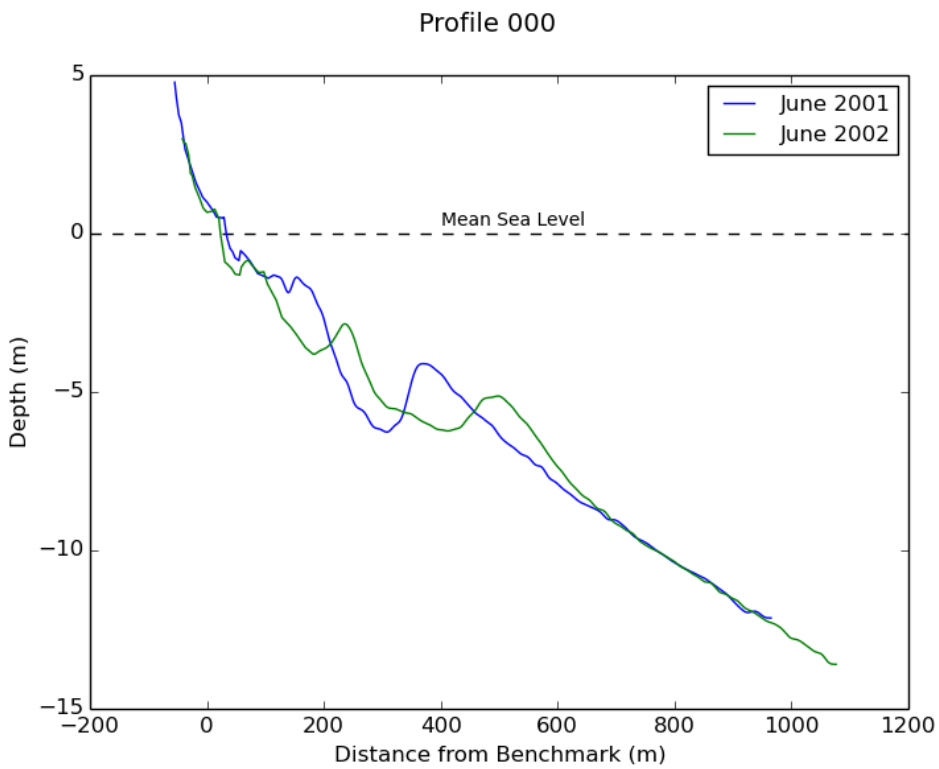

Figure 1.6. Profile 000, June 2001 and June 2002 [1].

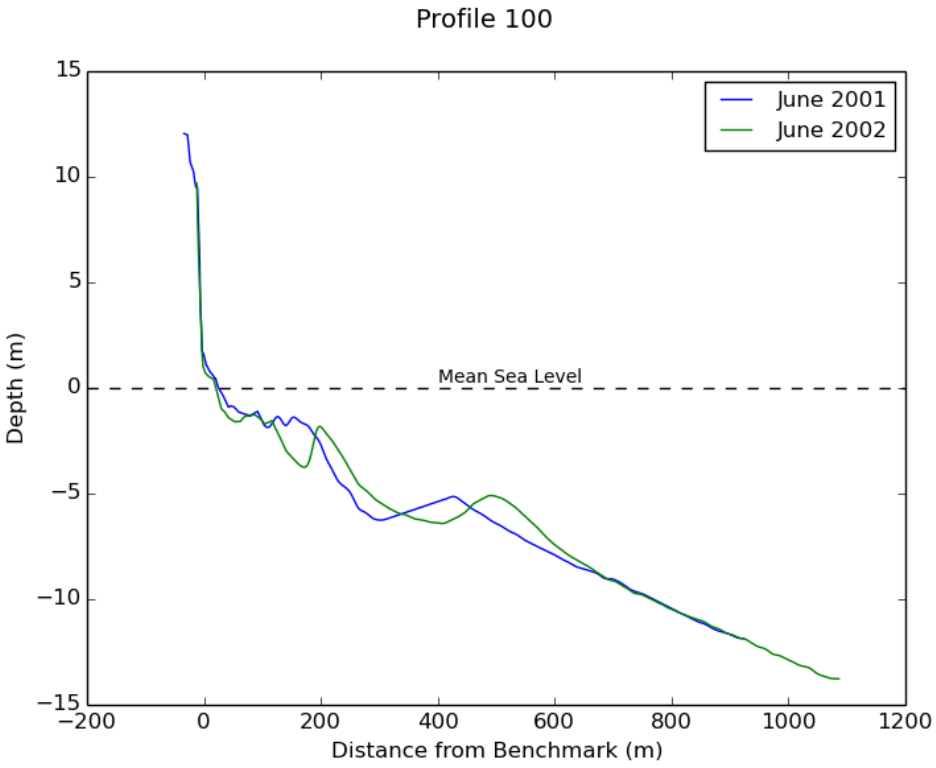

Figure 1.7. Profile 100, June 2001 and June 2002 [1].

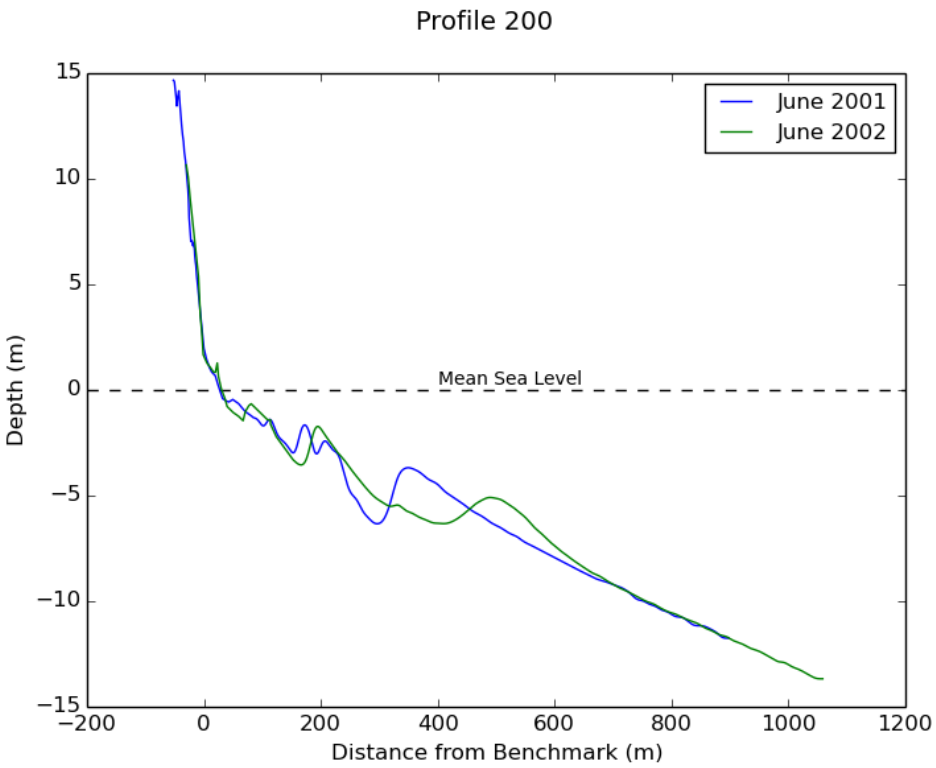

Figure 1.8. Profile 200, June 2001 and June 2002 [1].

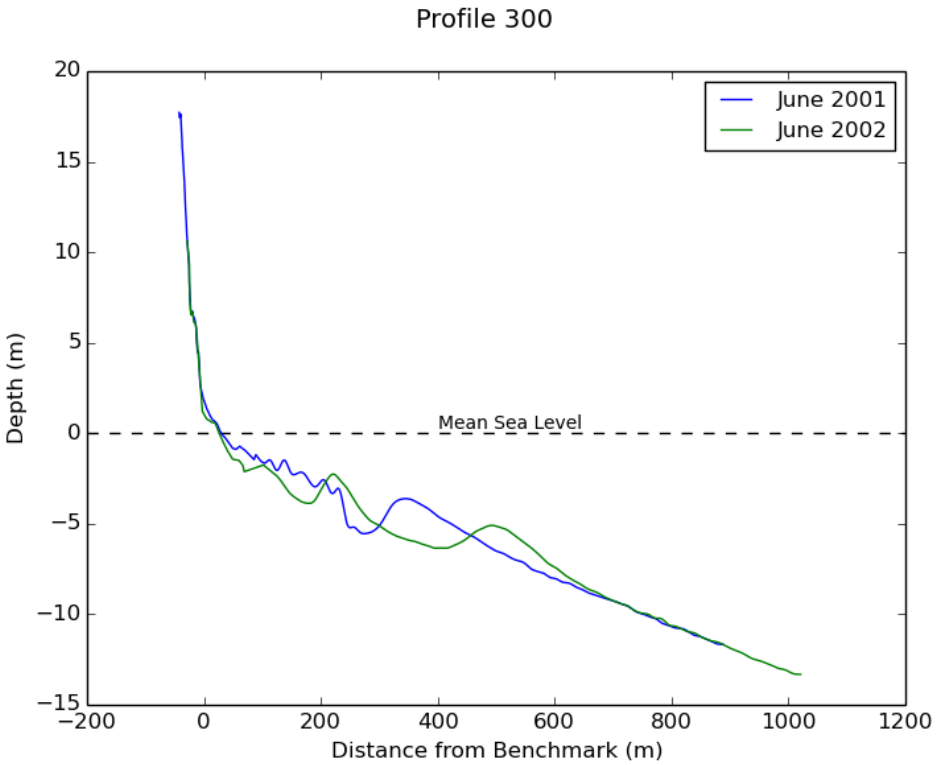

Figure 1.9. Profile 300, June 2001 and June 2002 [1].

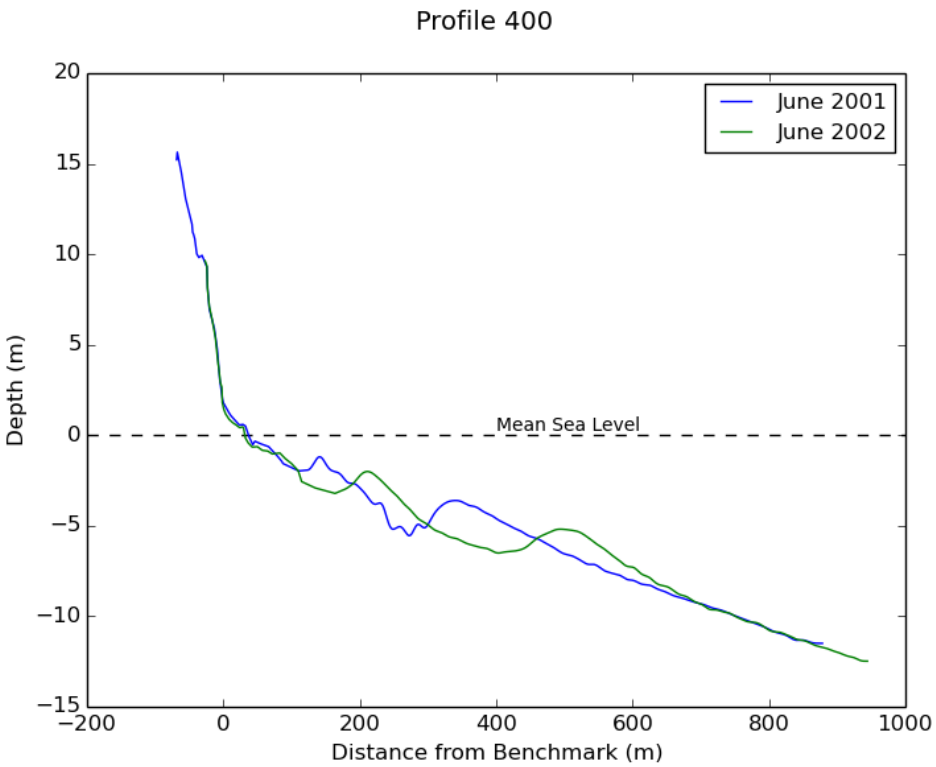

Figure 1.10. Profile 400, June 2001 and June 2002 [1].

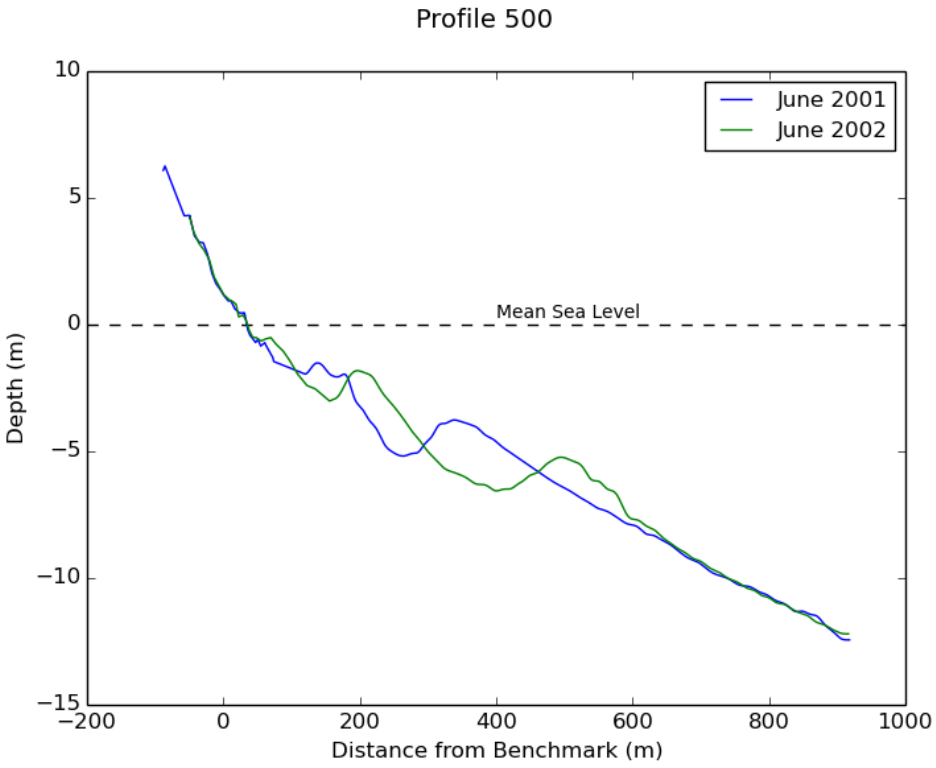

Figure 1.11. Profile 500, June 2001 and June 2002 [1].

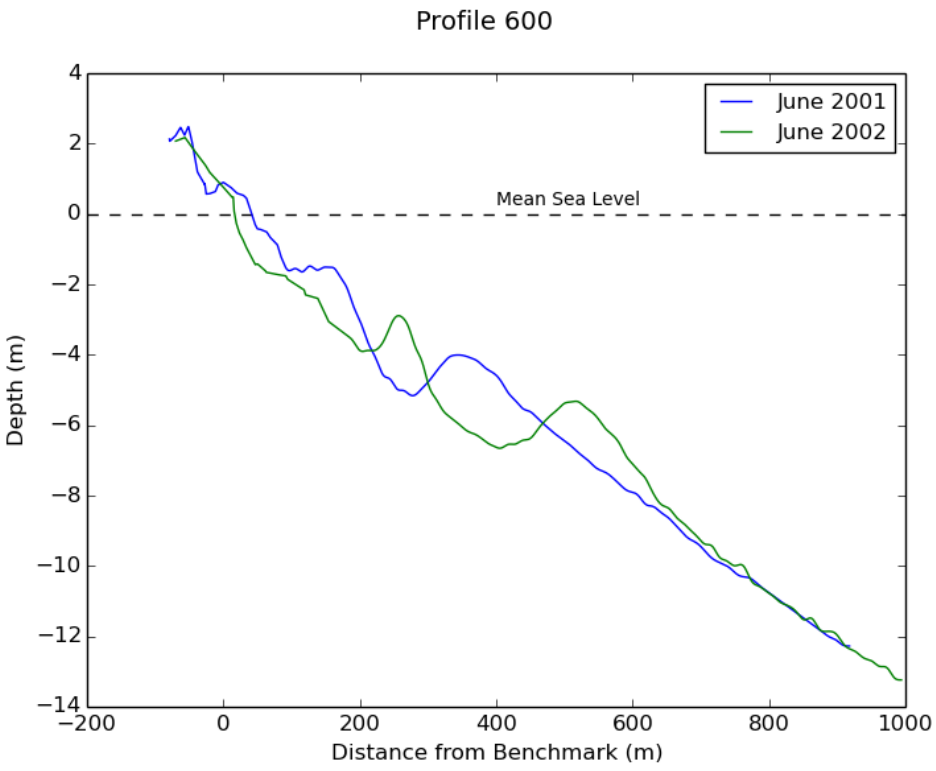

Figure 1.12. Profile 600, June 2001 and June 2002 [1].

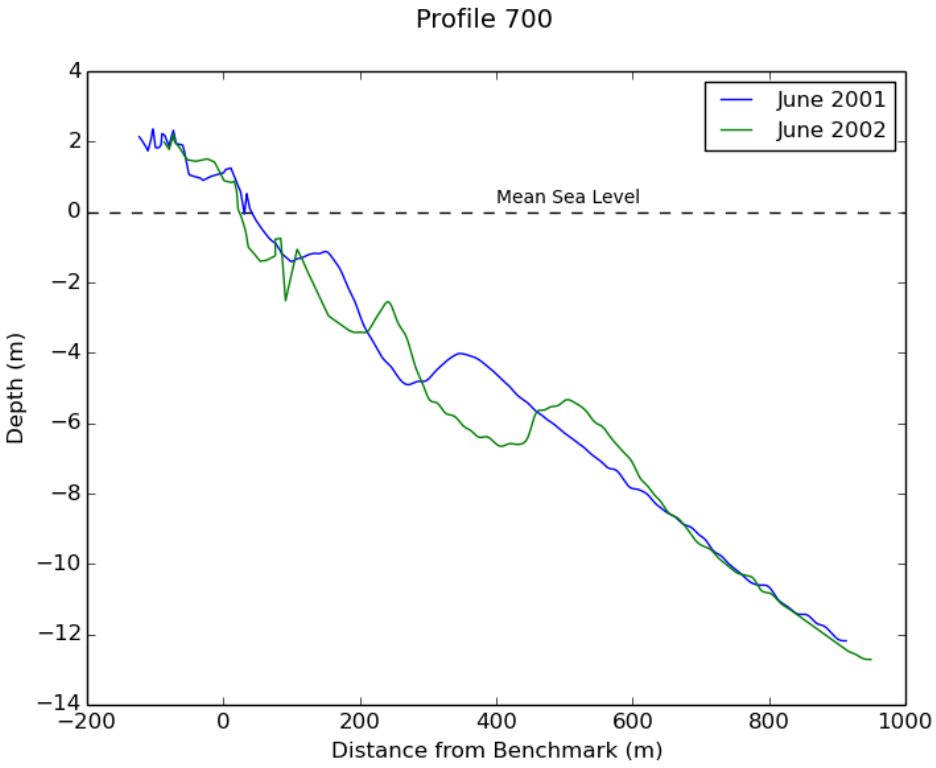

Figure 1.13. Profile 700, June 2001 and June 2002 [1].

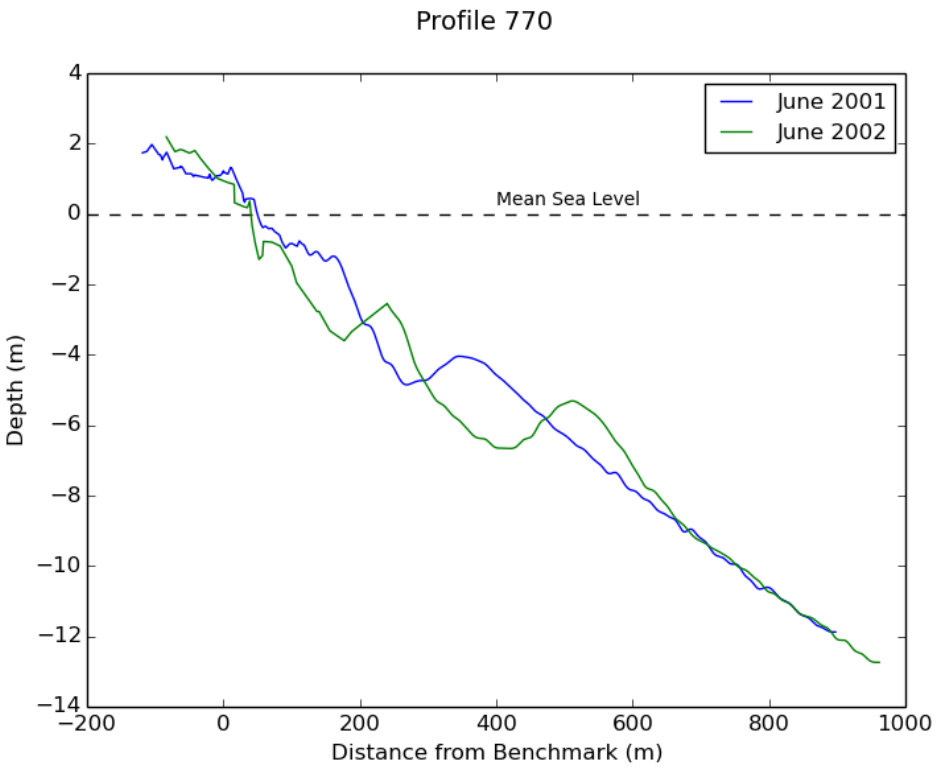

Figure 1.14. Profile 770, June 2001 and June 2002 [1].

Another 2002 study on the effects of dredge holes on the coastline was conducted in the same location as the survey area in the present study [31] [32]. In addition to reporting the findings from the study mentioned above, it was noted that further studies are needed to determine whether shoreline changes in the area are seasonal or can be attributed to long-term trends.

2. EXPERIMENTS AND RESULTS

2.1. Methodology

2.1.1. General Parameters of Study

One kilometer of the Black Sea coast in Kilyos, Turkey was used as the alongshore boundary of the study area in accordance with the location of the 2001 and 2002 surveys. Kilyos is located in northwestern Turkey approximately 50 km west of the mouth of the Bosphorous Strait. The study area lies to the north of Boğaziçi University's Sarıtepe Campus.

Surveys were conducted in September 2016 and March 2017 as initiatives of this study carried out by the Geodesy Department and Coastal Engineering Laboratory of Boğaziçi University. In December 2015, a similar survey was conducted by Boğaziçi University's Coastal Engineering Laboratory. Though less details are available for that survey, the results are included in the comparison.

2.1.2. GNSS Positioning

For the December 2015 and September 2016 surveys, the base station of the Topcon Hiper V Dual-Frequency RTK GNSS system was set up over a point with ITRF96/TM30 coordinates of 417307.916 m E, 4568276.98 m N and an elevation of 8.665 m. The elevation value was obtained in a previous survey according to the shoreline at the time. An explanation of the reduction of observed heights is found below.

For the March 2017 survey, the base was set up over concrete benchmark 5003 installed in 2001 for the 2001 and 2002 surveys. The location of this point as obtained in the 2001 survey was entered into the system as the base location: 417124.061 E and 4568275.965 N with an elevation of 54.362 m relative to the WGS 84 ellipsoid. During

each survey, the height of the base was measured with a metal measuring tape and entered into the system.

Figure 2.1. Base GNSS receiver, March 24, 2017 (preparation survey).

The radio-linked rover receiver was used in both the bathymetry and shoreline surveys. Topcon reports the horizontal and vertical accuracies of RTK surveys completed with their HiPer V receivers as 10 mm + 1 ppm and 15 mm + 1 ppm, respectively. Further accuracy details are found in the section titled *Accuracy of Observations*

2.1.3. Survey Conditions

Days with calm wind and waves were chosen for each of the surveys. Dates, times, and mean 10-m wind velocity during each of the surveys are found in Table 2.1. Wind data was collected through the wind turbine associated with the Wind Power Plant Project at Boğaziçi University's Sarıtepe Campus.

Table 2.1. Start and End Times of Bathymetry Surveys.

	Start Time	**End Time**	**Mean Wind Vel. (m/s)**
Dec 7, 2015	10:41 am	1:40 pm	2
Sept 29, 2016	11:15 am	1:30 pm	2.79
Mar 25, 2017 am	10:52 am	1:00 pm	3.34
Mar 25, 2017 pm	3:38 pm	5:46 pm	3.19
Mar 28, 2017	11:30 pm	6:00 pm	2.39

2.1.4. Bathymetric Surveys

The bathymetry surveys were carried out from a Zodiac Rigid Inflatable Boat equipped with the above-mentioned GNSS receiver secured at the top of a pole and an AirMar P66 echo sounder fixed at the opposite end of the same pole below the surface of the water. The offset between the GNSS antenna phase center and the surface of the water as well as that between the surface of the water and the transducer were measured with a metal tape measure during each survey. Offset values are listed in Table 2.2. Boat speed during all surveys was kept below 6 knots, approximately 3 m/s. Two bathymetry surveys were conducted on March 25, 2017 as the desired route was not followed closely enough during the first survey. Though the data from the two surveys was combined and processed as a single survey, when necessary, these surveys are referred to as the *March 2017 morning survey* and the *March 2017 afternoon survey*.

The single-beam echo sounder with a 200 kHz transducer frequency and an 11 degree beam width had been modified to achieve a pulsing rate of 5 Hz. The depth

Figure 2.2. Survey boat with pole for GNSS receiver and echo sounder, Aug 22, 2016 (preparation survey).

Table 2.2. Offsets from Surface of Water (m).

	Transducer to Surface	**Surface to GNSS Receiver**
Dec 2015	0.32	1.6
Sept 2016	0.38	1.54
Mar 2017 am	0.27	1.59
Mar 2017 pm	0.35	1.51

range is listed as 65 m in the log files, and the manufacturer reports a vertical accuracy of 2.5 cm. Though it is intended to be mounted to the transom, a reinforcing beam at the stern of a boat, mounting the echo sounder at the opposite end of the pole holding the GNSS receiver simplified calculations.

A Windows field computer was used for data collection and navigation using Kordil Navigation Pro. The GNSS receiver and transducer offsets mentioned above were entered into the program prior to data collection. The system was closely monitored for battery issues and GNSS disconnections.

Since the 2001 and 2002 surveys went to maximum depths of nearly 12.5 m and 14 m respectively, 14 m in depth was originally targeted as the seaward boundary of the study area. Additionally, the depth of closure, the depth beyond which sediment transport is negligible or non-existent, is estimated to be 12 m over one year and 26 m over ten years [31]. Both the morning and afternoon surveys in March 2017 and the December 2015 survey reached depths of at least 14 m. During the September 2016 survey, however due to concerns regarding battery life, maximum depths of 10 m were reached on all transects, and 12 m was reached along two of those transects.

Additionally, during the September 2016 and March 2017 morning survey a Conductivity-Temperature-Depth (CTD) device was used every 5 m in depth along a transect longer in length than the other transects. Further details are discussed in the section titled *Data Processing*.

2.1.4.1. Additional Observations during March 2017 Bathymetric Surveys. At the outset of the March 2017 morning survey, a sonar bar check was completed using a 5 m rod at depths of 1-4 m. A mean of 0.04 m was obtained from absolute values of the differences in each of 15 locations.

Table 2.3. March 2017 Sonar Bar Check Results.

	Sonar Depth (m)	**Bar Depth (m)**	**Difference (m)**
1	1.65	1.68	0.03
2	1.6	1.58	0.02
3	1.6	1.68	0.08
4	1.59	1.68	0.09
5	2.77	2.79	0.02
6	2.65	2.69	0.04
7	2.6	2.59	0.01
8	3.45	3.49	0.04
9	3.35	3.39	0.04
10	3.4	3.39	0.01
11	3.4	3.39	0.01
12	4.15	4.2	0.05
13	4.11	4.1	0.01
14	4.1	4	0.1
15	4.15	4.2	0.05

Sea level was also recorded from shore every 15 minutes during the March 2017 surveys. Table 2.4 shows minimum, maximum, and mean sea level for each survey with respect to the WGS 84 ellipsoid.

Table 2.4. March 25, 2017 Sea Level During Bathymetry Surveys.

	Min (m)	**Max (m)**	**Mean (m)**
Morning	36.57	36.64	36.61
Afternoon	36.59	36.63	36.61

Figure 2.3. View of the shore from the survey boat (Sept 29, 2016).

Figure 2.4. Point distribution from September 2016 survey, 26,360 usable data points.

Figure 2.5. Point distribution from March 2017 survey, 13,347 usable data points.

Figure 2.6. Point distribution from December 2015 survey, 54,726 usable data points.

2.1.5. Shoreline Surveys

As mentioned above, the same GNSS base and rover receivers were used for both the bathymetry and shoreline surveys. With the GNSS antenna on the land survey rod, the height shown on the rod was entered into the data collector.

2.1.5.1. September 2016 Shoreline Survey. The September 2016 shoreline survey was conducted between 4:00 and 6:00 pm on September 29.

The High Water Line (HWL) was used as a shoreline indicator so that the positions of the limits of run-up at the time of the survey were recorded as the shoreline. Positions were recorded every 20-30 m over a distance of approximately 800 m along the southern boundary of the bathymetry survey. After measuring HWL, two more

alongshore lines further seaward and one further inland were surveyed with the same approximate interval between points. The mean ellipsoidal height values of each of those survey lines as well as the mean value of the surface of the sea from the bathymetry survey are found in Table 2.7.

2.1.5.2. March 2017 Shoreline Survey. The March 2017 shoreline surveys were conducted between 6:15 and 8:00 pm on March 25 and between 4:15 and 5:00 pm on March 28.

Every 10-12 m in the alongshore direction, observations were made at run-up, run-down and one point 1-2 m seaward of run-down.

Approximately 80% of the shoreline survey was completed after the bathymetry surveys on the evening of March 25. Due to lack of daylight that evening, the remaining portion was completed on March 28 after the profile survey.

2.1.5.3. December 2015 Shoreline Survey. The December 2015 shoreline survey was conducted in a manner similar to the September 2016 survey, however aside from the data itself, no further details on its collection are available.

2.1.6. Profile Survey

The cross-shore transects surveyed in 2001 and 2002 were surveyed on March 28, 2017. Along each transect, the two to three benchmarks used in the original surveys were measured. Flags were placed at the two most landward benchmarks so the transect line could be followed to the shoreline and beyond to a depth of one meter.

Figure 2.7. Locations of points collected along transects March 28, 2017.

Figure 2.8 summarizes available data and methods employed during each of the surveys considered in this study.

	June 2001	Jan 2002	June 2002	Dec 2015	Sep 2016	Mar 2017
AVAILABLE DATA						
x-y (GPS)						
z (GPS, ellipsoidal heights)						
Sonar Depths						
Topographic Survey						
Wading Survey		?				
CTD Data						
Water line (GPS and/or Total Station)	Both			Measured only at run-up	Measured only at run-up	GNSS
Sea Level Measurements during Survey						
ACTION TAKEN						
Use of benchmarks						
Bar check for sonar						

data available and/or action taken
action may have been taken but no data in hand
data unavailable and/or action not taken

Figure 2.8. Summary of available data and methods employed during surveys.

2.1.7. Future Adjustments to Methodology

For future similar surveys at the study area, the following recommendations can be made. Many of the items below were carried out during one but not all of the surveys.

- All bathymetry surveys should be performed to a minimum depth of 14 meters.
- A topography study should be done in conjunction with each bathymetry survey.

Benchmarks from 2001 as well as the most landward portions of the 2001 profiles should be included.

- Sea level should be measured from shore every 15 minutes during each bathymetry and shoreline survey.
- Permanent benchmarks should be measured at each survey.
- A bar check should be performed during each bathymetry survey.
- A separate GPS/GNSS receiver should be used for boat navigation. While boat routes were loaded into the field computer for the March 2017 bathymetry surveys, they were not available while using the navigation and data collection application. As a backup, Google Maps was used on a smartphone, but eventually access to the map was lost. Inability to follow the desired boat route leads to greater reliance on interpolated data.

2.1.8. Data Processing

All data was collected using ITRF96/TM30 as a spatial reference, was output as geographic coordinates in WGS84 using Kordil Geodesy Tools, and transformed to ITRF96/TM30 in QGIS before processing.

2.1.8.1. Corrections for Local Velocity of Sound. The local velocity of sound in seawater can be obtained using salinity, temperature, and either depth or pressure. Since the exact values are unknown prior to the survey, an estimated value was entered to calculate depths in the field. Estimated values of 1,500 m/s, 1,515 m/s and 1,511 m/s were used in December 2015, September 2016, and March 2017, respectively.

During the September 2016 bathymetric survey, samples of the water's salinity, temperature, and pressure were collected at seven locations using a Conductivity-Temperature-Depth (CTD) instrument. Since the majority of the survey was conducted between depths of 1 m and 10 m, the values for the local velocity of sound at three locations with depths of 5-6 m were averaged to obtain a single value used for the entire survey. The UNESCO algorithm, the international standard for calculating

the velocity of sound in seawater, was chosen over the Del Grosso algorithm. Though the UNESCO algorithm is often preferred for deeper water, the salinity range of the Del Grosso algorithm is beyond that of the relatively low salinity of the Black Sea. Details on the UNESCO algorithm can be found in [33]. Table 2.5 displays the depths according to the SBES and the CTD, as well as the velocity of sound calculated using pressure, salinity, and temperature measured by the CTD.

Table 2.5. CTD Data for Calculation of Local Velocity of Sound for September 2016 survey.

	SBES(m)	**CTD(m)**	**P(dbar)**	**S(psu)**	**T(C)**	**Sound Vel.(m/s)**
CTD 467	5.81	5.75	6.38	17.23	21.91	1507.24
CTD 469	5.37	5.47	5.97	17.30	21.95	1507.43
CTD 472	5.98	5.85	6.28	10.95	21.99	1500.56

The mean of the three resulting values in Table 2.5 (1,505.08 m/s) was used as the local velocity of sound for the entire survey. Depths measured using the SBES were then adjusted for the difference between the entered sound velocity (1,515 m/s) and the sampled sound velocity using a calibration factor of 0.9934.

Measured depths were adjusted as follows where d_a represents adjusted depth and d_f represents depth acquired in the field:

$$d_a = 0.9934 d_f \tag{2.1}$$

CTD measurements for the March 2017 surveys resulted in a mean velocity of sound of approximately 1458 m/s. Since this value would adjust the depth values significantly beyond the error obtained from the bar check described above, a CTD

adjustment was not applied to the depths from those surveys. Due to the relatively low error obtained from the bar check, the velocity of 1,511 m/s selected prior to the survey was accepted for the March 2017 surveys.

CTD measurements were not included in the data use for the December 2015 survey. Since a choice had to be made between data that was adjusted for the local velocity of sound and data that included heights of the sea surface at collected points, the latter was preserved. Further explanation is found in the *Conversion of Depths to Ellipsoidal Heights* section.

2.1.8.2. Reduction of Heights. Elevations from the 2001 and 2002 surveys were reported with reference to the shoreline determined in the 2001 survey where the shoreline was considered to be at an elevation of zero. Horizontal locations were referred to the most landward temporary benchmark lying along each transect.

Though this local coordinate system was used in the 2001 and 2002 surveys, ellipsoidal heights for 33 shoreline points and two concrete benchmarks (benchmarks 5002 and 5003) were obtained during the June 2001 survey. Since the shoreline points were taken as zero elevation in the original surveys, the current study began by adding the mean of the ellipsoidal heights of these values (36.6435 m) to all 2001 and 2002 elevations. Excluding one shoreline point, P2_0020 in the list below, due to its extreme variation from the dataset, the mean was calculated as 36.6435 m. Horizontal coordinates were converted to ITRF96/TM30 using the distances from and angles between the above-mentioned temporary benchmarks and each point along the corresponding transects.

Figure 2.9. Shoreline and benchmark locations measured with GPS on June 14, 2001.

ID	Latitude (Global)	Longitude (Global)	Height (Global) (Meter)	Benchmark
P2_____	N41°14'43,25052"	E29°00'45,37979"	47,697	5002
P2__0001	N41°14'43,10127"	E29°01'13,10433"	36,531	
P2__0002	N41°14'43,28417"	E29°01'11,57730"	36,548	
P2__0003	N41°14'43,54151"	E29°01'10,19360"	36,508	
P2__0004	N41°14'43,35550"	E29°01'08,30203"	36,448	
P2__0005	N41°14'42,87137"	E29°01'05,91938"	36,680	
P2__0006	N41°14'43,17358"	E29°01'03,48397"	36,609	
P2__0007	N41°14'43,71508"	E29°01'01,31404"	36,473	
P2__0008	N41°14'43,81112"	E29°01'00,50121"	36,566	
P2__0009	N41°14'43,53193"	E29°00'58,64918"	36,547	
P2__0010	N41°14'43,35708"	E29°00'56,03582"	36,702	
P2__0011	N41°14'43,59566"	E29°00'54,20875"	36,569	
P2__0012	N41°14'44,03765"	E29°00'52,06069"	36,674	
P2__0013	N41°14'44,03922"	E29°00'51,74763"	36,667	
P2__0014	N41°14'44,26403"	E29°00'50,39473"	36,728	
P2__0015	N41°14'44,28499"	E29°00'48,76414"	36,782	
P2__0016	N41°14'44,39749"	E29°00'47,24027"	36,615	
P2__0017	N41°14'44,45400"	E29°00'45,31675"	36,514	
P2__0018	N41°14'44,83811"	E29°00'43,55502"	36,548	
P2__0019	N41°14'44,90325"	E29°00'41,23079"	36,587	
P2__0020	N41°14'45,49988"	E29°00'38,54611"	37,777	
P2__0021	N41°14'45,65072"	E29°00'37,99814"	36,606	
P2__0022	N41°14'46,12838"	E29°00'35,07945"	36,637	
P2__0023	N41°14'46,33741"	E29°00'33,37620"	36,495	
P2__0024	N41°14'46,64278"	E29°00'29,42182"	36,620	
P2__0025	N41°14'46,64354"	E29°00'29,42506"	36,610	
P2__0026	N41°14'46,91667"	E29°00'27,17308"	36,709	
P2__0027	N41°14'47,59431"	E29°00'23,82881"	36,652	
P2__0028	N41°14'48,00213"	E29°00'20,14953"	36,644	
P2__0029	N41°14'48,49995"	E29°00'17,22118"	36,519	
P2__0030	N41°14'48,41482"	E29°00'14,97506"	36,612	
P2__0031	N41°14'49,07144"	E29°00'11,47586"	36,593	
P2__0032	N41°14'49,89048"	E29°00'07,69480"	36,663	
P2__0033	N41°14'50,59175"	E29°00'03,91050"	36,803	
P3_____	N41°14'42,72728"	E29°00'40,68104"	54,362	5003

Figure 2.10. Coordinates of ellipsoidal heights from June 14, 2001 as received from Geodesy Department (Benchmark field added during current study).

Since the March 2017 survey was performed with the base GNSS receiver over benchmark 5003 with the coordinates obtained in 2001 entered into the system, elevations from that survey were referenced to the WGS84 ellipsoid.

The location of the base GNSS used in December 2015 and September 2016 was found to be 44.909 m above the WGS84 ellipsoid on May 18, 2017. After subtracting the original value of 8.665 m used as the location's elevation, the difference of 36.224 was added to all values to obtain ellipsoidal heights of all data.

2.1.8.3. Conversion of Depths to Ellipsoidal Heights. Included in the bathymetry data are ellipsoidal heights of the water surface at each point that positions and depths are observed. After subtracting the antenna height from the elevation observed by the GNSS receiver, height of the sea surface, or *RTK Tide* is found. Figure 2.11 shows a sample table for calculation of RTK Tide values.

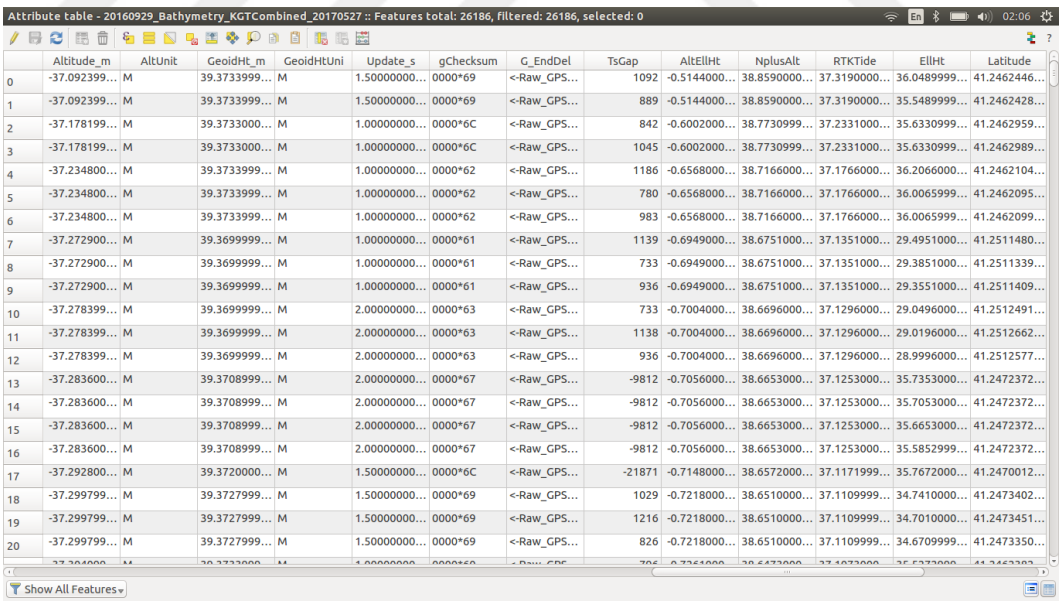

	Altitude_m	AltUnit	GeoidHt_m	GeoidHtUni	Update_s	gChecksum	G_EndDel	TsGap	AltEllHt	NplusAlt	RTKTide	EllHt	Latitude
0	-37.092399...	M	39.3733999...	M	1.50000000...	0000*69	<-Raw_GPS...	1092	-0.5144000...	38.8590000...	37.3190000...	36.0489999...	41.2462446...
1	-37.092399...	M	39.3733999...	M	1.50000000...	0000*69	<-Raw_GPS...	889	-0.5144000...	38.8590000...	37.3190000...	35.5489999...	41.2462428...
2	-37.178199...	M	39.3733000...	M	1.00000000...	0000*6C	<-Raw_GPS...	842	-0.6002000...	38.7730999...	37.2331000...	35.6330999...	41.2462959...
3	-37.178199...	M	39.3733000...	M	1.00000000...	0000*6C	<-Raw_GPS...	1045	-0.6002000...	38.7730999...	37.2331000...	35.6330999...	41.2462989...
4	-37.234800...	M	39.3733999...	M	1.00000000...	0000*62	<-Raw_GPS...	1186	-0.6568000...	38.7166000...	37.1766000...	36.2066000...	41.2462104...
5	-37.234800...	M	39.3733999...	M	1.00000000...	0000*62	<-Raw_GPS...	780	-0.6568000...	38.7166000...	37.1766000...	36.0065999...	41.2462095...
6	-37.234800...	M	39.3733999...	M	1.00000000...	0000*62	<-Raw_GPS...	983	-0.6568000...	38.7166000...	37.1766000...	36.0065999...	41.2462099...
7	-37.272900...	M	39.3699999...	M	1.00000000...	0000*61	<-Raw_GPS...	1139	-0.6949000...	38.6751000...	37.1351000...	29.4951000...	41.2511480...
8	-37.272900...	M	39.3699999...	M	1.00000000...	0000*61	<-Raw_GPS...	733	-0.6949000...	38.6751000...	37.1351000...	29.3851000...	41.2511339...
9	-37.272900...	M	39.3699999...	M	1.00000000...	0000*61	<-Raw_GPS...	936	-0.6949000...	38.6751000...	37.1351000...	29.3551000...	41.2511409...
10	-37.278399...	M	39.3699999...	M	2.00000000...	0000*63	<-Raw_GPS...	733	-0.7004000...	38.6696000...	37.1296000...	29.0496000...	41.2512491...
11	-37.278399...	M	39.3699999...	M	2.00000000...	0000*63	<-Raw_GPS...	1138	-0.7004000...	38.6696000...	37.1296000...	29.0196000...	41.2512662...
12	-37.278399...	M	39.3699999...	M	2.00000000...	0000*63	<-Raw_GPS...	936	-0.7004000...	38.6696000...	37.1296000...	28.9996000...	41.2512577...
13	-37.283600...	M	39.3708999...	M	2.00000000...	0000*67	<-Raw_GPS...	-9812	-0.7056000...	38.6653000...	37.1253000...	35.7353000...	41.2472372...
14	-37.283600...	M	39.3708999...	M	2.00000000...	0000*67	<-Raw_GPS...	-9812	-0.7056000...	38.6653000...	37.1253000...	35.7053000...	41.2472372...
15	-37.283600...	M	39.3708999...	M	2.00000000...	0000*67	<-Raw_GPS...	-9812	-0.7056000...	38.6653000...	37.1253000...	35.6653000...	41.2472372...
16	-37.283600...	M	39.3708999...	M	2.00000000...	0000*67	<-Raw_GPS...	-9812	-0.7056000...	38.6653000...	37.1253000...	35.5852999...	41.2472372...
17	-37.292800...	M	39.3720000...	M	1.50000000...	0000*6C	<-Raw_GPS...	-21871	-0.7148000...	38.6572000...	37.1171999...	35.7672000...	41.2470012...
18	-37.299799...	M	39.3727999...	M	1.50000000...	0000*69	<-Raw_GPS...	1029	-0.7218000...	38.6510000...	37.1109999...	34.7410000...	41.2473402...
19	-37.299799...	M	39.3727999...	M	1.50000000...	0000*69	<-Raw_GPS...	1216	-0.7218000...	38.6510000...	37.1109999...	34.7010000...	41.2473451...
20	-37.299799...	M	39.3727999...	M	1.50000000...	0000*69	<-Raw_GPS...	826	-0.7218000...	38.6510000...	37.1109999...	34.6709999...	41.2473350...

Figure 2.11. Calculation of RTK Tides for September 2016 Bathymetry.

As explained above,

$$h = H + N \tag{2.2}$$

where: h = ellipsoidal height, H = orthometric height (referenced to MSL), N = geoid separation, the distance between the ellipsoid and the geoid.

In Figure 2.11, the fields titled *Altitude_m* and *GeoidHt_m* are found in the NMEA message for the GNSS receiver and refer to orthometric height and geoid separation, respectively. If heights in a given survey were not referenced to the ellipsoid, i.e. December 2015 or September 2016 surveys, the 36.244-m difference between the MSL-referenced base elevation and the ellipsoidal height of that base location, must be added to the orthometric height. The result is found in the *AltEllHt* field above. After adding the geoid height N (*NPlusAlt* field above) and subtracting the antenna height, the RTK Tide values are obtained. Seafloor ellipsoidal heights are obtained by subtracting the depths (field not shown) from the RTK Tide values. Further details on this method of surveying can be found in [34].

Table 2.6. RTK Tide Statistics, all values are given in meters. Minimum, maximum, and mean values are ellipsoidal heights.

	Min	**Max**	**Mean**	**Std. Dev.**
Dec 2015	35.78	36.71	36.33	0.06
Sept 2016	36	37.32	36.85	0.075
Mar 2017	36.29	36.87	36.53	0.07

The asterisks (*) denote mean of High Water Line observations as opposed to the mean of all observations for both runup and rundown.

When sufficient RTK Tide data is available, the observed value for sea level during a survey serves as a check rather than an essential value used to determine elevations

Table 2.7. Comparison of mean values for sea level, ellipsoidal heights in meters.

	Observed	**GNSS Shoreline**	**Estimated**	**RTK Tide**
Dec 7, 2015	Not Observed	37.12*	36.93	36.33
Sept 29, 2016	Not Observed	36.83*	36.65	36.85
Mar 25, 2017	36.61	36.64	NA	36.53
Mar 28, 2017	36.52	36.56	NA	36.53

of the seafloor from depths.

In one case in this study however, the data that was output with RTK tide data did not produce expected results. The original plots of the September 2016 data showed significant variation from the 2001 data at the most seaward portions of the survey where sediment transport is known to be negligible. For this reason, the data was reprocessed with Kordil Geodesy Tools using a different method. The output of this method includes only horizontal coordinates and elevations, and the input requires a value for *Tide Height* or local sea level. Since sea level was not observed during that survey, it had to be estimated from values available from the set of surveys.

In Table 2.7, *GNSS Shoreline* represents the mean of GNSS-observed elevations at both runup and rundown. Using differences between this value and GNSS HWL (runup only), the same differences were estimated for December 2015 and September 2016 and adjusted proportionally according to mean wind velocity. Those values were subtracted from the *GNSS HWL* value to obtain an estimate for *GNSS Shoreline*. According to the differences between observed *GNSS Shoreline* and observed sea level in the March surveys, 0.03 m was then subtracted from the estimated GNSS Shoreline to get estimates for sea level in the December 2015 and September 2016 surveys.

In the 2001 and 2002 surveys, GPS equipment was used for horizontal positions during the bathymetry survey, but since no GPS data was collected for vertical positions, elevations at the sea surface are not available. As described above, the 2001 and

Table 2.8. Variables for estimation of sea level. All values are mean values or estimates for mean values. Asterisks denote estimated values.

	3.25.17	**3.28.17**	**9.29.2016**	**12.7.2015**
Observed Sea Level (m)	36.61	36.52	NA	NA
Est. Sea Level (m)	NA	NA	36.65*	36.93*
Wind Velocity (m/s)	3.29	2.39	2.79	2
GNSS HWL (m)	36.781	36.713	36.83	37.115
GNSS Shoreline (m)	36.639	36.556	–	–
Est. GNSS Shoreline (m)	NA	NA	36.68*	36.96*
HWL minus Shoreline (m)	0.142	0.157	–	–
Est. HWL minus Shoreline (m)	NA	NA	0.15*	0.16*

2002 data were converted from the original local vertical datum to ellipsoidal heights using the mean of the shoreline points for which ellipsoidal height values were measured. When the single value of 36.224 m is added to the elevation values from 2001 and 2002, they are considered to be referenced to ellipsoidal heights.

2.1.8.4. Correction for Heave, Tides, Wind and Wave Setup. A vessel at sea experiences heave, or vertical movement resulting from swell, waves, currents, and the wake of other boats. The multiple sources resulting in heave are random in terms of period and amplitude thus introducing errors in measurements that are generally difficult to detect and remove.

A nearshore survey must also account for tides caused by the gravitational effects of the Moon on the Earth. Since the Black Sea is isolated from oceans by multiple straits, tidal effects in the survey area are quite low. Magnitudes of local tides are estimated at 3-5 cm [31].

Nearshore mean water levels also undergo variation due to both wind stresses

over the surface of the water and to the presence of breaking waves. Although no long-term wave measurements are available for the survey area, statistical data based on hindcast models is available from the two projects. According to both models, waves predominantly propagate from the northeast across the survey area with a mean significant wave height of 1.0 m and mean period of 5.2 s [31].

Vertical variations due to tide, heave, wind and wave setup, as well as dynamic draft, and loading are inherently addressed in an RTK survey in that both the GNSS antenna and the transducer undergo the same vertical movements. When either observed or adjusted depths are subtracted from ellipsoidal heights at the surface of the water, any variation due to the factors listed above is removed [34].

2.1.8.5. Intentional Horizontal Shift of Data. While benchmark 5003 was used as the location for the base GNSS receiver during the March 2017 surveys, the concrete benchmarks themselves were measured in May 2017. Measurement of 5003 was conducted with the base GNSS receiver set up over benchmark 5002. Coordinates obtained for 5002 in 2001 were input into the system. Benchmark 5002 was measured in the same way with the base set up over 5003.

Table 2.9 shows differences between the coordinates obtained in 2001 and those obtained in 2017.

Table 2.9. Differences between 2017 and 2001 measurements of benchmarks (2017 values minus 2001 values).

	X (m)	**Y (m)**	**Z (m)**
5002	0.022816	0.059977	-0.044
5003	-0.007565	-0.065001	0.023667

Uncertainty values for the 2001 measurement of the benchmarks as provided by the Geodesy Department are found in Table 2.10.

Table 2.10. Horizontal error values of 2001 measurement of benchmarks.

	Easting Error (m)	**Northing Error (m)**
5001	0.004	0.006
5002	0.007	0.008
5003	0.004	-0.005

The 6-cm difference in opposite directions (north-south) over 16 years was of particular interest. Figure 2.12 shows the possible scenarios that explain the difference. While every survey has its own associated error, the term *match* is used, in this case, to refer to a match on the order of millimeters while *non-match* refers to a difference on the order of a few centimeters.

Case 1	**5002**	**5003**
2001	Match	Match
2017	Non-match	Non-match

Case 2	**5002**	**5003**
2001	Match	Non-match
2017	Non-match	Match

Case 3	**5002**	**5003**
2001	Non-match	Match
2017	Match	Non-match

Case 4	**5002**	**5003**
2001	Non-match	Non-match
2017	Match	Match

Figure 2.12. Possible explanations for discrepancy between 2001 and 2017 benchmark observations.

Since Case 1 and Case 4 involve both benchmarks not matching in a single survey, and since an error in a single survey would shift all points in the same direction, these two cases were eliminated. Both Cases 2 and 3 are possible, but a determination as to which of them explains the reality is not possible. Correcting the error in both cases would mean shifting the data to the south and west of the original coordinates. This shift was made to reduce the horizontal uncertainty from this source from a possible 6 cm to a definite 3 cm.

The following values were added to each of the coordinates:

X: -0.0037826 Y: -0.03250575

2.1.8.6. Interpolation. Interpolation was performed using the GRASS GIS *Bicubic Spline Interpolation* tool in a QGIS environment.

For each of the surveys, all available observations for each period were combined into one shapefile which was input into the tool. For each dataset, grid cell size was set to 0.1 m with a spline step of 4 and a Tykhonov regularization parameter of 0.1. A screen shot of parameters is found in Figure 2.13.

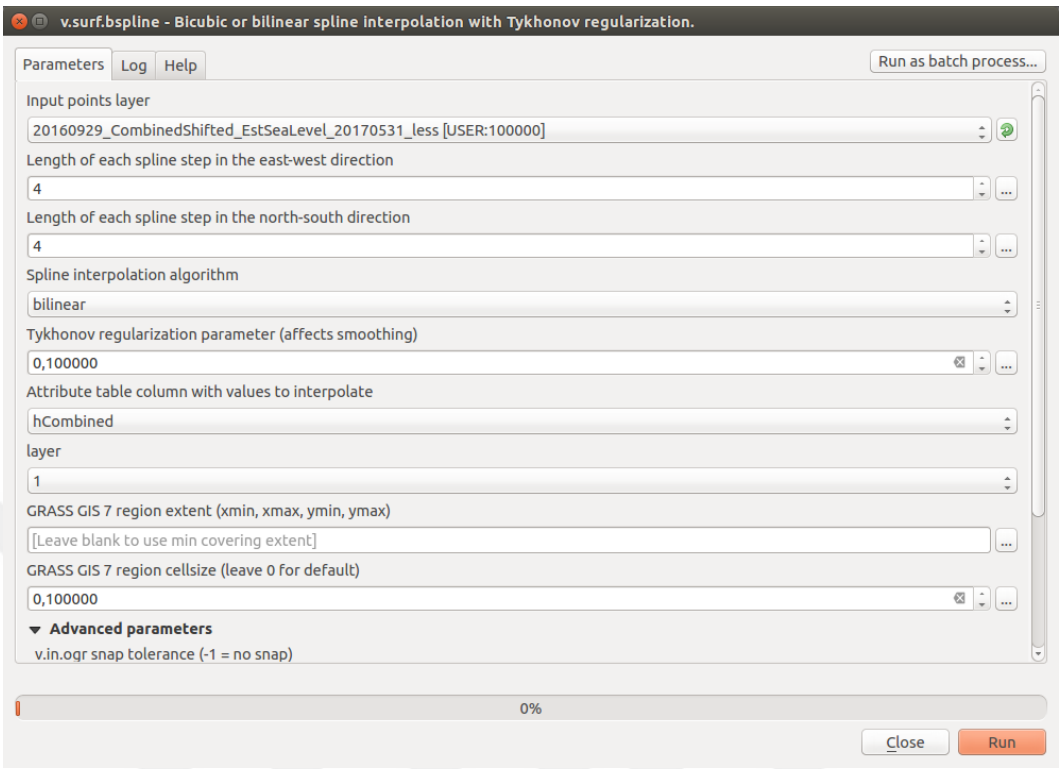

Figure 2.13. Bicubic Spline Parameters.

Using the QGIS *Point Sampling Tool*, interpolated values were then extracted to the profile points used to report the results from the 2001 survey.

A separate interpolation was also performed in order to use depth rather than distance as the variable of integration when analyzing the results. In order to minimize the error introduced by this process, distance values were interpolated at every 0.0001 m of elevation. Figure 2.14 shows plots of the interpolated and original data for a sample profile.

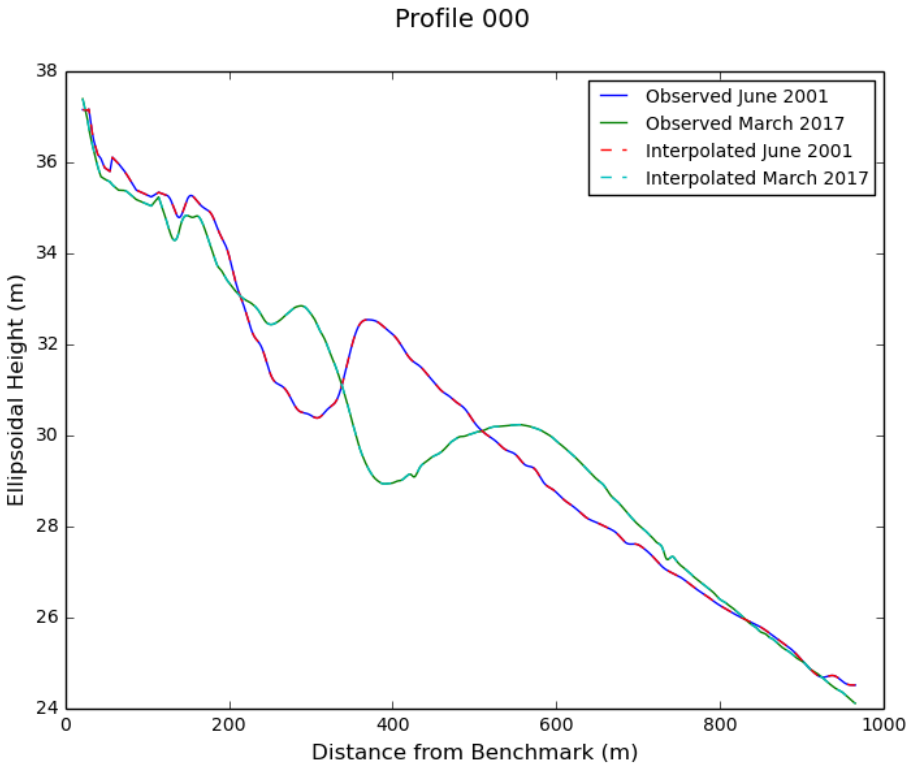

Figure 2.14. Comparison of original and interpolated plots of sample June 2001 and March 2017 data.

2.1.9. Accuracy of Observations

In addition to the horizontal and vertical uncertainty associated with the GNSS equipment and the echo sounder, the accuracy of the entire survey can be estimated by considering the sources of error listed above and remaining factors for which corrections have not been made.

As mentioned above, Topcon reports the horizontal and vertical accuracies of RTK surveys conducted with their HiPer V receivers as 10 mm + 1 ppm and 15 mm + 1 ppm, respectively. Since the rover receiver was never more than 1200 m from the base receiver, these values can be assumed to be 0.115 cm and 0.165 cm, respectively.

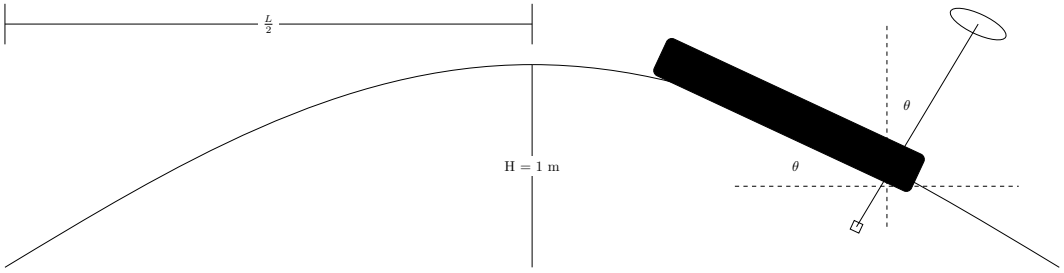

Figure 2.15. Maximum angle (θ) of GNSS antenna displacement caused by pitch.

Airmar reports the vertical accuracy of their P66 echo sounder as 2.5 cm.

Since an inertial measurement unit (IMU) was not used during the survey, maximum values for pitch and roll were estimated using the local values for mean wave height (1 m) and mean wave period (5.2 s).

The equation for wave length in deep waters (where water depth is greater than half of the wavelength) is given below:

$$L_o = \frac{gT^2}{2\pi} \tag{2.3}$$

where g is the acceleration due to gravity and T is period.

The local mean wave period of 5.2 s results in a deep-water wave length of approximately 42.2 m.

The maximum angle between the pitching boat and the flat surface of the sea was found. The sine of that angle was then multiplied by the distance between the GNSS antenna and the surface of the water to obtain the horizontal error. The magnitude of vertical error was found by multiplying the GNSS antenna height by the cosine of the angle produced by the pitching boat.

The equation for wavelength in intermediate and shallow waters is given below:

$$L = L_o \sqrt{\tanh 2\pi \frac{h}{L_o}} \tag{2.4}$$

where L_o is deep-water wavelength and h is water depth.

The maximum displacement of the antenna due to pitch is given as:

$$\theta = \arctan \frac{H}{0.5L} \tag{2.5}$$

where H is the mean wave height.

Table 2.11. Maximum error values due to pitch.

	Depth (m)	**Horizontal (cm)**	**Vertical (cm)**
1	Min (0.69)	28.18	2.08
2	Max (12.94)	9.3	0.22

Although the survey boat experiences relatively minimal roll due to its design, wave-induced roll does occur. While maximum uncertainty due to roll should be less than that of pitch, in the absence of estimated uncertainty values for roll, the greatest pitch uncertainty values are multiplied by a factor of two.

Considering all sources of uncertainty, total horizontal and vertical uncertainty associated with the observed data are under 0.6 m and 0.1 m respectively.

Table 2.12. Total Error/Uncertainty.

	Source	Horizontal (cm)	Vertical (cm)
1	GNSS	0.115	0.165
2	Echo sounder	NA	2.5
3	Pitch	28.18	2.08
4	Roll	28.18	2.08
5	Intentional Shift	3	NA
6	Total	<60	<7

While the horizontal uncertainty could have been decreased with the use of an IMU, the uncertainty values are well within the IHO Standards for the most rigorous survey classification. The *Special Order* classification requires a 2 m THU and a TVU of 0.25-0.27 m (calculated by substituting the minimum and maximum depths in formula (1.1))

TPU can be conservatively estimated by summing the THU and TPU, resulting in 0.7 m [15].

While an effort was made to minimize error associated with interpolated data, an estimate of uncertainty after interpolating the collected data was not calculated.

2.2. Results

The June 2001 data was used as a reference to determine change along the profiles in each of the surveys from the last few years.

2.2.1. Shoreline Change

In order to compare the shoreline location between the surveys, a single ellipsoidal height near the shoreline was selected, and corresponding horizontal coordinates of

surveys were compared. Selection of this common shoreline ellipsoidal height value began with the mean value of all water level values (36.63 m) observed at all surveys and transects (Table 2.13). The value was then adjusted to ensure that all profiles from all considered surveys would have horizontal coordinates available for comparison. Shoreline values were compared at the ellipsoidal height value of 36.5 m.

Table 2.13. Water levels by survey and profile, ellipsoidal heights in meters.

Profile	**June 2001**	**Dec 2015**	**Sept 2016**	**Mar 2017**
000	36.7	37.2	36.62	36.63
100	36.56	37.14	36.61	36.6
200	36.57	36.91	36.55	36.65
300	36.61	36.85	36.68	36.64
400	36.57	36.89	36.55	36.58
500	36.62	37	36.86	36.58
600	36.68	36.99	36.65	36.61
700	36.65	37.14	36.77	36.59
770	36.58	36.76	36.77	36.56

Horizontal coordinates at the ellipsoidal height value of 36.5 m originated in the form of distances to the benchmarks used in 2001 and 2002. Since the benchmarks used as reference points for each transect were not situated along a single line in the long shore direction, the distances to corresponding benchmarks were converted to ITRF96/TM30 using the values within each transect.

The values for shoreline shift at each survey with respect to the June 2001 survey are found in Table 2.14, and the associated plots are found in Figure 2.16.

Table 2.14. Horizontal change between shorelines of given surveys and June 2001 shoreline observations at the ellipsoidal height of 36.5 m. Values are distances given as meters where negative values indicate shoreline recession.

Profile	**Dec 2015**	**Sept 2016**	**Mar 2017**
000	23.62	19.65	-2.96
100	19.04	27.65	1.43
200	15.41	32.29	12.21
300	9.59	2.54	6.27
400	14.22	11.44	-10.01
500	12.32	14.3	-3.27
600	12.26	5.92	-14.89
700	10.89	Not available	7.24
770	Not available	Not available	Not available
Mean	14.67	16.26	-0.50

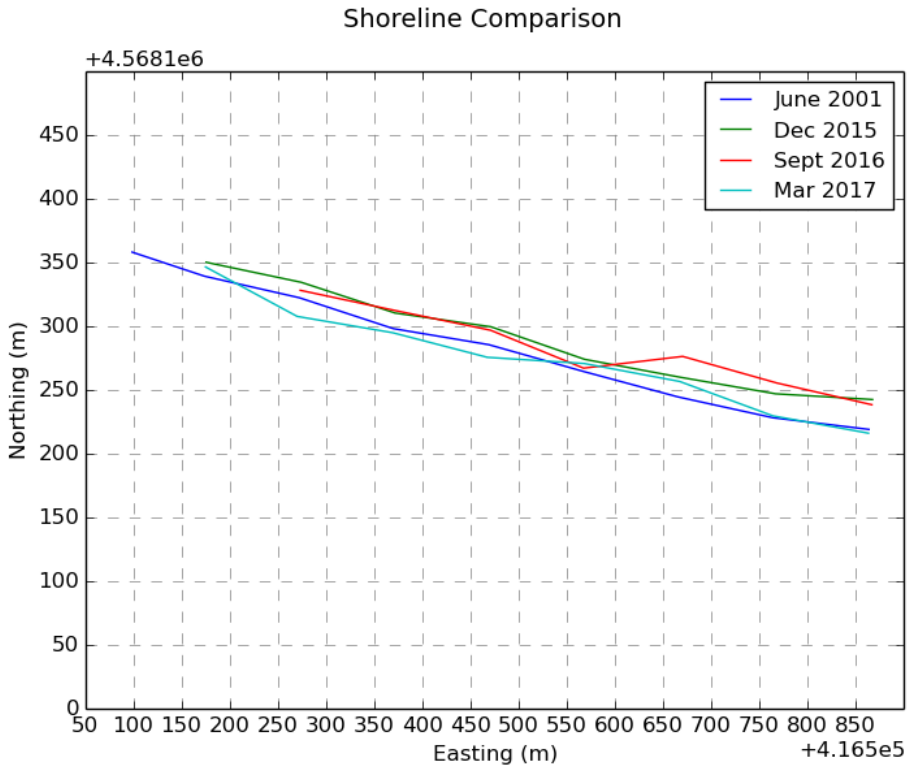

Figure 2.16. Comparison of shoreline locations at ellipsoidal height of 36.5 m.

2.2.2. Nearshore Bathymetry Change

2.2.2.1. Bathymetry Profiles. When the profiles along each transect are plotted, sections of loss or gain of sediment along each transect can be seen in areas between the intersecting profile lines. Profiles from all surveys on a single plot are found in Appendix A, and individual comparisons of profiles are found in Appendices B-F.

Areas in these sections were calculated with the trapezoidal rule for integration with elevation used as the variable of integration. Distance values interpolated at every 0.0001 m of elevation were used (see the section entitled *Interpolation*). The integral of the lower area was subtracted from that of the upper area in each segment and resulting values in each section were then summed to obtain net change for the given profile. The transects range in distance between 900 and 1000 m with an average of

8093 points per transect.

Net changes in area along each transect are found in the lower left corner of the plots. Positive values reflect a gain in sediment with respect to the given transect observed in 2001 while negative values reflect a loss or migration of sediment from the particular transect. It should be noted that the scales along the x- and y-axes differ greatly from each other resulting in overlapping areas that are not drawn to scale.

Due to either a lack of deepwater observations or boat routes that did not sufficiently approach the transects in one or more of the surveys, certain areas were removed from the comparison of recent-year surveys. The plots in the appendices display only the compared portions of the profile data. Similarly, the net change values were calculated using only the portions of the data that would receive feasible values through interpolation.

Associated water levels found in Table 2.13 are also shown within each profile comparison figure. Values shown are derived from the shoreline surveys and are the mean of the two observations nearest to each transect.

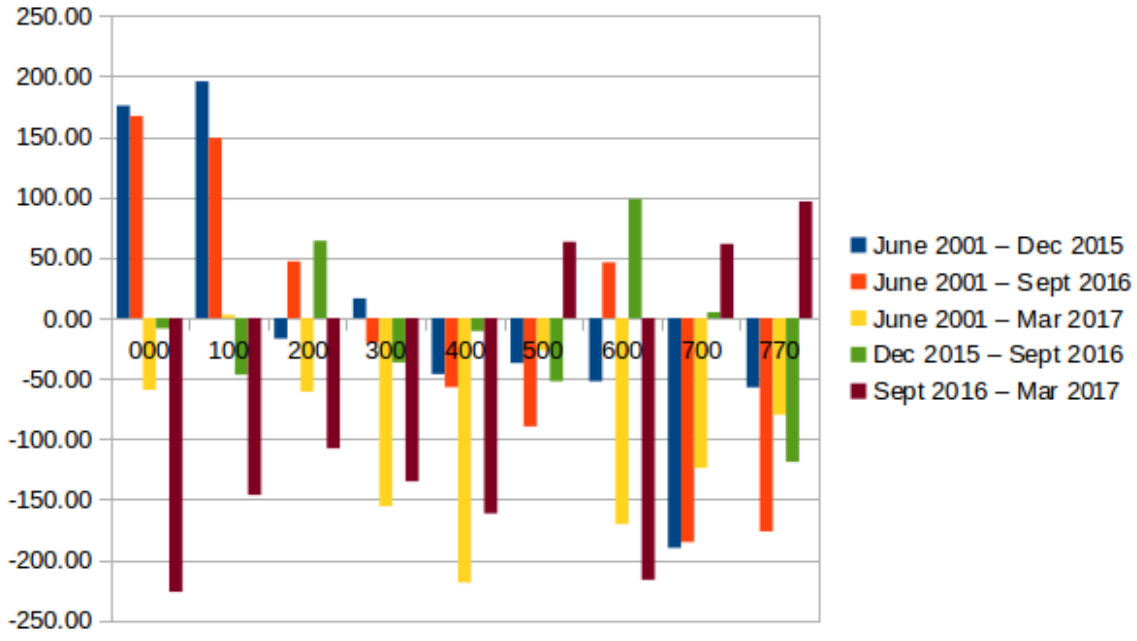

Figure 2.17. Comparison of net changes in area by survey and transect. Transect names are shown across the center of the figure. Values are given as areas in square meters (m^2).

Tables 2.15 summarizes changes in area between a given initial survey (row headings) and a subsequent survey (column headings). Negative values reflect a loss of sediment over the period between two given surveys.

Table 2.15. Net changes found in recent-year surveys (column headings) with respect to given previous surveys (row headings) between the shoreline and approximate depth of closure. Values shown are areas in square meters (m^2).

	Dec 2015	**Sept 2016**	**Mar 2017**
June 2001	-13	-120	-893
Dec 2015	–	-107	–
Sept 2016	–	–	-773

2.2.2.2. Bar Migration. In both the original and current studies, sandbar migration has been observed to be in the offshore direction, but the current study has found a much slower rate of migration. In the single year between 2001 and 2002, offshore bar migration ranged between 100-150 m. The current study, however, reveals a maximum offshore migration of 10 m over the thirteen years between 2002 and 2015, less than 1 m/yr.

3. CONCLUSION

The results of the original study in 2001 and 2002 suggested that a similar study conducted after a period of more than 15 years would reveal significant erosion and shoreline recession. While the surveys of December 2015, September 2016, and March 2017 revealed movement in the expected direction, with respect to the original study, a much more gradual degree of change was observed.

As in the original study, the current study has revealed shoreline recession, but the rate of change observed in the current study is significantly lower. While the 2001 and 2002 surveys showed an average shoreline recession of 11 m, this survey found a recession of 0.5 m over 15 years, or 3-4 cm/yr. This level of erosion is slight compared to that found in the 2001 and 2002 surveys.

Though the absence of nearly 900 m^3/m of sediment in March 2017 with respect to June 2001 may initially resemble medium-term erosion on the order of the short-term erosion observed in 2002, seasonal effects must first be considered and removed as much as possible. The fact that the degree of erosion observed between September 2016 and March 2017 approaches that observed over the nearly sixteen-year period between June 2001 and March 2017 suggests that the majority of the difference between June 2001 and March 2017 may be the effect of a single typical winter on the study area. Additionally, despite the noise in the September 2016 data, the trend shows that the majority of the sediment along the transects is replenished with respect to both June 2001 and December 2015. The remaining approximately 100-125 m^3/m of sediment represents the mid-term nearshore erosion. On a yearly basis, this erosion which is independent of expected seasonal changes has been observed to be occurring at 6-8 m^3/m.

Last, though it is possible that the sandbar shifted to a greater degree during the thirteen years for which no data exists and now happens to be back in the same location, the data from 2015, 2016, and 2017 suggests that the bar's typical location

varies by approximately 50 m depending on the season. Several of the December 2015 and September 2016 plots show the bar in almost the exact same location.

The faculty at the Coastal Engineering Laboratory reported a major storm between 2001 and 2002 that buried research equipment placed at the seafloor prior to the storm. The equipment still has not been found at the time of the writing of this report. The drastic bar migration and shoreline erosion between 2001 and 2002 may be attributed to that storm.

According to the recent surveys, though shoreline recession and nearshore erosion have continued over the mid-term in Kilyos, the process has been found to be much more gradual than the 2001 and 2002 data suggested.

APPENDIX A: ALL SURVEY PROFILES

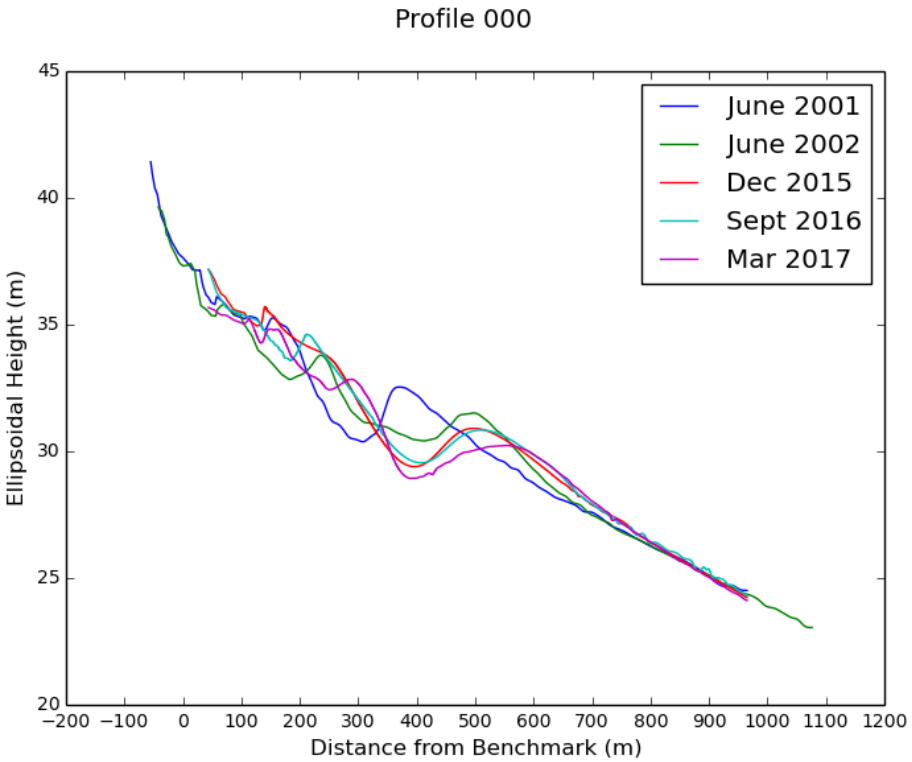

Figure A.1. Profile 000, All Surveys.

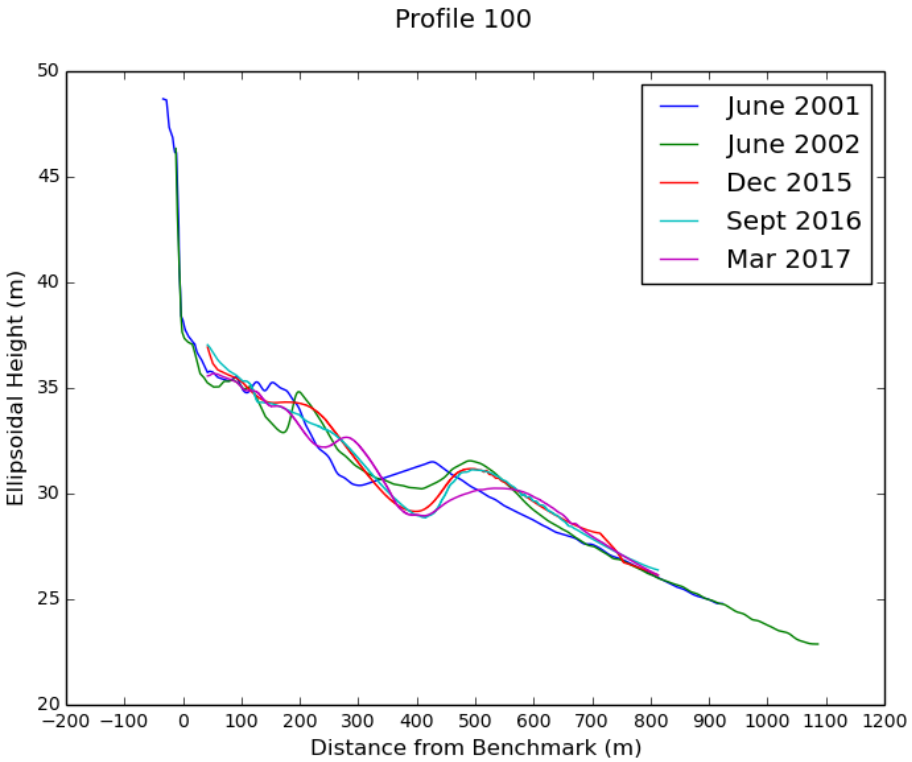

Figure A.2. Profile 100, All Surveys.

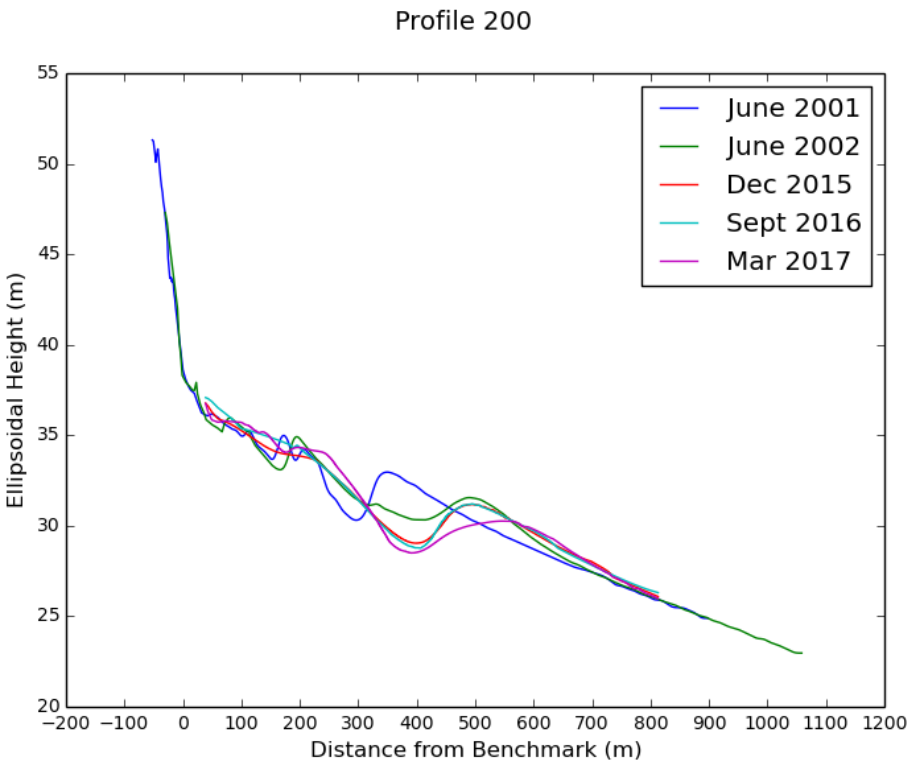

Figure A.3. Profile 200, All Surveys.

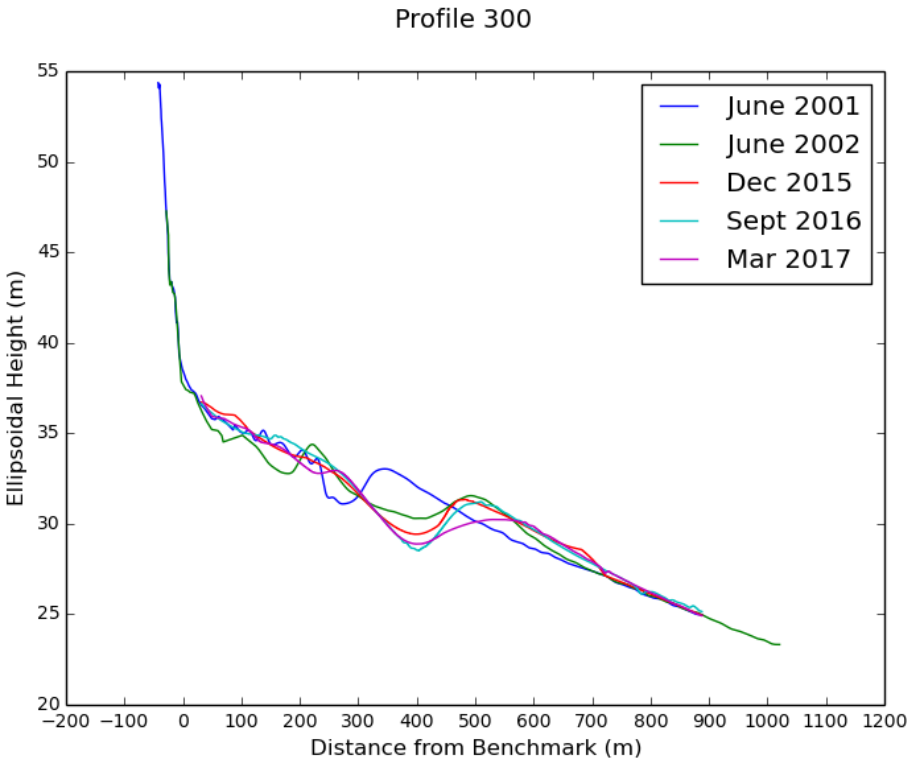

Figure A.4. Profile 300, All Surveys.

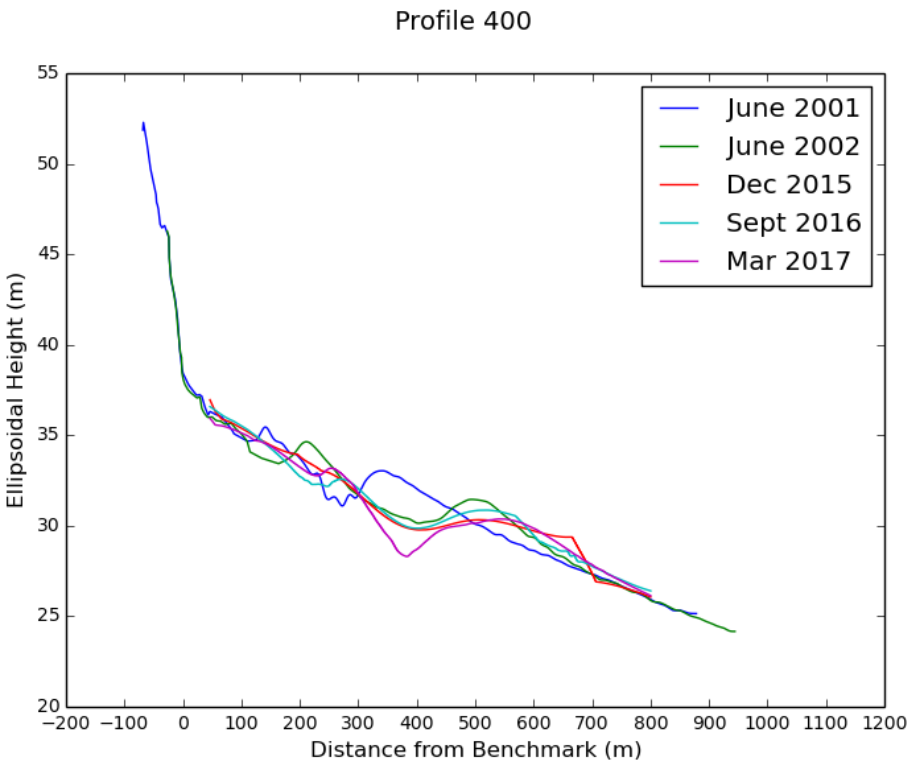

Figure A.5. Profile 400, All Surveys.

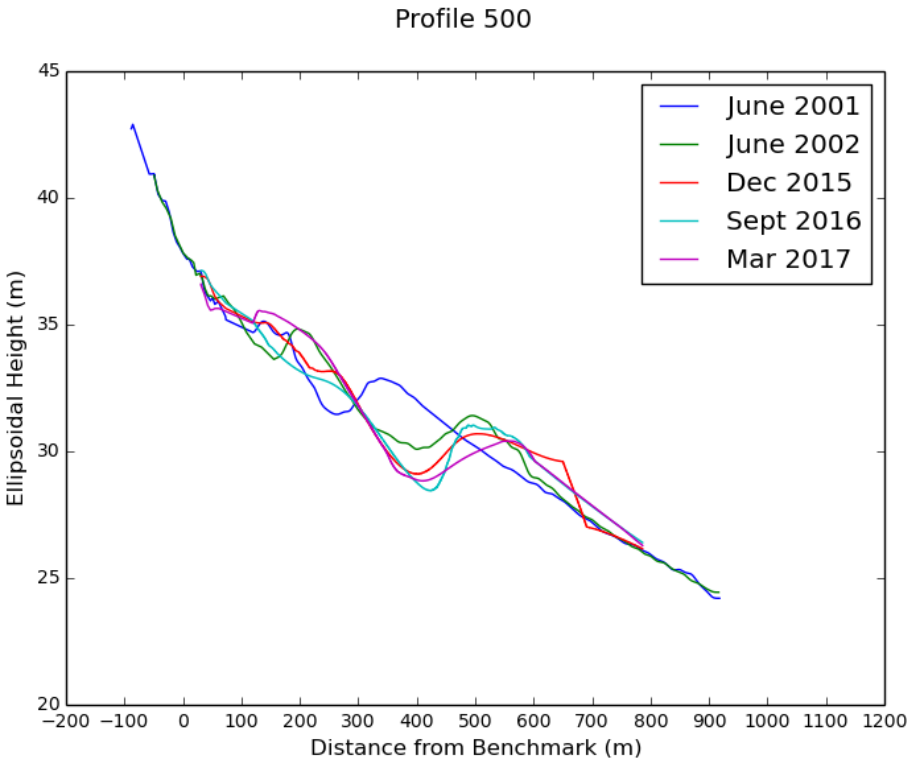

Figure A.6. Profile 500, All Surveys.

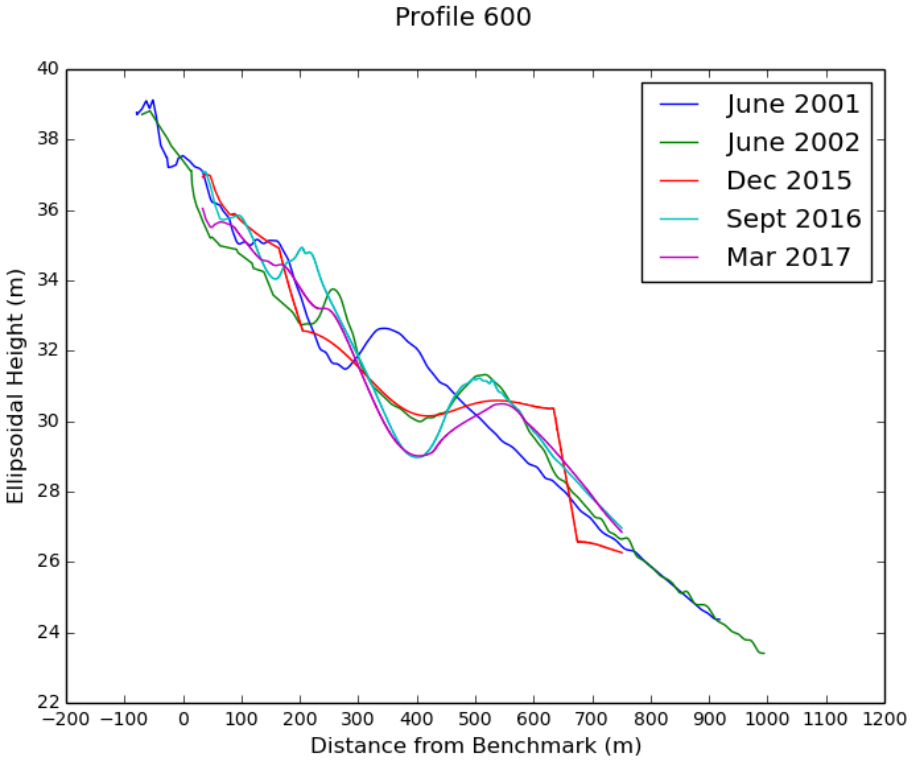

Figure A.7. Profile 600, All Surveys.

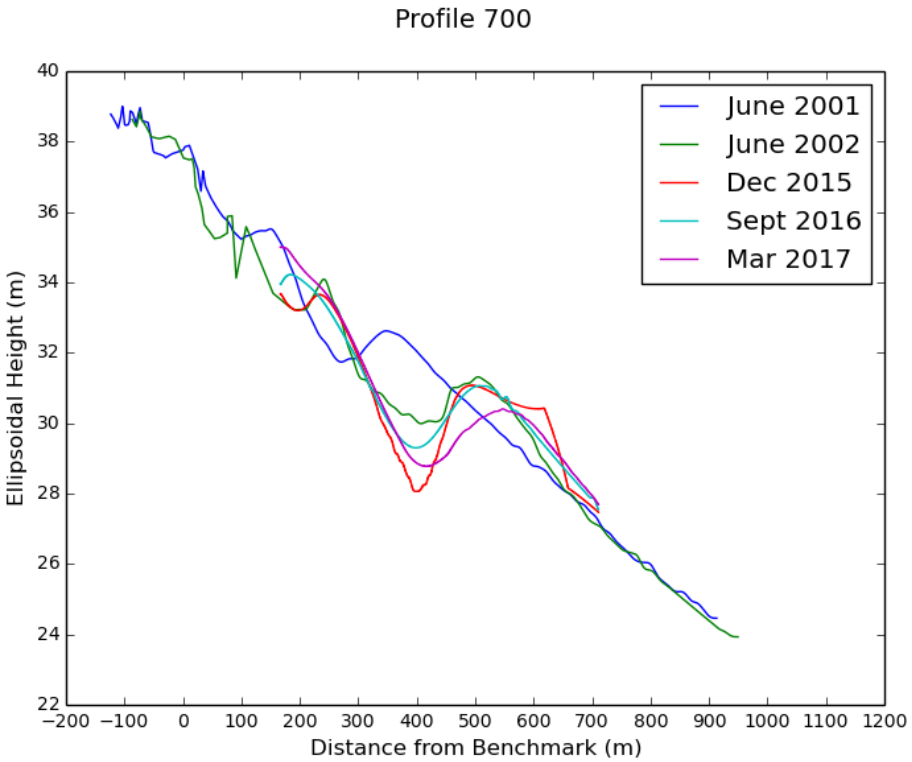

Figure A.8. Profile 700, All Surveys.

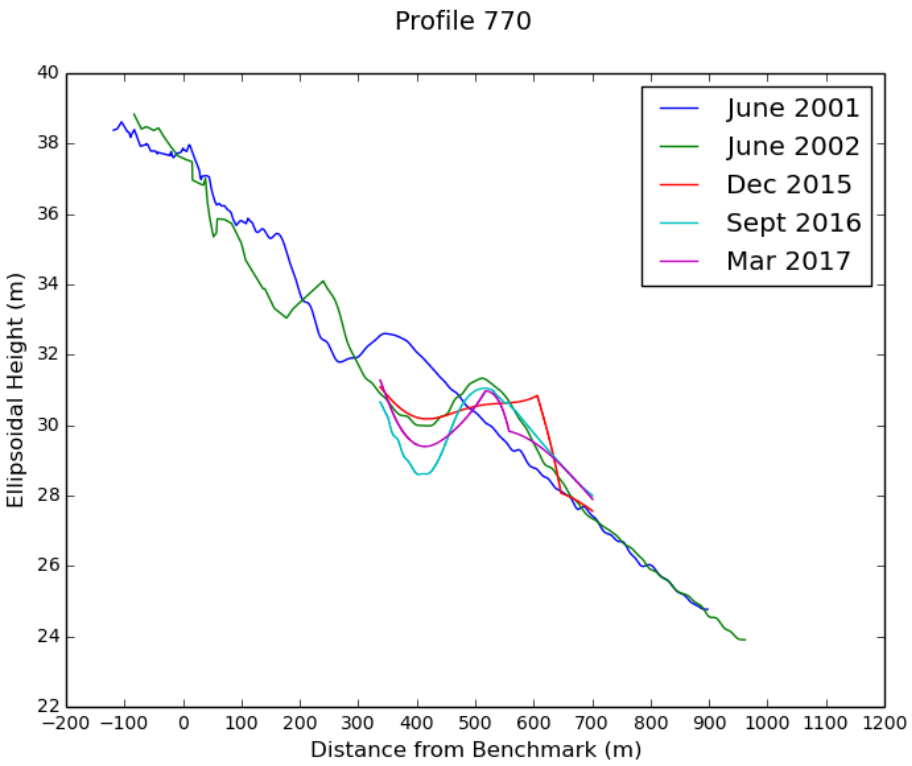

Figure A.9. Profile 770, All Surveys.

APPENDIX B: JUNE 2001 AND DECEMBER 2015 PROFILES

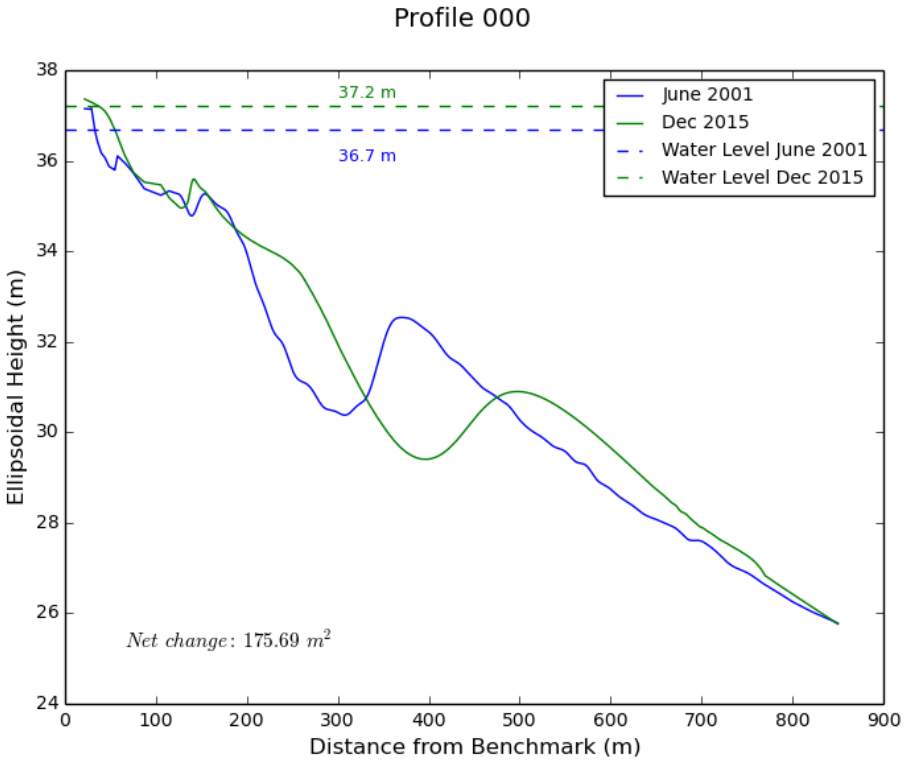

Figure B.1. Profile 000, June 2001 and December 2015.

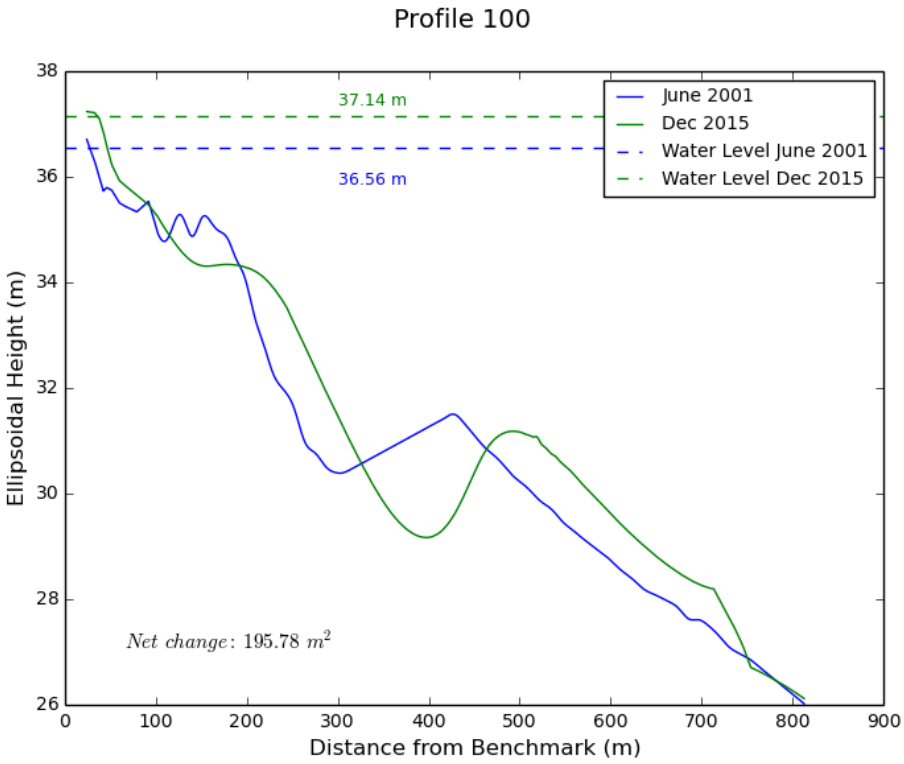

Figure B.2. Profile 100, June 2001 and December 2015.

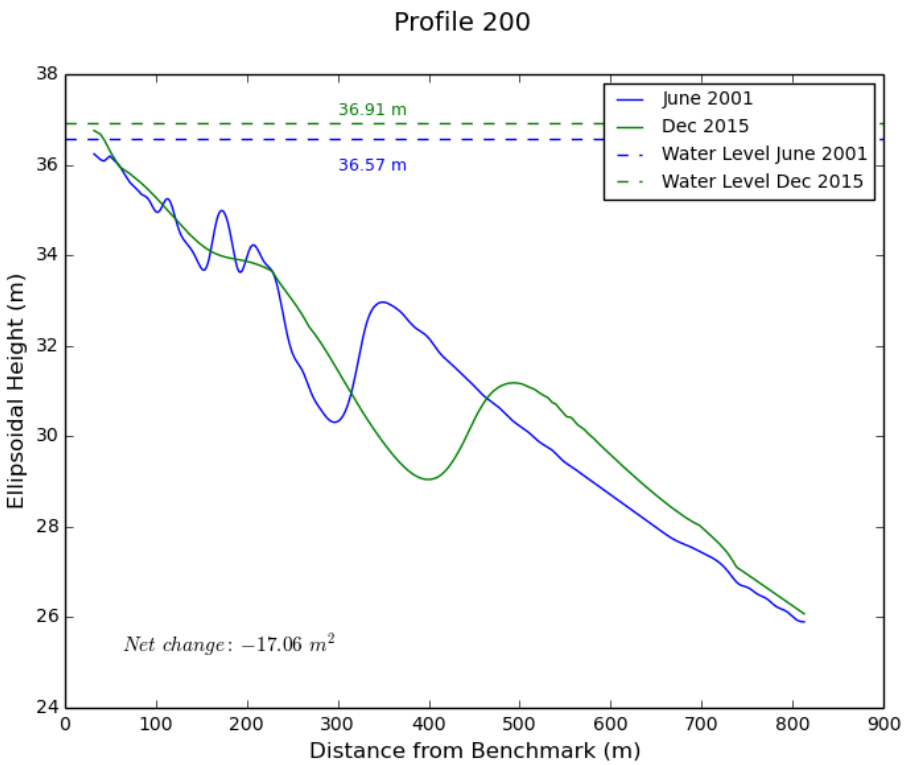

Figure B.3. Profile 200, June 2001 and December 2015.

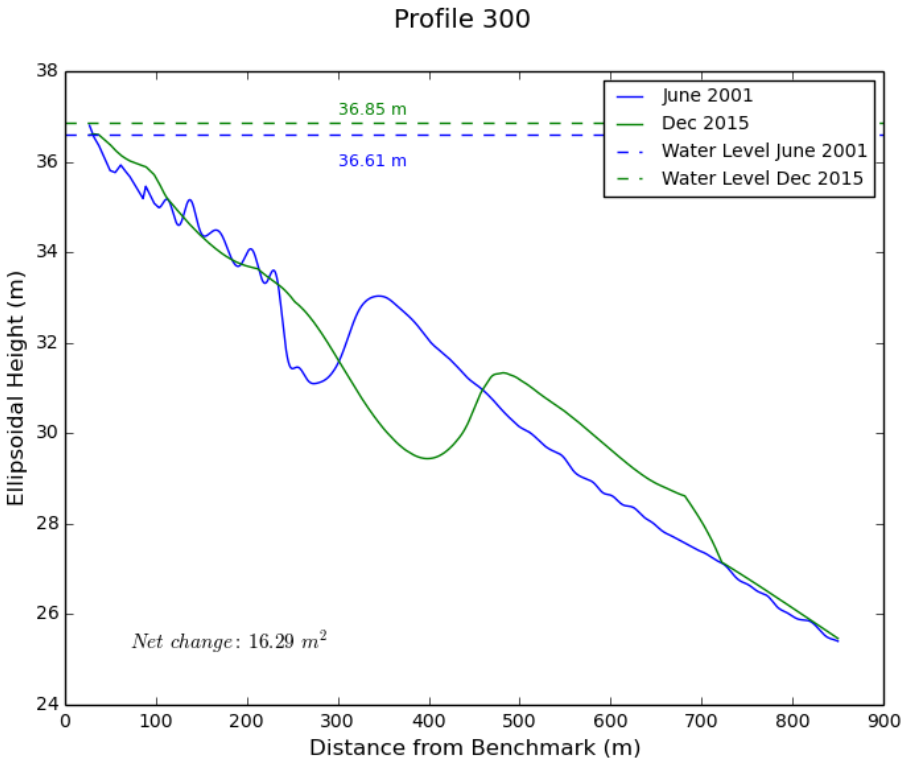

Figure B.4. Profile 300, June 2001 and December 2015.

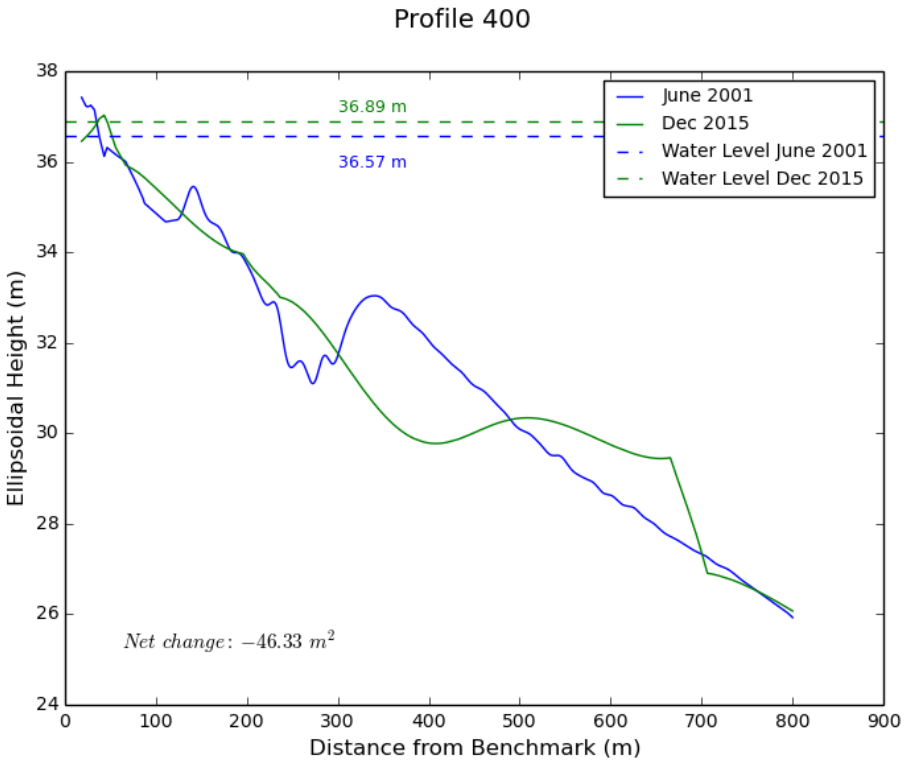

Figure B.5. Profile 400, June 2001 and December 2015.

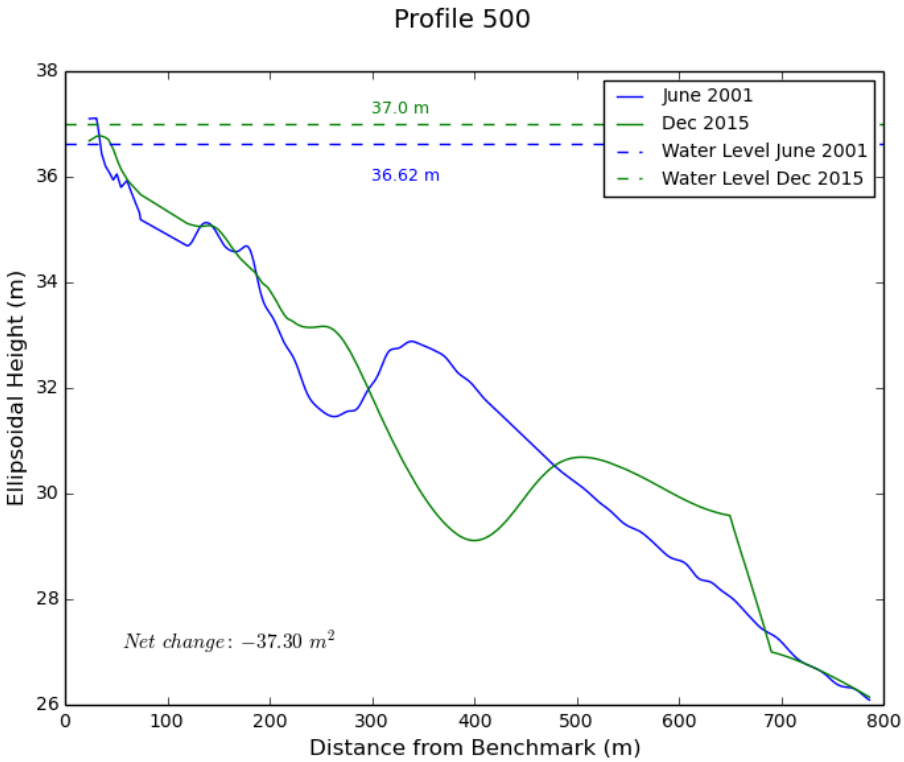

Figure B.6. Profile 500, June 2001 and December 2015.

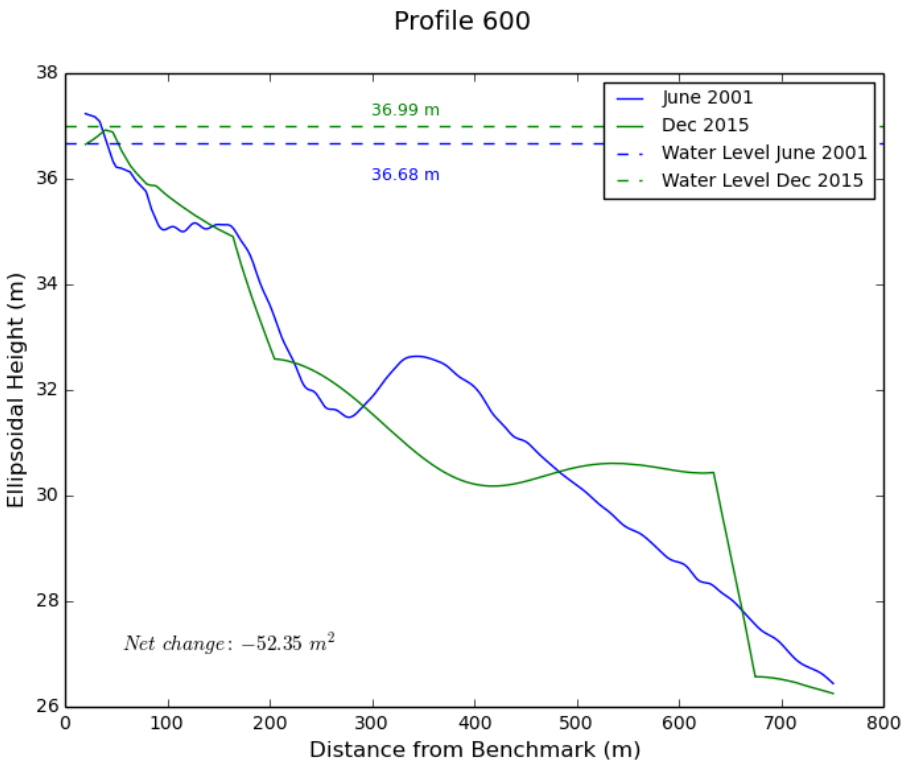

Figure B.7. Profile 600, June 2001 and December 2015.

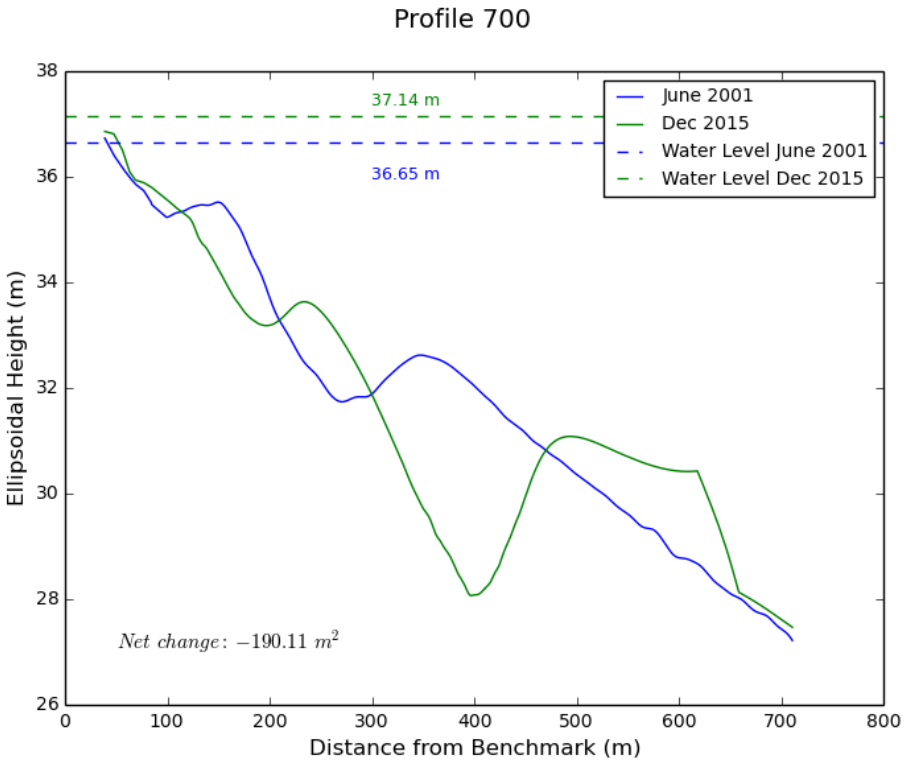

Figure B.8. Profile 700, June 2001 and December 2015.

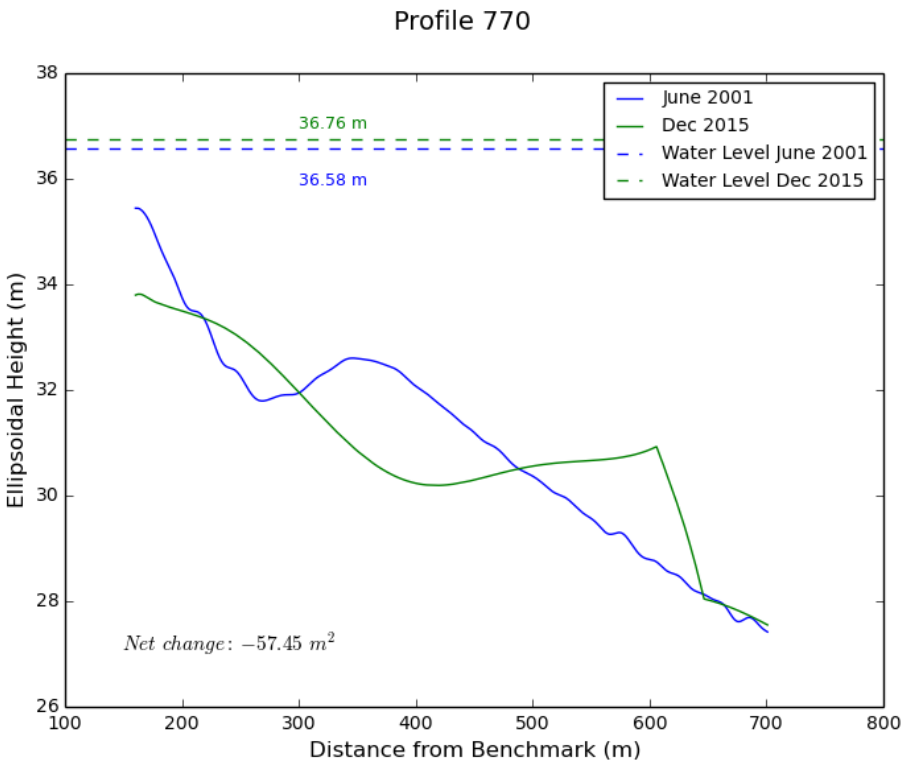

Figure B.9. Profile 770, June 2001 and December 2015.

APPENDIX C: JUNE 2001 AND SEPTEMBER 2016 PROFILES

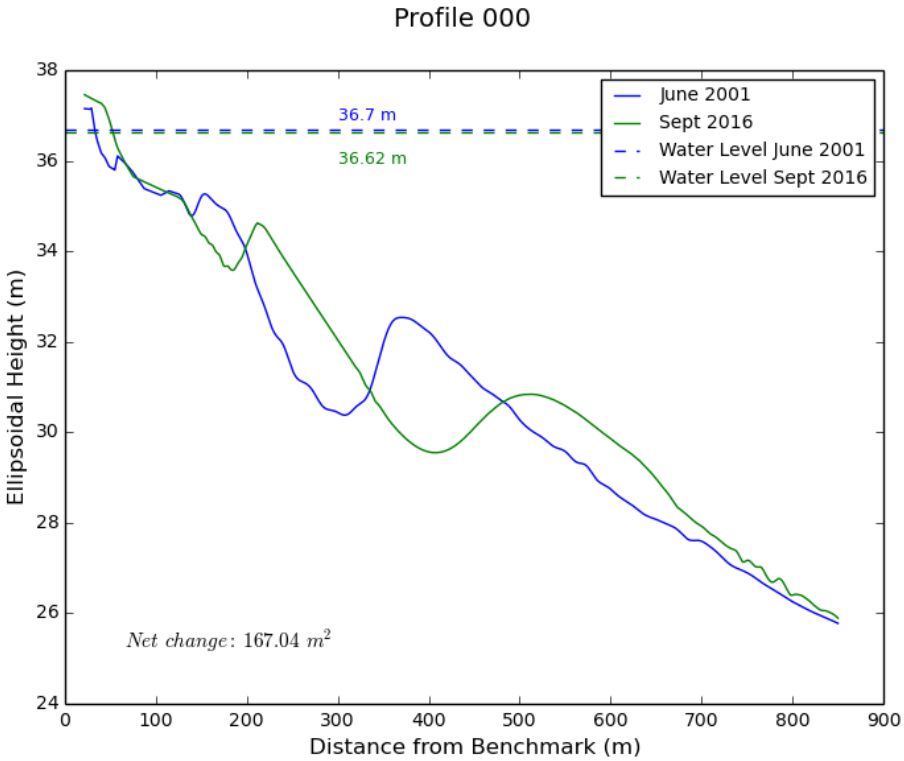

Figure C.1. Profile 000, June 2001 and September 2016.

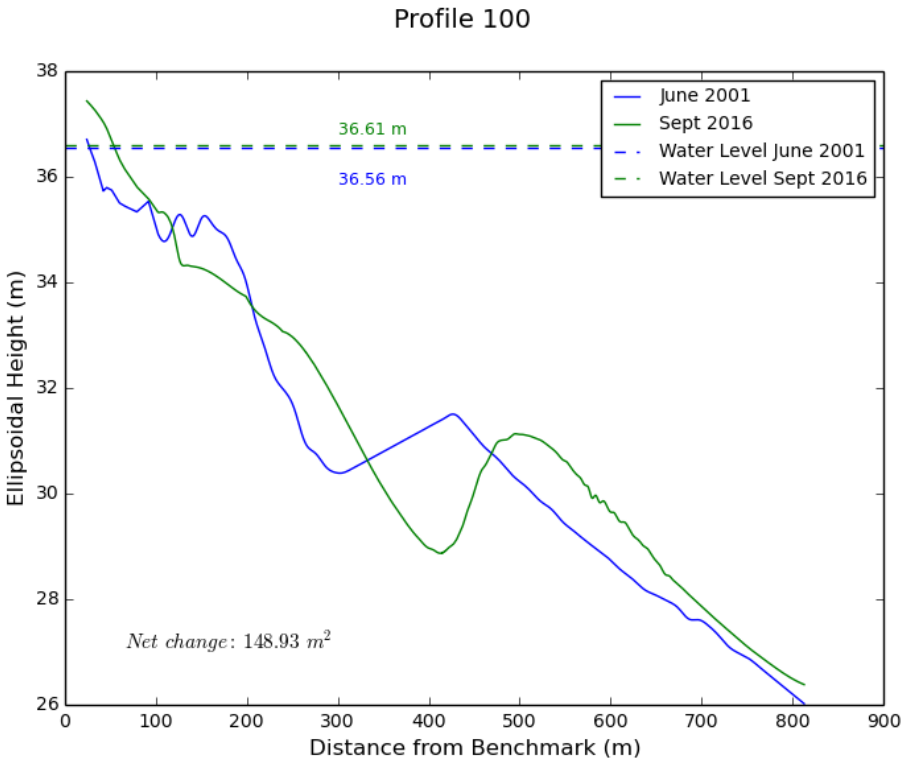

Figure C.2. Profile 100, June 2001 and September 2016.

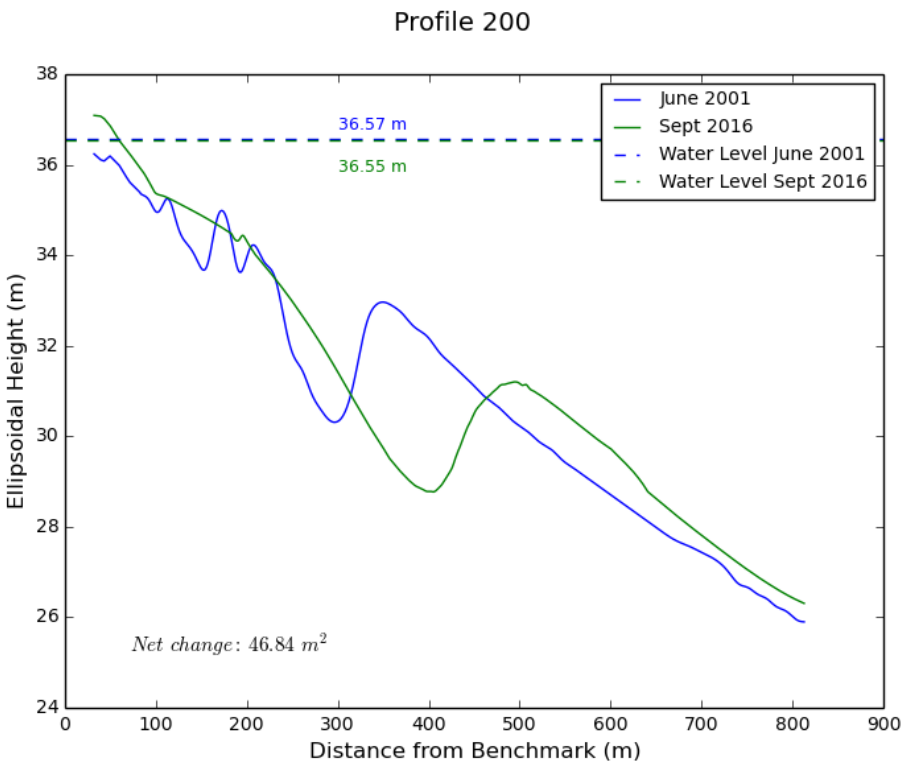

Figure C.3. Profile 200, June 2001 and September 2016.

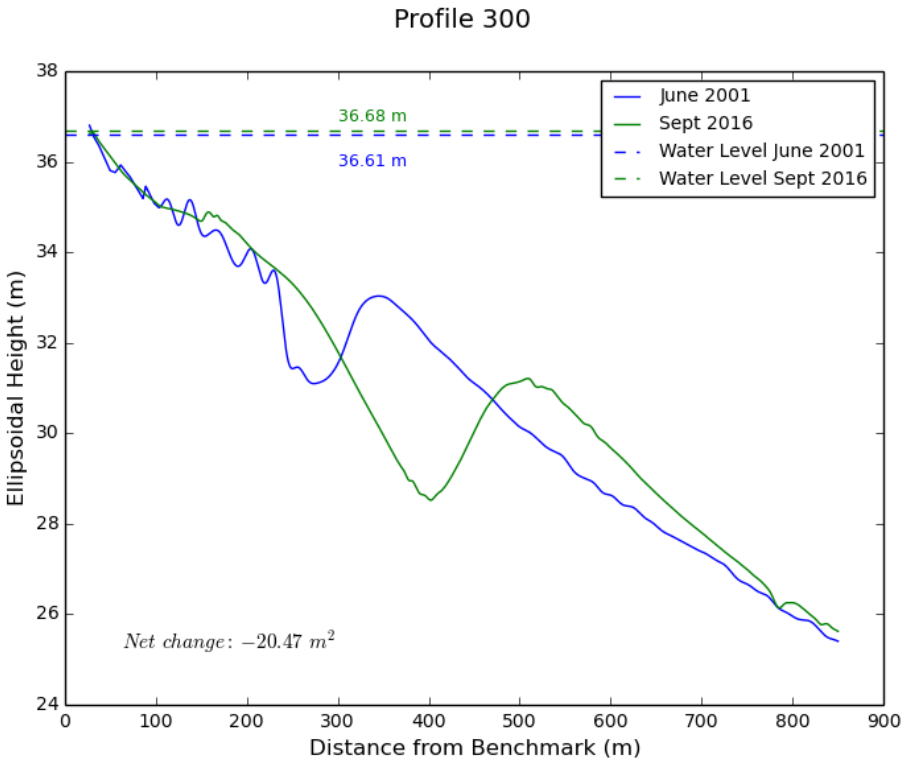

Figure C.4. Profile 300, June 2001 and September 2016.

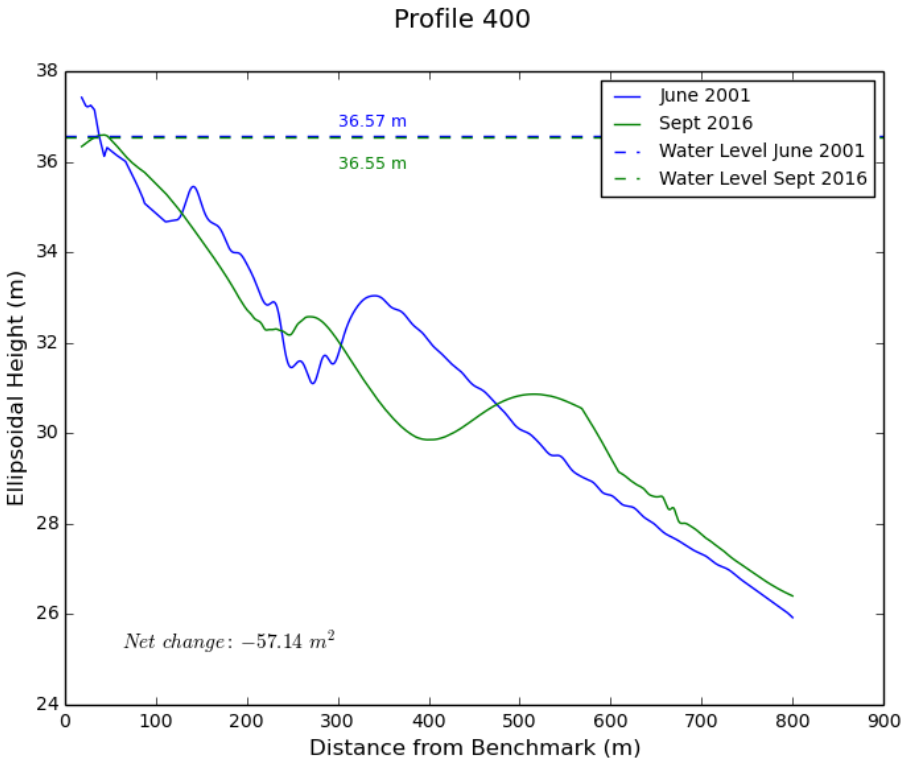

Figure C.5. Profile 400, June 2001 and September 2016.

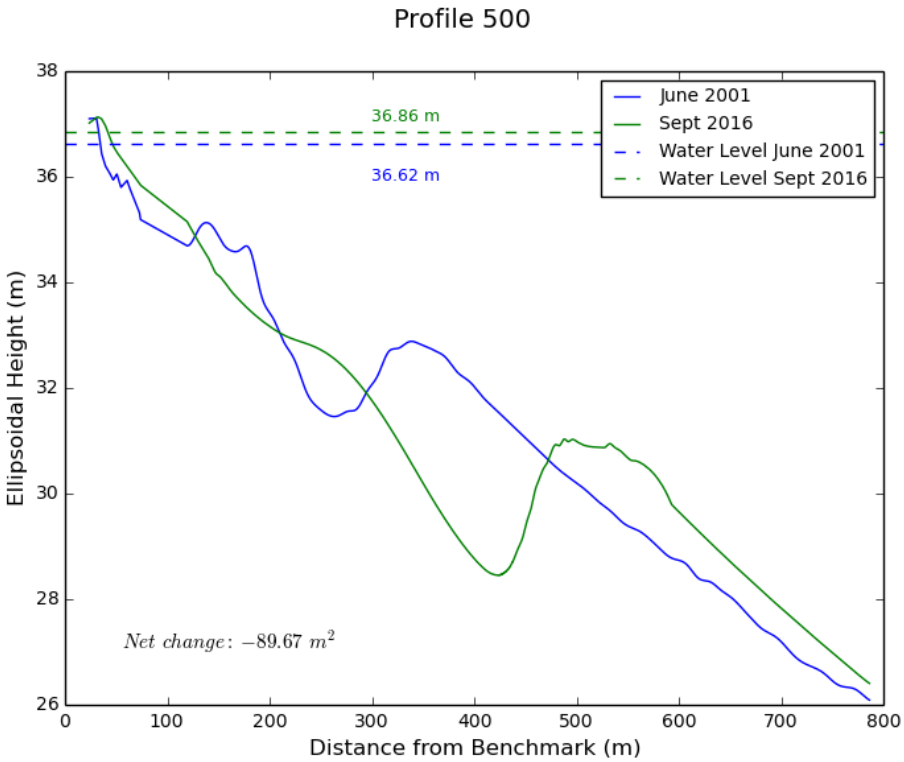

Figure C.6. Profile 500, June 2001 and September 2016.

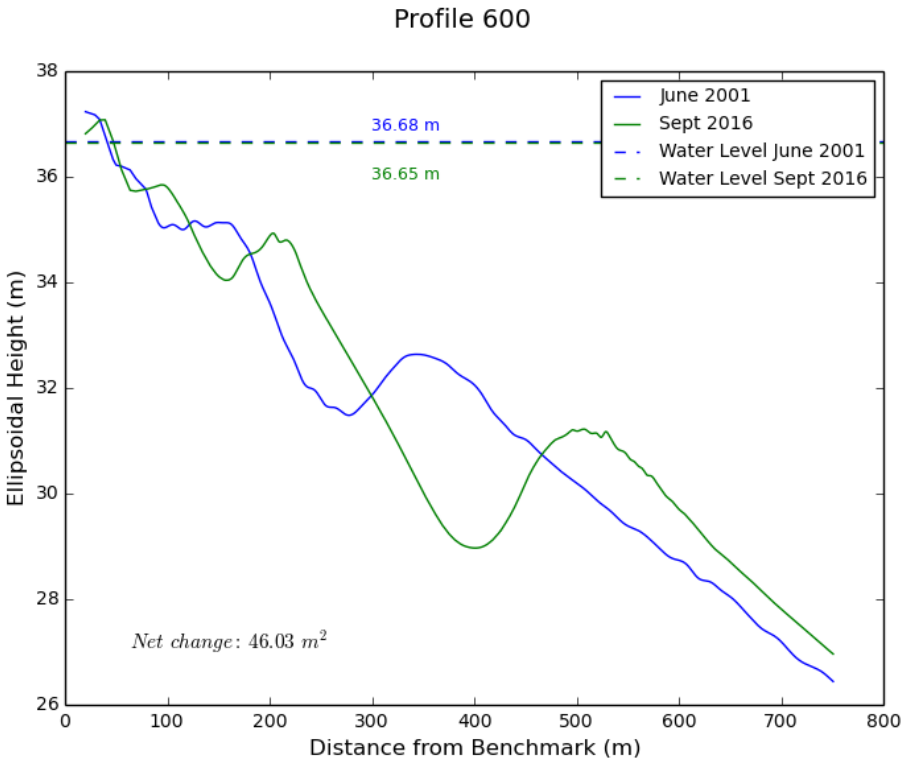

Figure C.7. Profile 600, June 2001 and September 2016.

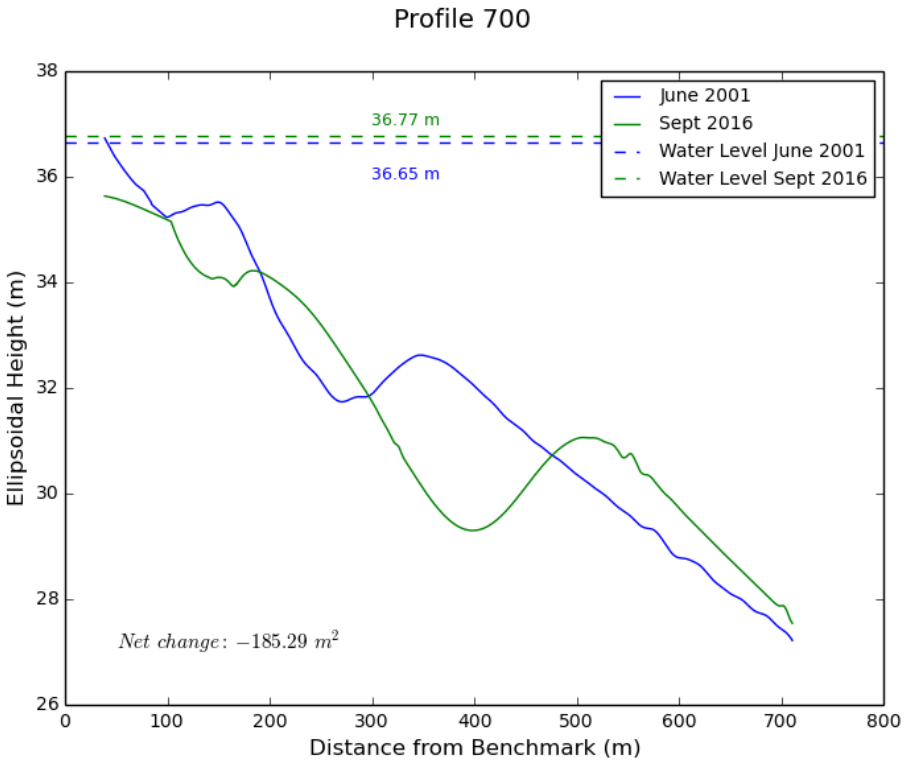

Figure C.8. Profile 700, June 2001 and September 2016.

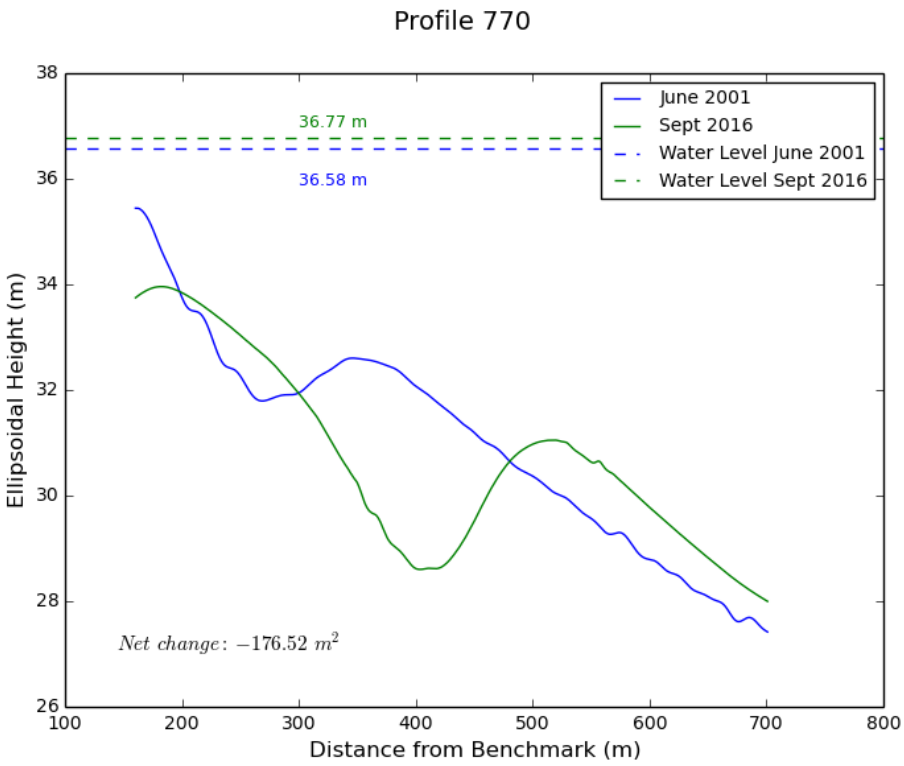

Figure C.9. Profile 770, June 2001 and September 2016.

APPENDIX D: JUNE 2001 AND MARCH 2017 PROFILES

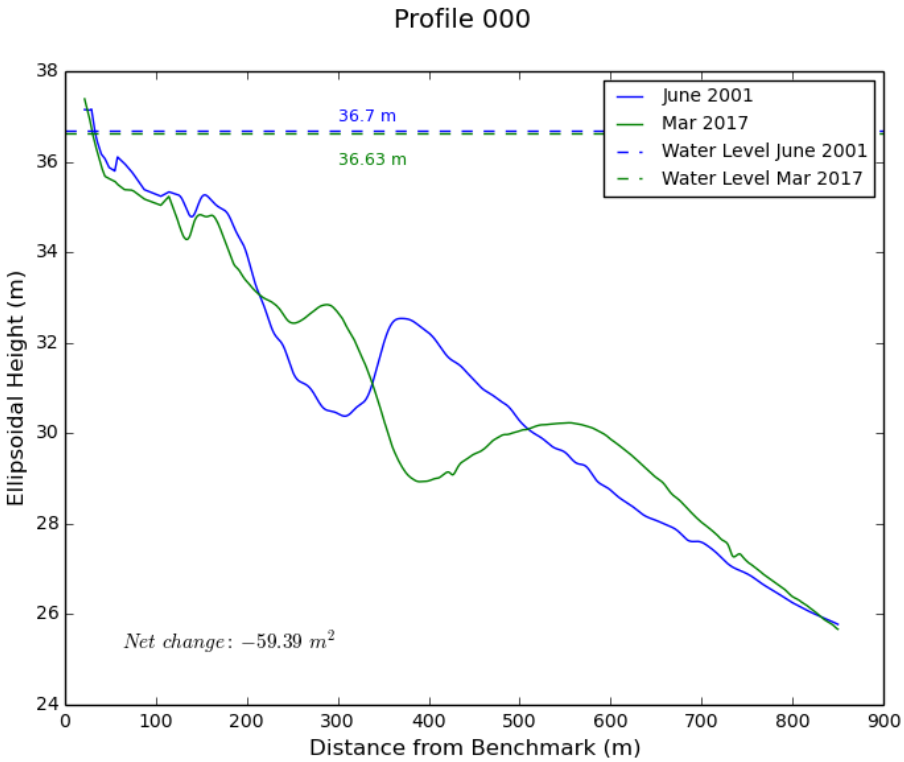

Figure D.1. Profile 000, June 2001 and March 2017.

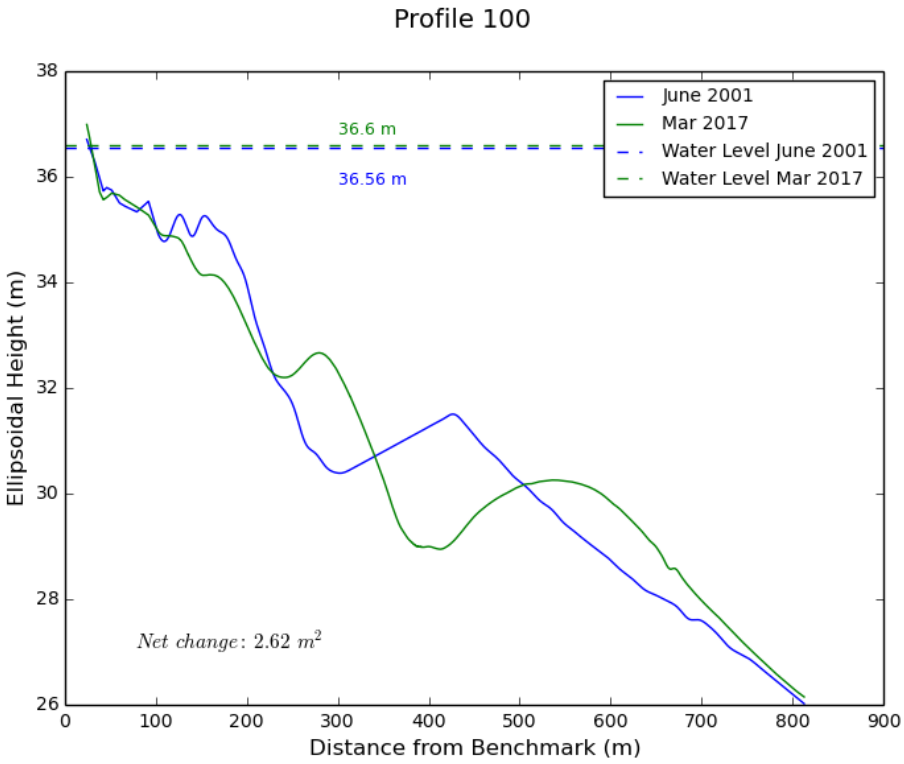

Figure D.2. Profile 100, June 2001 and March 2017.

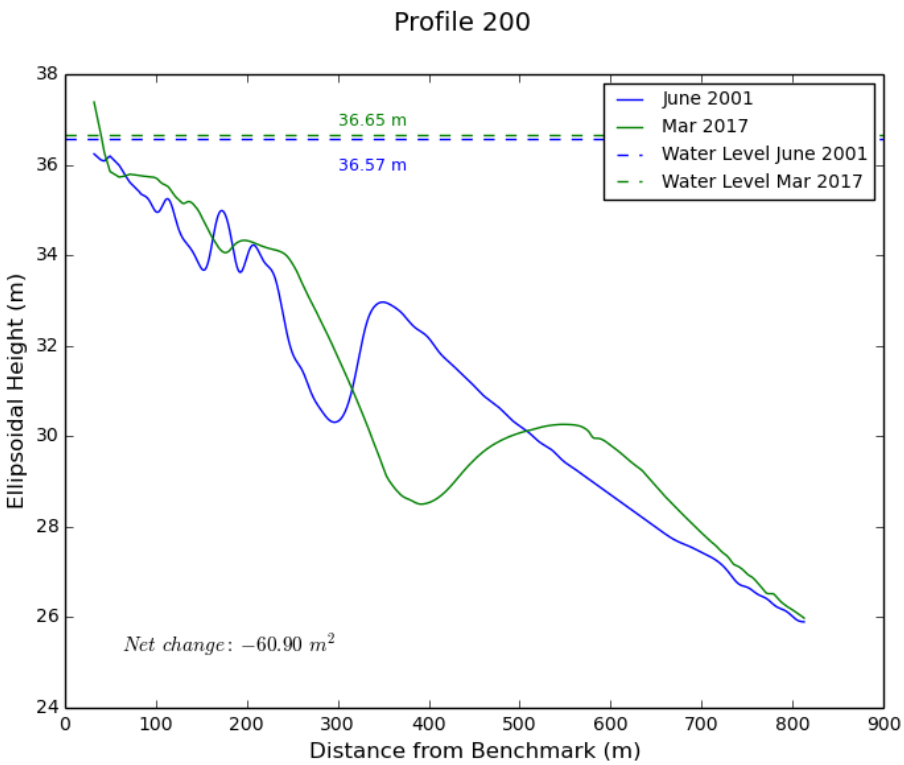

Figure D.3. Profile 200, June 2001 and March 2017.

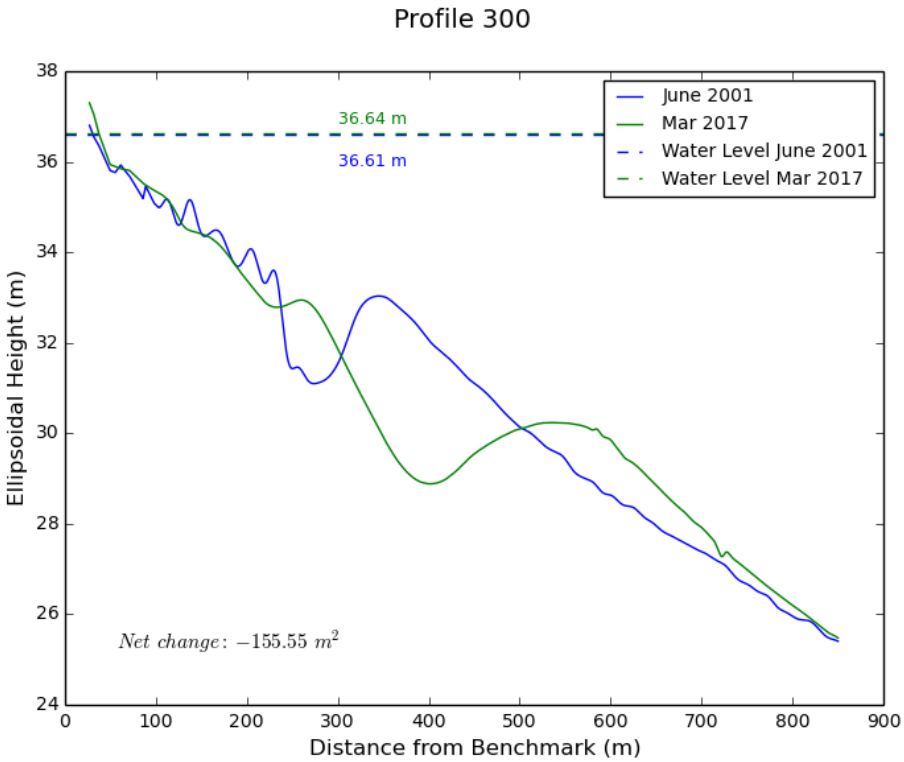

Figure D.4. Profile 300, June 2001 and March 2017.

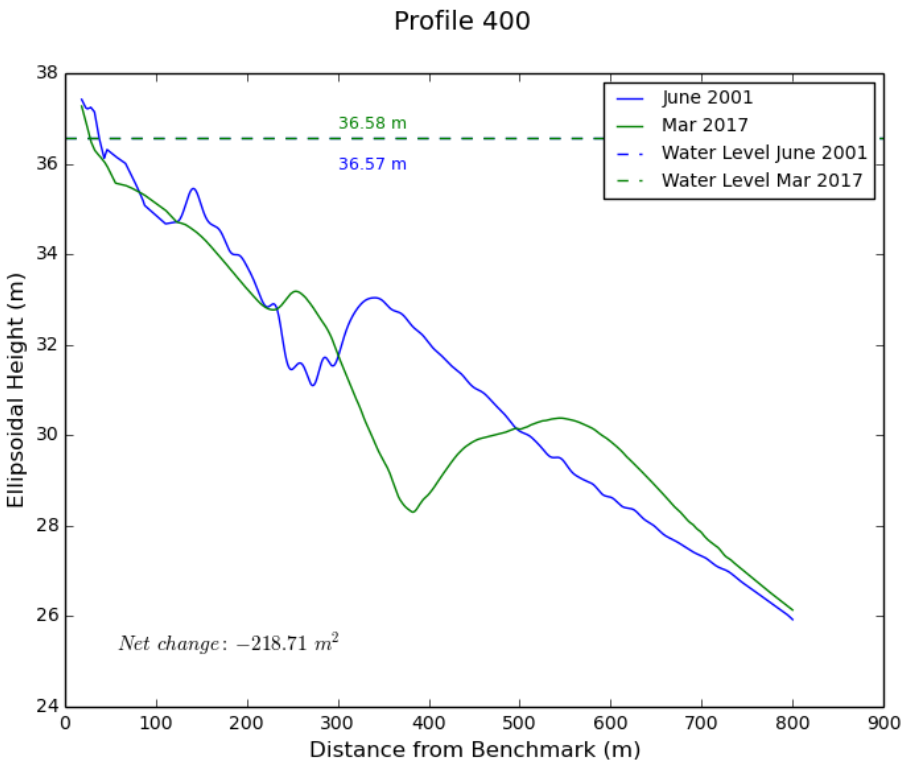

Figure D.5. Profile 400, June 2001 and March 2017.

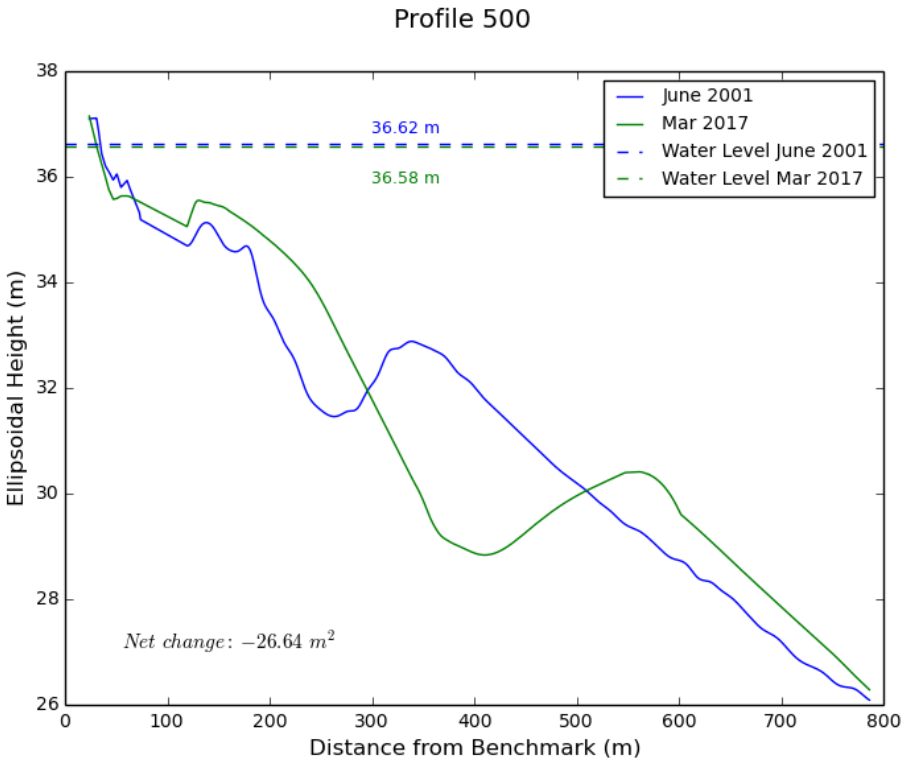

Figure D.6. Profile 500, June 2001 and March 2017.

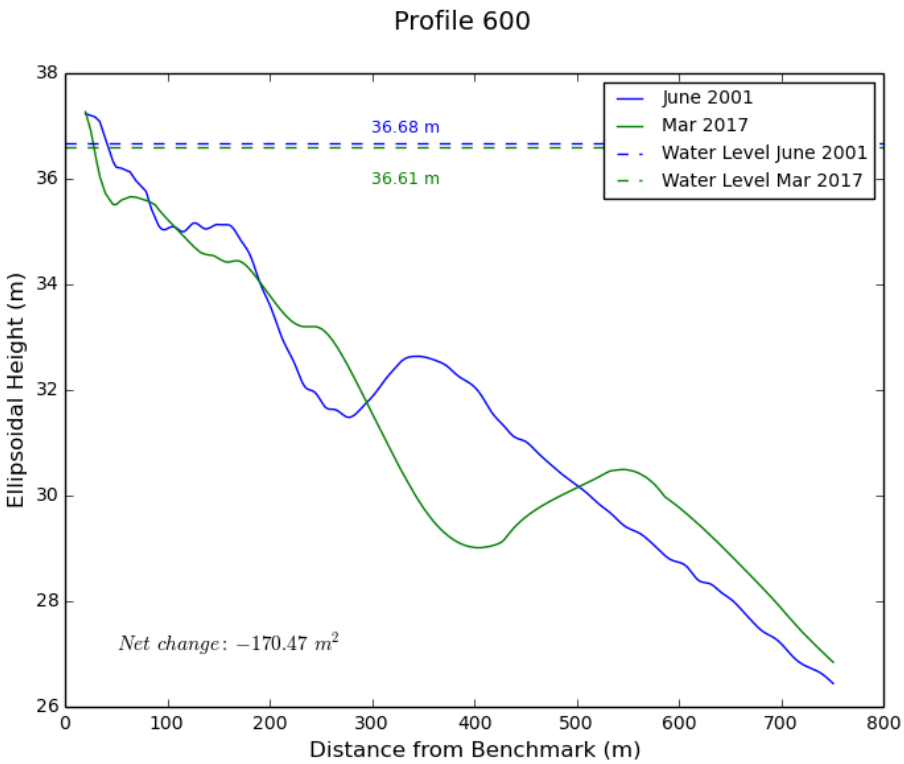

Figure D.7. Profile 600, June 2001 and March 2017.

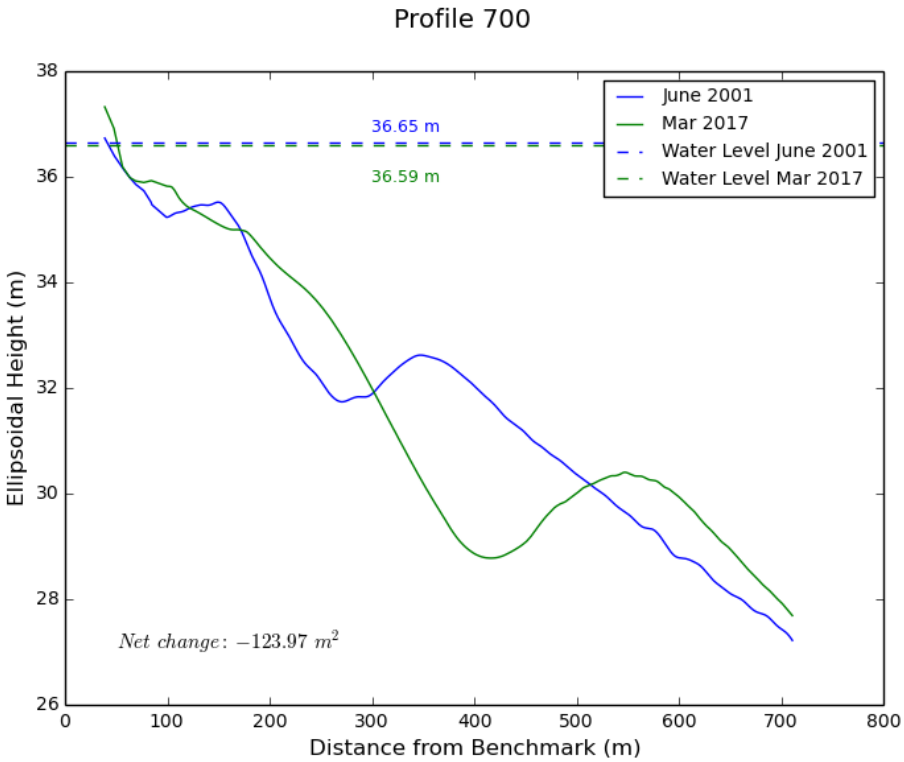

Figure D.8. Profile 700, June 2001 and March 2017.

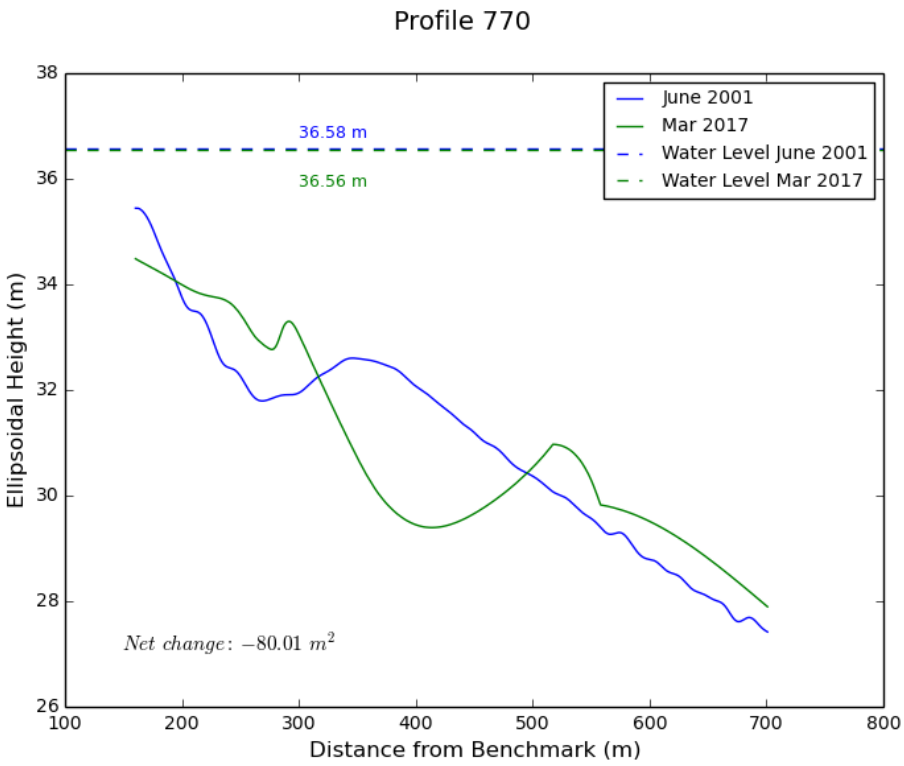

Figure D.9. Profile 770, June 2001 and March 2017.

APPENDIX E: DECEMBER 2015 AND SEPTEMBER 2016 PROFILES

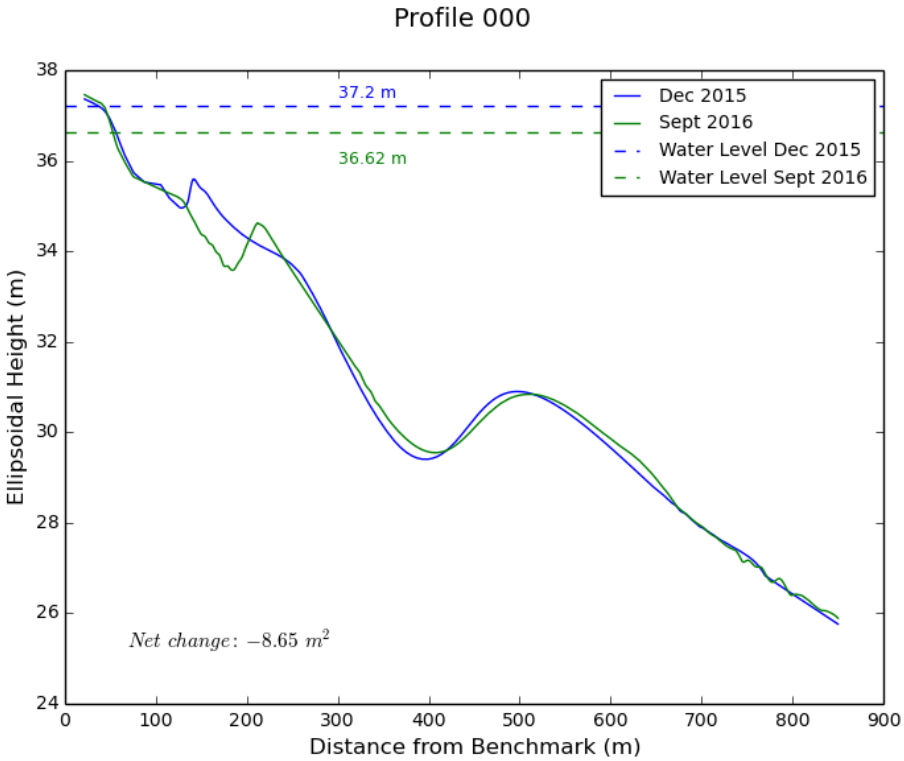

Figure E.1. Profile 000, December 2015 and September 2016.

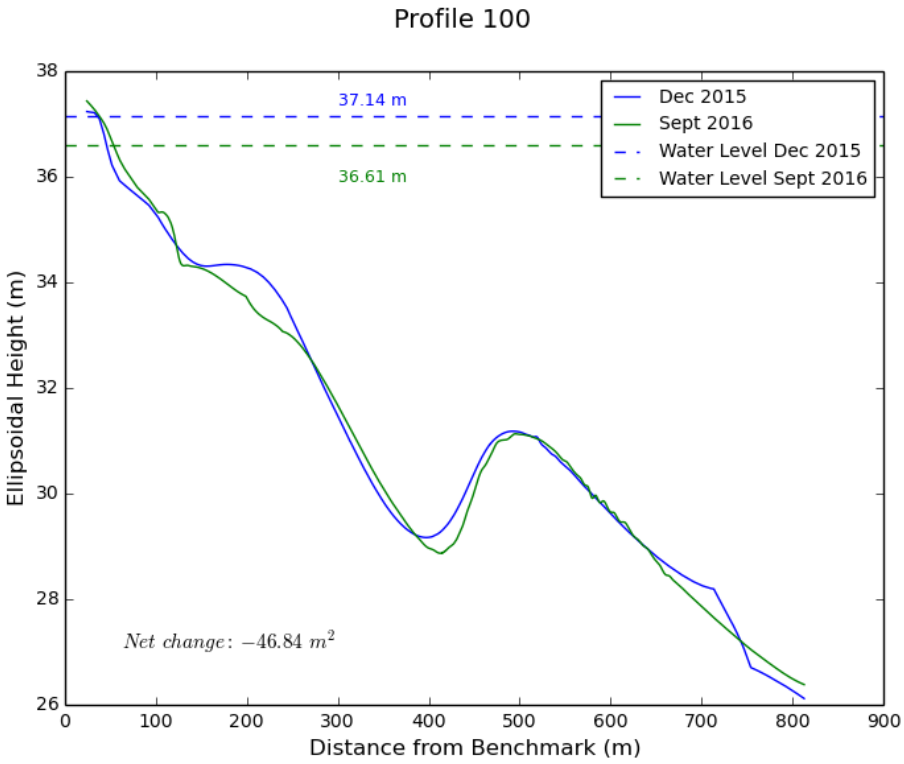

Figure E.2. Profile 100, December 2015 and September 2016.

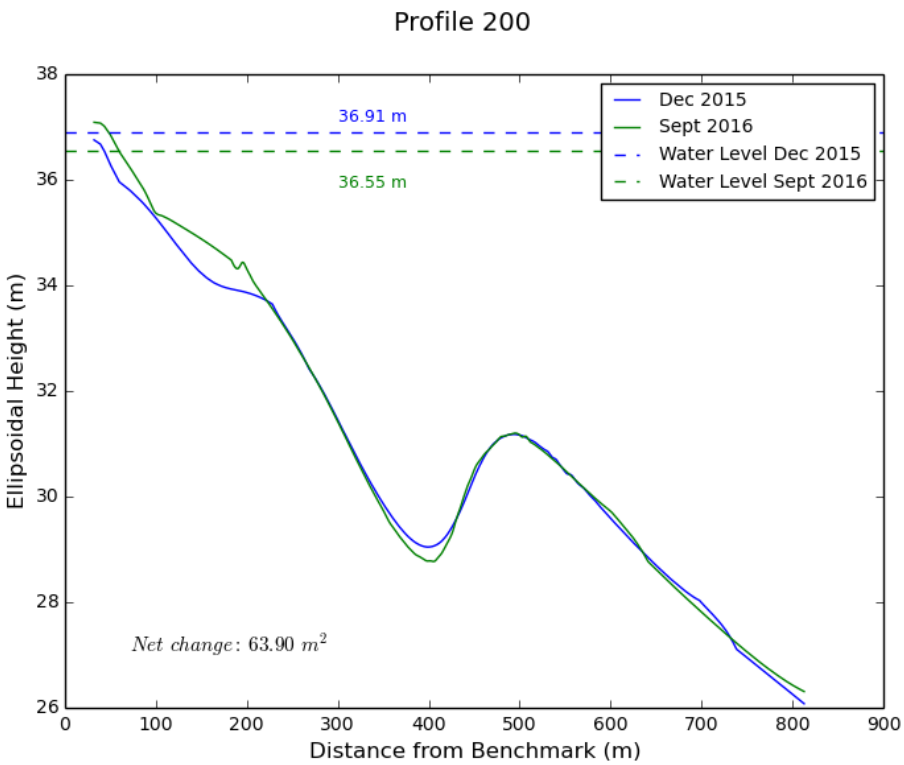

Figure E.3. Profile 200, December 2015 and September 2016.

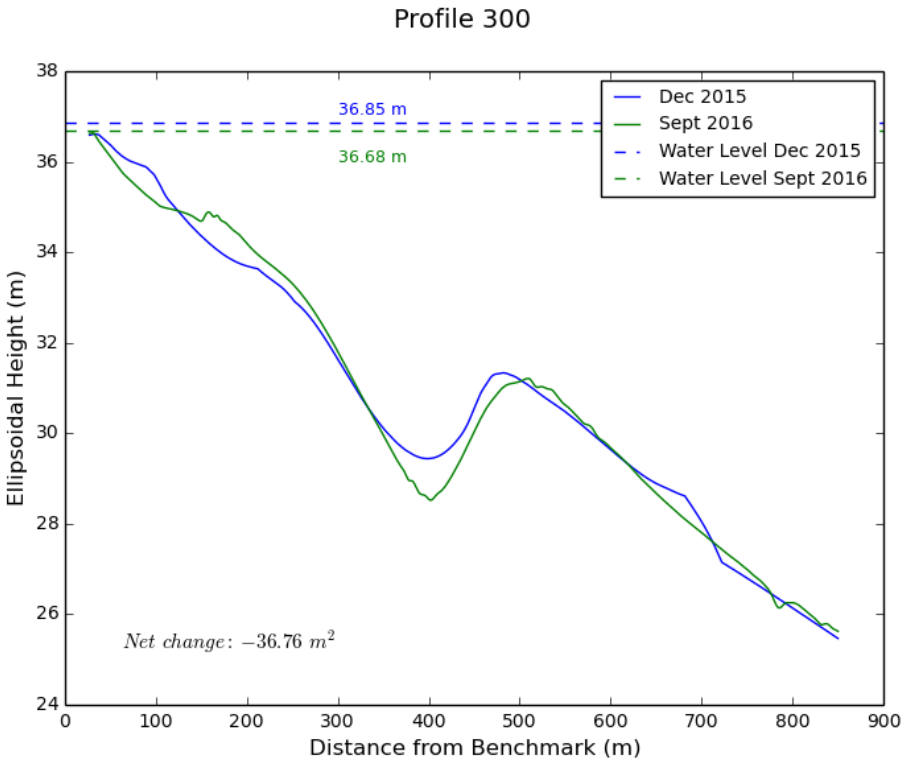

Figure E.4. Profile 300, December 2015 and September 2016.

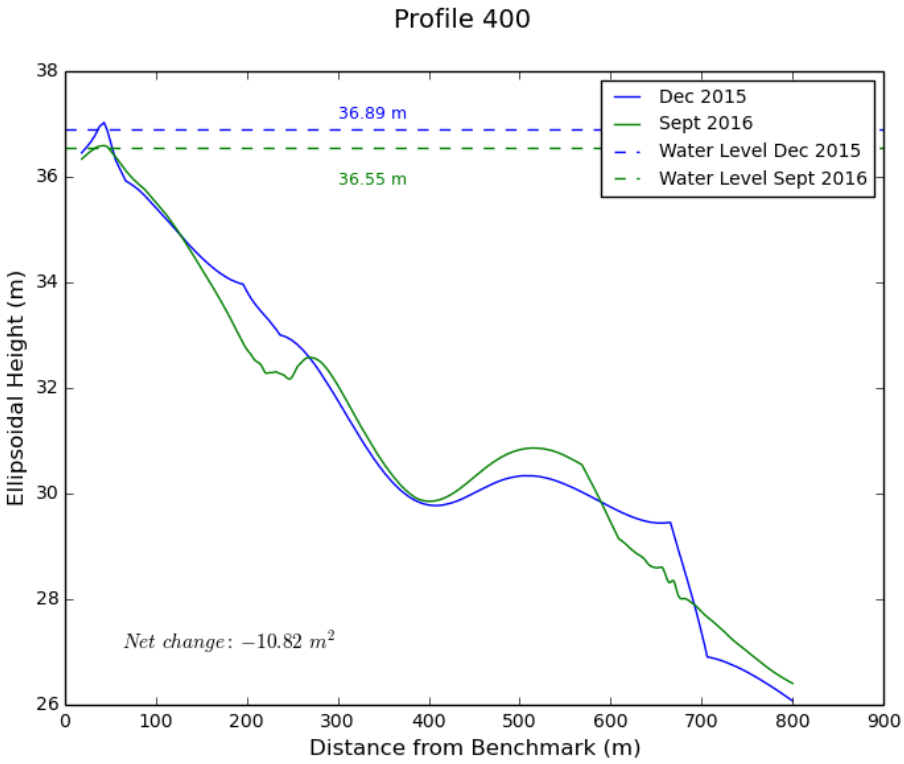

Figure E.5. Profile 400, December 2015 and September 2016.

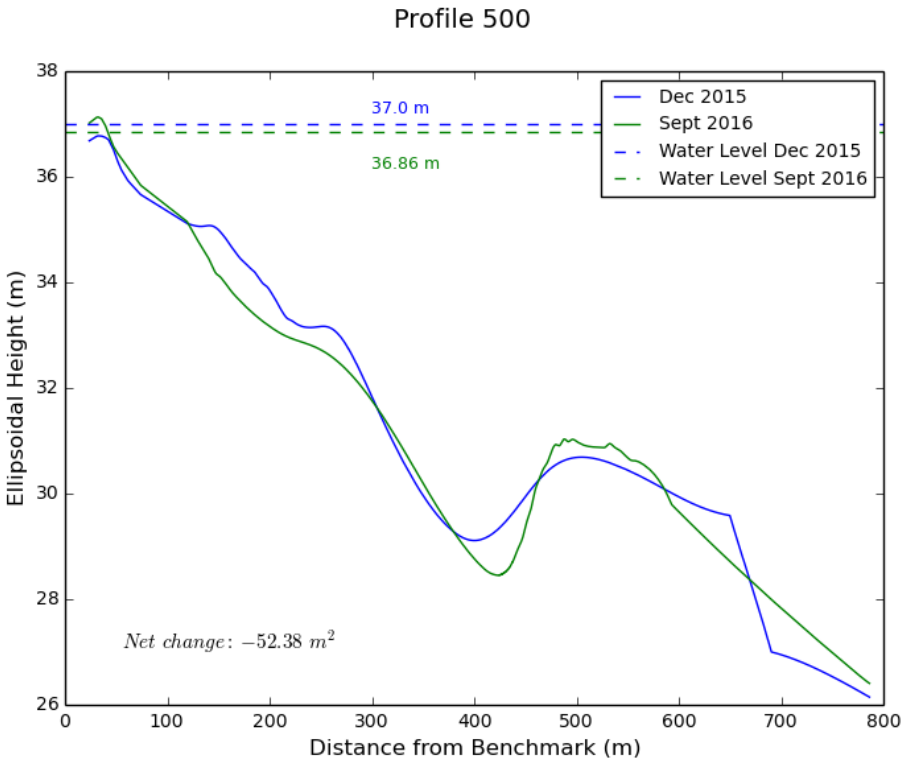

Figure E.6. Profile 500, December 2015 and September 2016.

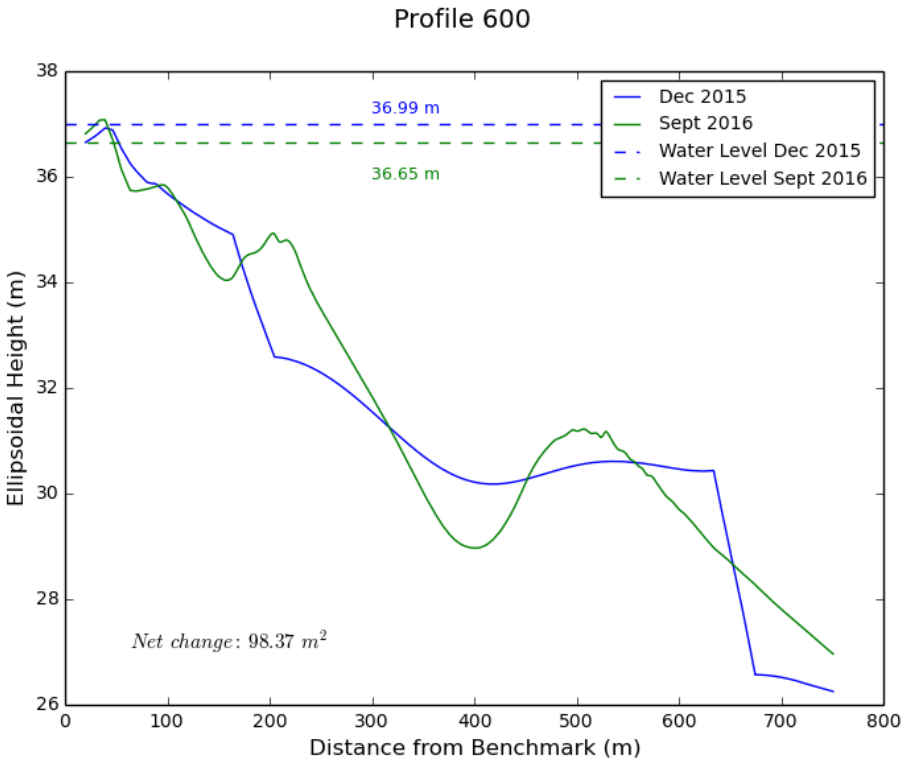

Figure E.7. Profile 600, December 2015 and September 2016.

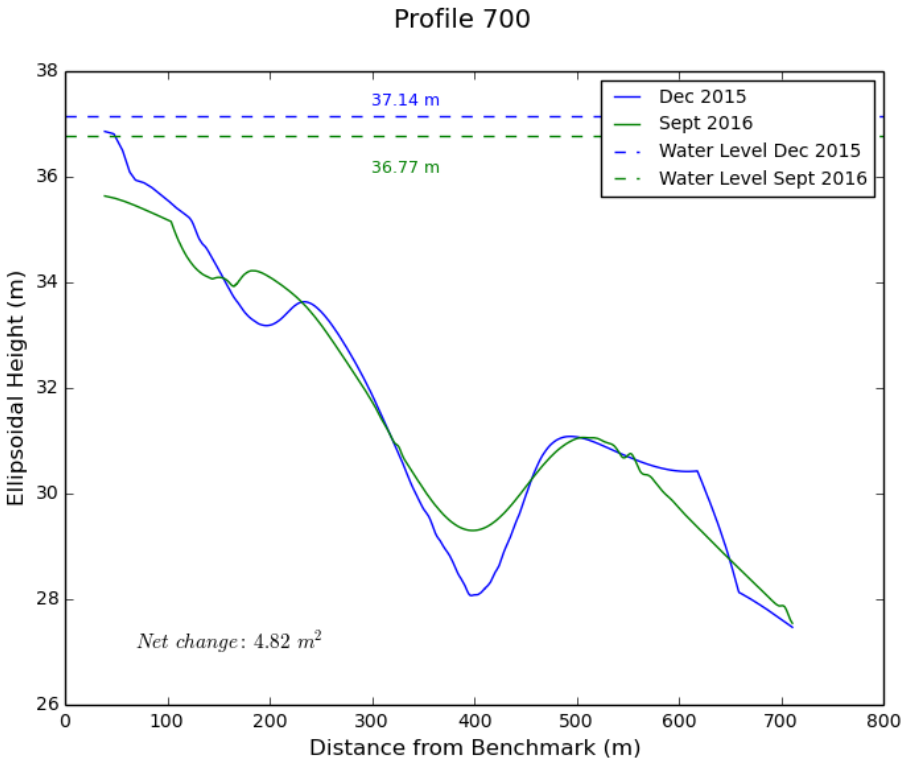

Figure E.8. Profile 700, December 2015 and September 2016.

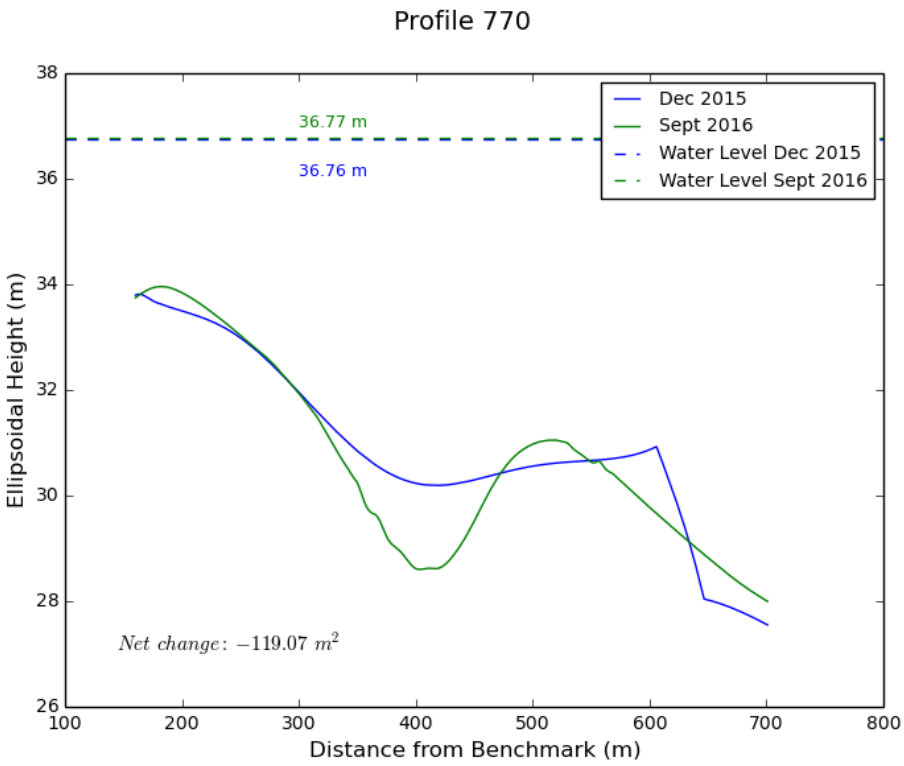

Figure E.9. Profile 770, December 2015 and September 2016.

APPENDIX F: SEPTEMBER 2016 AND MARCH 2017 PROFILES

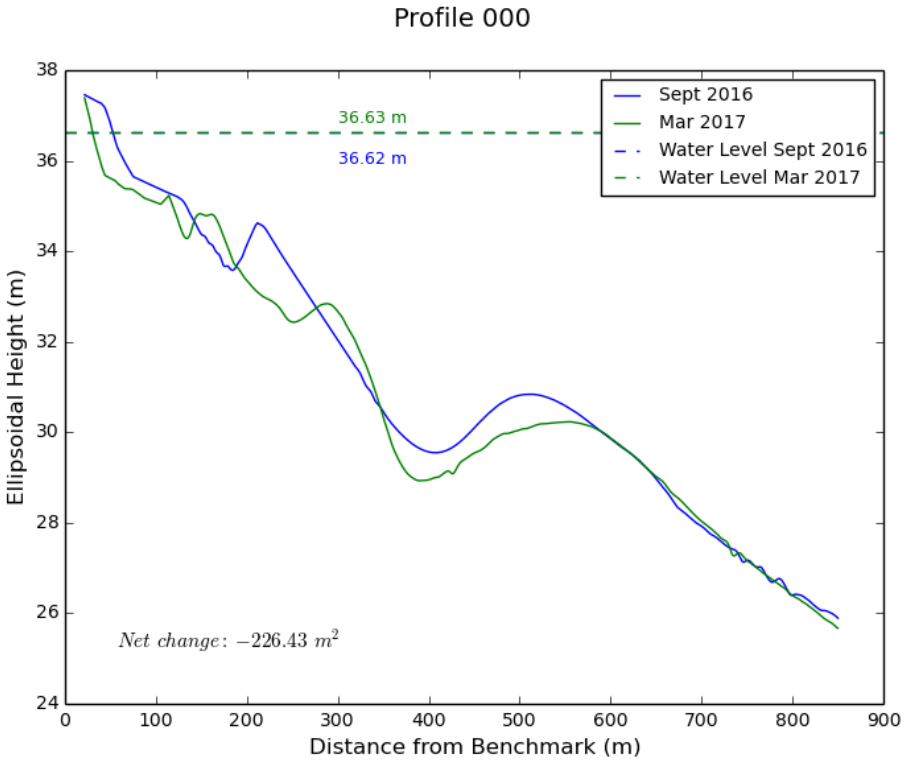

Figure F.1. Profile 000, September 2016 and March 2017.

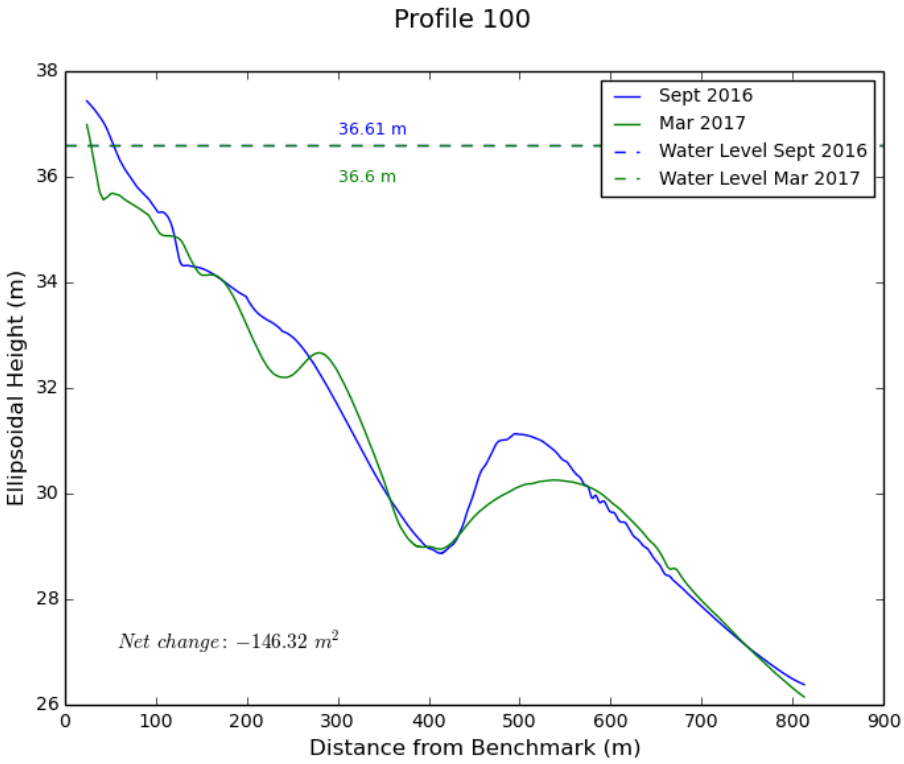

Figure F.2. Profile 100, September 2016 and March 2017.

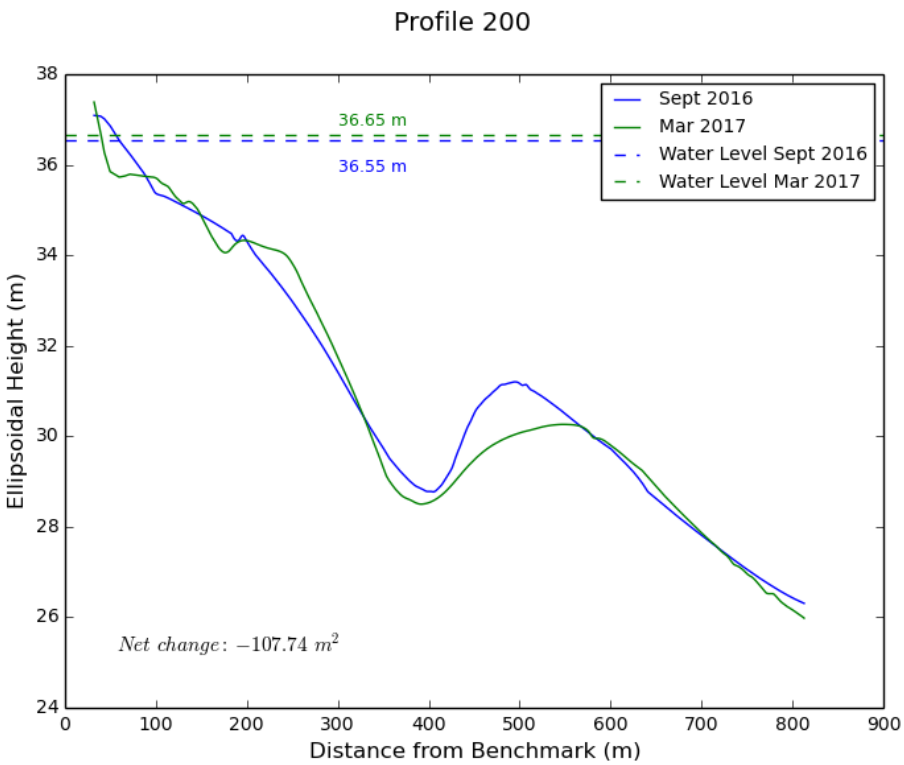

Figure F.3. Profile 200, September 2016 and March 2017.

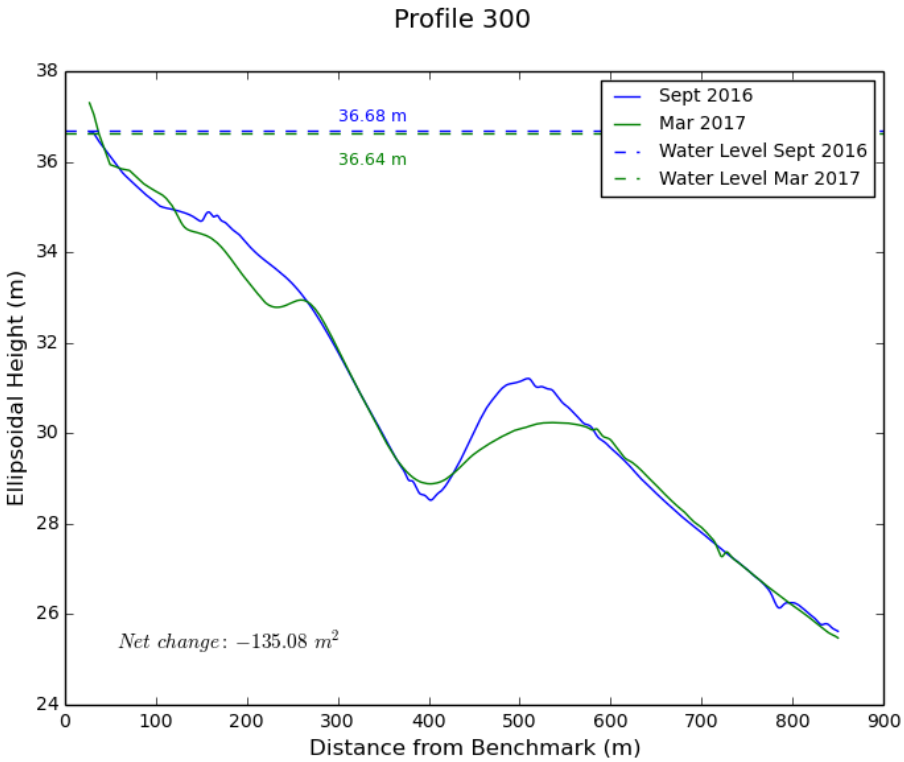

Figure F.4. Profile 300, September 2016 and March 2017.

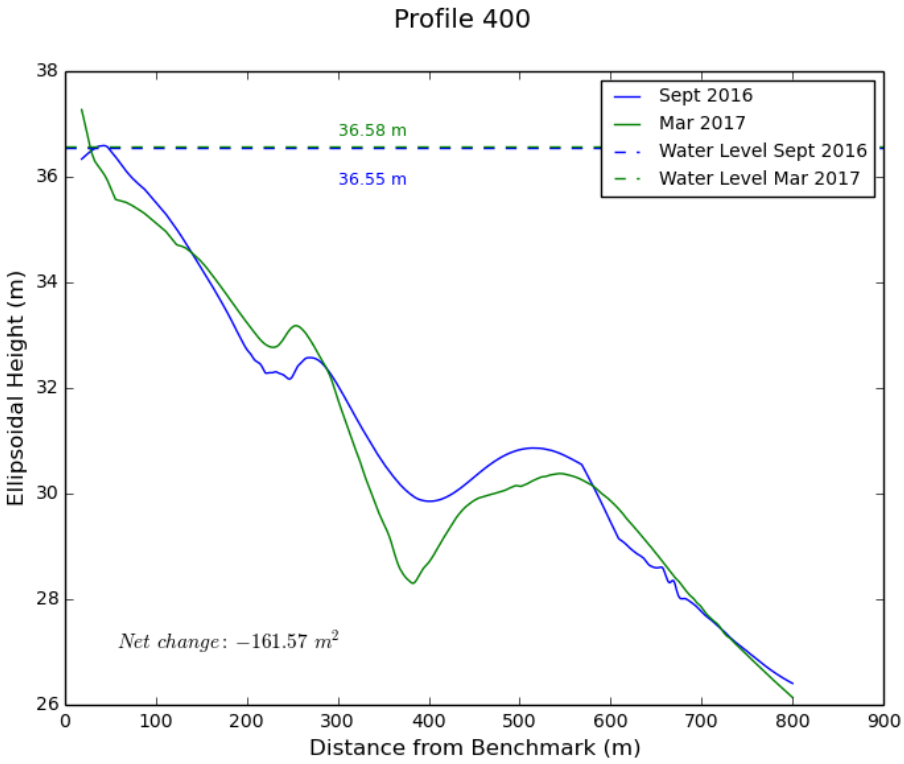

Figure F.5. Profile 400, September 2016 and March 2017.

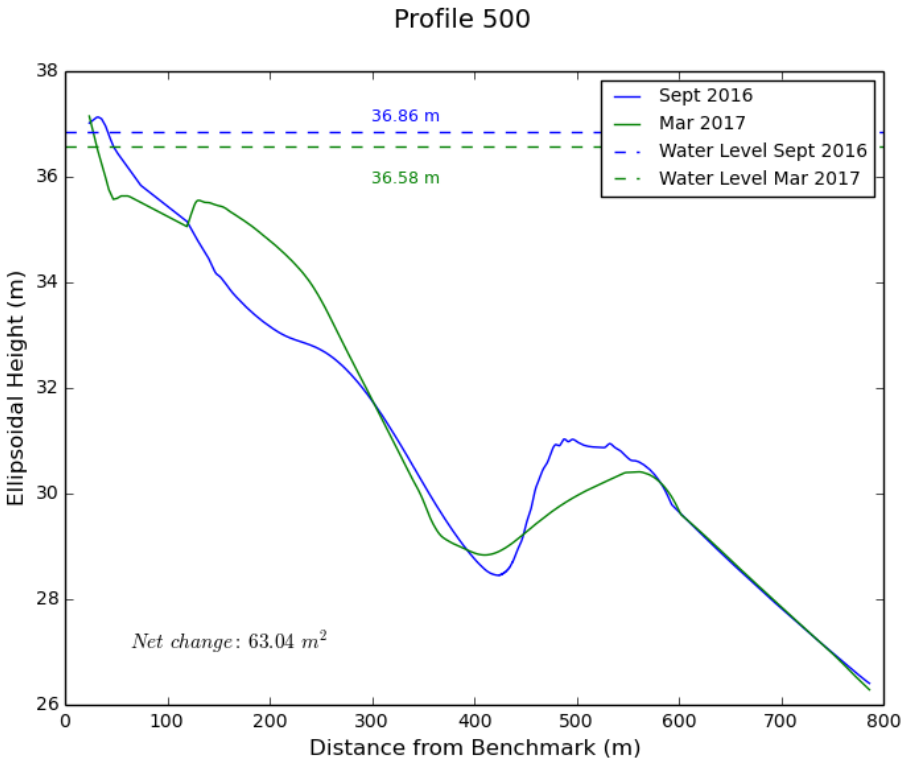

Figure F.6. Profile 500, September 2016 and March 2017.

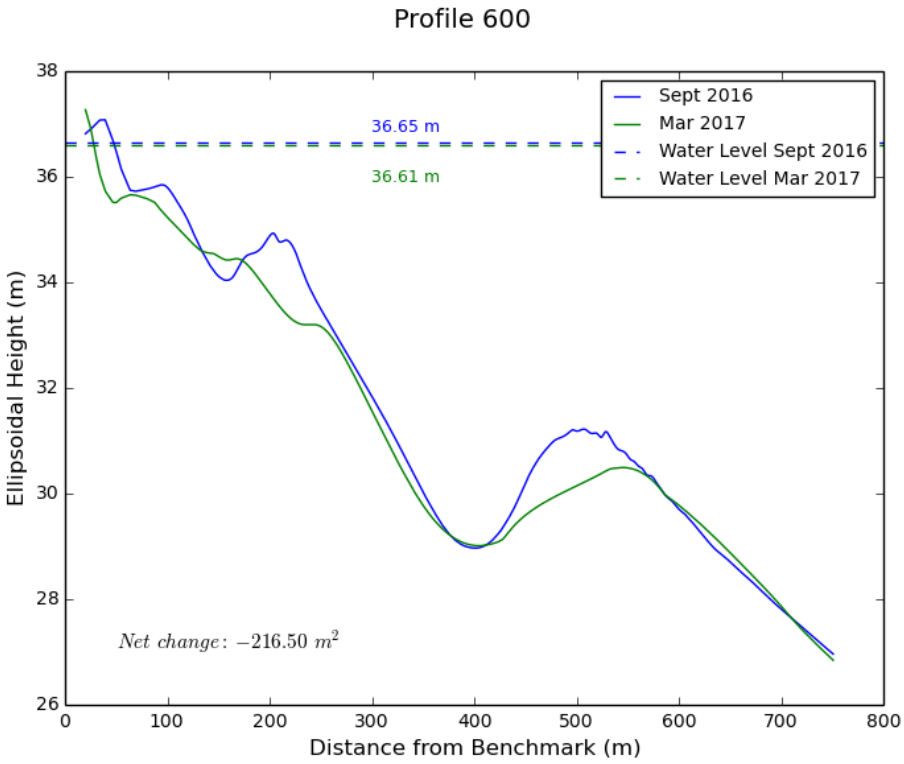

Figure F.7. Profile 600, September 2016 and March 2017.

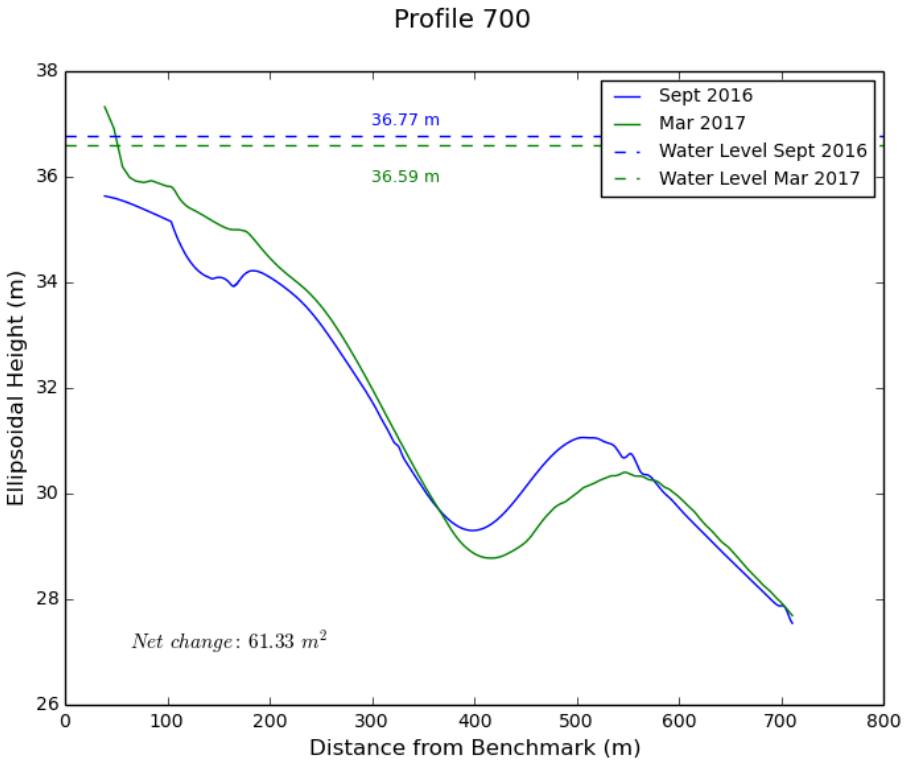

Figure F.8. Profile 700, September 2016 and March 2017.

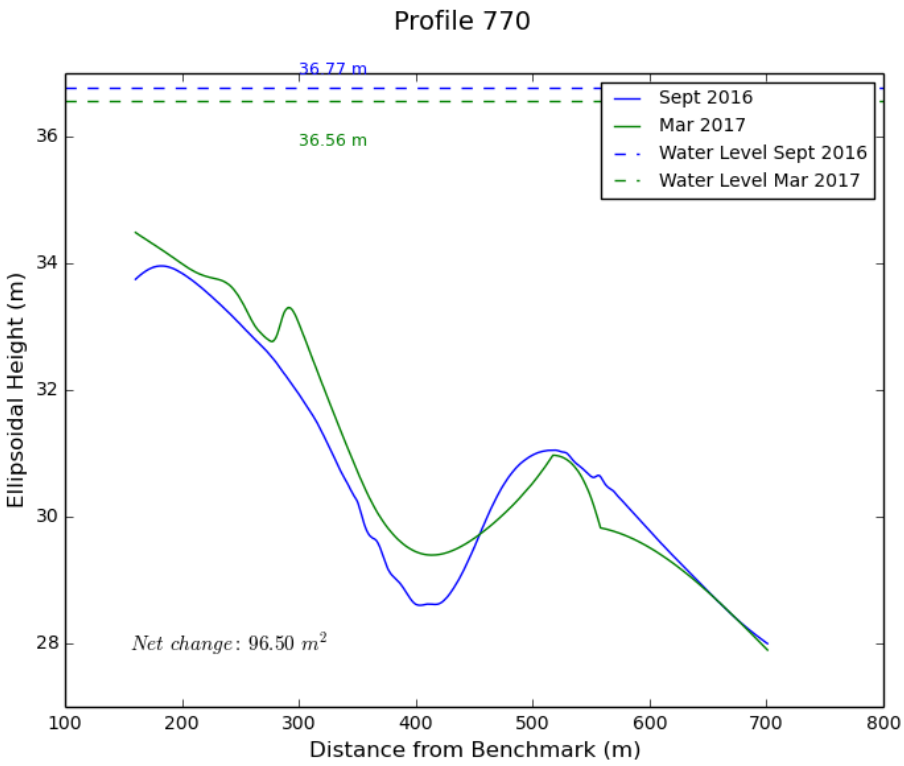

Figure F.9. Profile 770, September 2016 and March 2017.

REFERENCES

1. Börekçi, O. and E. Otay, "Deniz Kumu Üretiminin Kıyı Erozyonuna Etkileri ve Rasyonel Üretim, Kriterlerinin Geliştirilmesi, Kapanış Raporu. (Turkish) [Effects of Marine Dredging on Coastal Erosion and the Development of Rational Sand Production Criteria, Final Report]", *TÜBITAK (Turkish National Science Foundation)*, 2004.

2. McGranahan, G., D. Balk and B. Anderson, "The Rising Tide: Assessing the Risks of Climate Change and Human Settlements in Low Elevation Coastal Zones", *Environment and Urbanization*, pp. 17–37, 2007.

3. Neumann, B., A. Vafeidis, J. Zimmermann and R. Nicholls, "Future Coastal Population Growth and Exposure to Sea-Level Rise and Coastal Flooding - A Global Assessment", *PLoS One*, Vol. 10, 2015.

4. Bird, E., *Coastal Geomorphology*, John Wiley & Sons, Ltd., West Sussex, England, 2008.

5. Council, N. R., D. on Earth, L. Studies, O. S. Board, M. S. Committee, C. on National Needs for Coastal Mapping and Charting, *A Geospatial Framework for the Coastal Zone: National Needs for Coastal Mapping and Charting*, National Academies Press, Washington, D.C., 2004.

6. Holman, R. and M. Haller, "Remote Sensing of the Nearshore", *Annual Review of Marine Science*, Vol. 5, pp. 95–113, 2012.

7. Mangor, K., *Shoreline Management Guidelines*, DHI Water and Environment, Horsholm, Denmark, 2004.

8. Ramsey, D. and R. B. (NIWA), "Coastal Hazards and Climate Change. A Guidance Manual for Local Government in New Zealand.", *Ministry for the Environment*,

pp. viii–127, 2008.

9. Charlier, R. and C. DeMeyer, *Coastal Erosion: Response and Management*, Springer-Verlag, Berlin, Heidelberg, Germany, 1998.

10. Uren, J. and W. Price, *Surveying for Engineers*, Palgrave Macmillan, London, 2010.

11. (IGN), I. G. N., *International Terrestrial Reference Frame*, 2016, `http://itrf.ign.fr/` [accessed January 14, 2017].

12. NOAA, *Tides and Currents*, 2016, `https://tidesandcurrents.noaa.gov/datum_options.html` [accessed January 15, 2017].

13. Van Sickle, J., *GEOG862 - GPS and GNSS for Geospatial Professionals*, 2014, `https://www.e-education.psu.edu/geog862/` [accessed January 15, 2017].

14. Pharaoh, A., *International Hydrographic Organization*, 2016, `https://www.iho.int/srv1/index.php?option=com_content&view=article&id=298&Itemid=297&lang=en` [accessed January 15, 2016].

15. Organization, I. H., *IHO Standards for Hydrographic Surveys, 5th edition. Special Publication No. 44*, International Hydrographic Bureau, Monaco, 2008.

16. Birkemeier, W. and C. Mason, "The CRAB: A Unique Nearshore Surveying Vehicle", *The Journal of Surveying Engineering*, Vol. 110, pp. 1–7, 1984.

17. Sallenger, A., P. Howard, C. Fletcher and P. Howd, "A system for measuring bottom profile, waves and currents in the high-energy nearshore envrionment", *Marine Geology*, Vol. 51, pp. 63–76, 1983.

18. Bell, P. and J. Osler, "Mapping bathymetry using X-band marine radar data recorded from a moving vessel", *Ocean Dynamics*, Vol. 61, pp. 2141–2156, 2011.

19. Otay, E. and R. Dean, "Nearshore Surveying: Accuracy and Techniques for Improvement", *Journal of Surveying Engineering*, Vol. 122, 1995.

20. Zhang, W., J. Zao, S. Zhu and S. Lin, "2nd International Conference on Remote Sensing, Environment and Transportation Engineering (RSETE)", *A Review of the Methods to Determine Nearshore Shallow Bathymetry by Remote Sensing*, 2012.

21. for Photogrammetry, A. S. and R. S. (ASPRS), "ASPRS Positional Accuracy Standards for Geospatial Data", *Photogrammetric Engineering and Remote Sensing*, Vol. 81, pp. A1–A26, 2015.

22. Lyzenga, D., "Passing Remote Sensing Techniques for Mapping Water Depth and Bottom Features", *Applied Optics*, Vol. 17, pp. 379–383, 1978.

23. Holman, R., N. Plant and T. Holland, "cBathy: A Robust Algorithm for Estimating Nearshore Bathymetry", *Journal of Geophysical Research: Oceans*, Vol. 118, pp. 2595–2609, 2012.

24. Hoogeboom, P., J. Kleijweg and D. van Halsema, "IGARSS '86 Symposium", *Seawave Measurements Using a Ships Radar*, pp. 819–823, 1986.

25. Boccia, V., A. Renga, G. Rufino, M. D'Errico, A. Moccia, C. Aragno and S. Zoffoli, "Linear Dispersion Relation and Depth Sensitivity to Swell Parameters: Application to Synthetic Aperture Radar Imaging and Bathymetry", *The Scientific World Journal*, Vol. 2015, pp. 1–10, 2015.

26. Wackerman, C., D. Lyzenga, E. Ericson and D. Walker, "Geoscience and Remote Sensing Symposium Proceedings. IGARSS. 1998 IEEE International, Volume: 3.", *Estimating Nearshore Bathymetry Using SAR*, 1998.

27. van Dongeren, A., N. Plant, A. Cohen, D. Roelvink, M. Haller and P. Catalán, "Beach Wizard: Nearshore Bathymetry Estimation through Assimilation of Model Computations and Remote Observations", *Coastal Engineering*, Vol. 55, pp. 1016–

1027, 2008.

28. Ludeno, G., F. Reale, F. Dentale, E. P. Carratelli, A. Natale and F. Serafino, *Coastal Ocean Observing Systems*, Elsevier, 2015.

29. Boak, E. and I. Turner, "Shoreline Definition and Detection: A Review", *Journal of Coastal Research*, Vol. 21, pp. 688–703, 2005.

30. Özener, H., "Detection of Shoreline and Bathymetry Changes", *Sea Technology*, Vol. 45, pp. 19–21, 2004.

31. Demir, H., E. Otay, P. Work and O. Borekci, "Effects of Dredgeholes on the Shoreline Change in the Black Sea", *Journal of Waterway, Port, Coastal, and Ocean Engineering*, Vol. 130, pp. 170–178, 2004.

32. Otay, E., H. Demir, O. Börekçi and P. Work, "Littoral", *Marine Sand Exploitation Off the Turkish Black Sea Coast*, 2002.

33. Chen, C.-T. and F. Millero, "Speed of Sound in Seawater at High Pressures", *Journal of the Acoustical Society of America*, Vol. 62, pp. 1129–1135, 1977.

34. Mills, J. and D. Dodd, "Ellipsoidally Referenced Surveying for Hydrography", *International Federation of Surveyors (FIG)*, Vol. 62, pp. 1–62, 2014.